MARCH 1981

SAND 81-8178
SANDIA CONTRACT
83-2729E

SECOND GENERATION HELIOSTAT DEVELOPMENT

FOR

SOLAR CENTRAL RECEIVER SYSTEMS

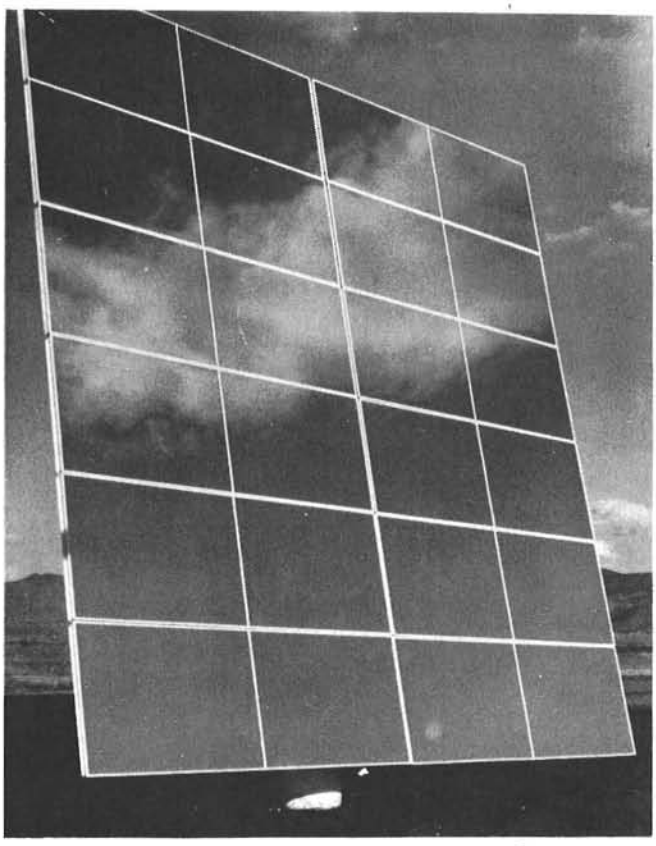

FINAL REPORT

VOLUME I

SECTIONS 1.0-3.0

INTRODUCTION
SUMMARY
HELIOSTAT DESCRIPTION

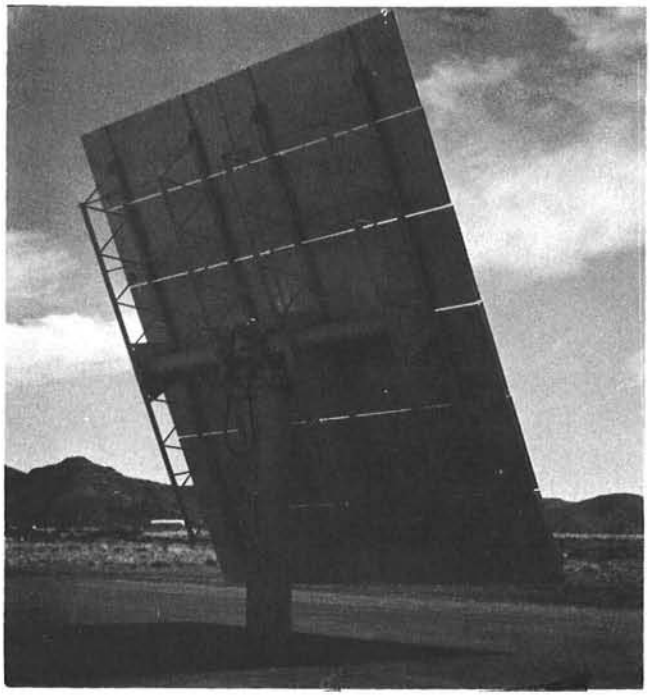

PREPARED BY

NORTHRUP, INCORPORATED

A SUBSIDIARY OF
ATLANTIC RICHFIELD CO.

AND

BECHTEL NATIONAL, INC. AND **BOOZ-ALLEN AND HAMILTON, INC.**

SECOND GENERATION HELIOSTAT DEVELOPMENT

FINAL REPORT

Volume I

Sections 1.0 - 3.0

Sandia Contract No. 83-2729E
Sandia Requestor - C. L. Mavis/8451
Contracting Representative - R. C. Christman

Work performed during the period
July 16, 1979 through March 31, 1981

by

Northrup Incorporated
302 Nichols Drive
Hutchins, Tx. 75141

and Subcontractors:

Bechtel National, Inc.
50 Beale St.
San Francisco, California 94119
and
Booz-Allen and Hamilton, Inc.
8801 E. Pleasant Valley Rd.
Cleveland, Ohio 44131

This report is presented in 4 Volumes. The content of these volumes is as follows:

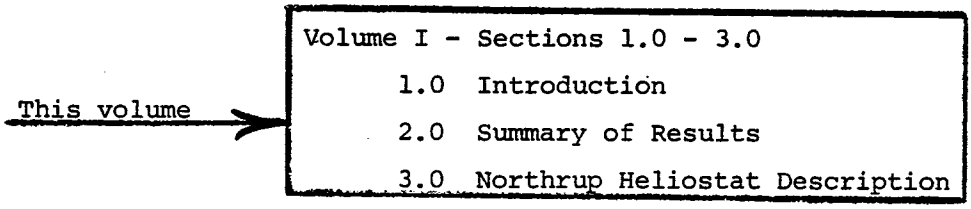

Volume II - Sections 4.0 - 8.0

- 4.0 Manufacturing
- 5.0 Transportation
- 6.0 Field Assembly and Installation
- 7.0 Maintenance
- 8.0 Cost Estimates

Volume III - Appendices A - E

- A. Bill of Materials
- B. Part Drawings (Subassemblies)
- C. Assembly Drawings
- D. Trade Studies
- E. System Studies

Volume IV - Appendices F - J

- F. Control Software
- G. Test Results
- H. Manufacturing
- I. Specification S-101
- J. Specification S-102

TABLE OF CONTENTS

TABLE OF CONTENTS (Continued)

TABLE OF CONTENTS (Continued)

TABLE OF CONTENTS (Continued)

TABLE OF CONTENTS (Continued)

TABLE OF CONTENTS (Continued)

LIST OF FIGURES

LIST OF FIGURES (Continued)

LIST OF FIGURES (Continued)

LIST OF FIGURES (Continued)

LIST OF TABLES

LIST OF TABLES (Continued)

LIST OF TABLES (Continued)

SECTION 1.0
INTRODUCTION

This report presents the results obtained in the development of a second generation heliostat by Northrup, Incorporated under Sandia Laboratories contract 83-2729E during the period July 16, 1979 through March 31, 1981.

Northrup, Incorporated, a subsidiary of Atlantic Richfield Company, is headquartered at 302 Nichols Drive, Hutchins, Texas, 75141 and has offices at Suite 306, 7061 South University Blvd., Littleton, Colorado, 80122. Work relating to this project was performed at both locations. The report includes contributions by Northrup's major subcontractors, Booz-Allen and Hamilton for portions of the Manufacturing subtask and Bechtel National for the Field Assembly and Installation subtask.

The report covers the results obtained in the program which includes the design of the second generation heliostat, the development of the manufacturing plan, the method of transporting the heliostat components from the factory to the installation site, heliostat field assembly and installation procedures, and the maintenance routines. These plans are then cost estimated to provide inputs required to develop the installed cost of the heliostat and further, the cost of owning, operating and maintaining a collector field which utilizes these heliostats.

Two prototype heliostats which were representative of production hardware were constructed. Some initial testing was performed at Northrup's Hutchins site prior to delivery to Sandia's Central Receiver Test Facility at Albuquerque, New Mexico for further evaluation by Sandia Laboratories. The results of the Northrup test program are contained in this report.

The report is presented in four volumes. Volumes I and II includes all the technical presentations and Volumes III and IV contain back-up appendices.

SECTION 2.0
SUMMARY OF RESULTS

2.1 DESCRIPTION OF NORTHRUP II HELIOSTAT

Northrup's second generation heliostat is appropriately identified as Northrup II. It is a dual axis tracking heliostat with a central pedestal mount. The normal stow position is vertical but under anticipated extreme high wind conditions it is driven to a horizontal orientation with the reflective surfaces facing upward. The gross face area of the heliostat is approximately 25 feet by 25 feet. Due to mirror module spacing and edge treatment the net reflective area is 568 square feet or 52.8 square meters. Each mirror module is nominally 4 feet by 12 feet with a 3 inch depth. Twelve modules comprise the mirror array for each heliostat. The mirror support rack consists of open-web roof-type trusses which are combined with tubular members which connect to the drive unit. The drive unit is gear-driven with separate motors and gear systems for azimuth and elevation. The foundation for the drive consists of a one-piece cylindrical pipe which is planted into the ground with conventional techniques.

The 4 ft. x 12 ft. mirror modules have a fabricated steel substrate which provides the flatness and rigidity needed for good performance. Second surface silvered float glass is attached to the substrate by a unique method designed to maintain mirror flatness along with low glass stress over the full range of operating conditions and temperatures. A silicone grease layer between the mirror and substrate permits the two parts to move relative to one another as temperature changes introduce dimensional changes. To provide for a more concentrated image at the receiver the module is constructed using two 4 feet by 6 feet mirrors. A slight pre-cant is designed into the substrate to provide convergence of the two images at prescribed distances. Twelve modules make up the heliostat array. Three point mounting of each module permits individual canting of the pre-canted dual mirror element.

The module support rack is of steel construction consisting of identical left and right hand sections. Each section consists of two open-web roof-type trusses coupled together by a cylindrical torque tube. The torque tubes are appropriately flanged to mate with the arms of the elevation drive. When fully assembled, the support rack has a high volume to weight ratio so it is shipped knocked-down for minimum shipping cubage. The support structure is field-assembled at the installation site.

The heliostat is positioned by a drive unit which provides azimuth and elevation tracking. Drive motor outputs are geared down to positioning speeds through precision gear drives of low backlash. All the gearing is enclosed and bathed in oil to promote long life. D-C stepping motors are used to power the drive. Step counting from zero reference positions simplifies the control system as complex encoders are not required. Flanges on the elevation drive mate with the mirror support racks. The drive unit also has a bottom mounting flange which mates with the top of the foundation pedestal.

The foundation of the heliostat is provided by a one piece cylindrical steel pipe which is inserted into the ground. The single continuous pipe extends above grade up to the bottom of the drive unit. Conventional methods are used for planting the pedestal. The pedestal is topped off with a flange which mates with the bottom flange of the drive unit.

The heliostat presents a square appearance with no unusual irregularities or slots. The dual mirrors used in the mirror modules provide a 24 facet design although only 12 modules are used. All exposed steel and iron parts are painted white. Most of the cabling and all of the controls are contained within the volume of the hollow pedestal. These features result in a clean, uncluttered appearance which is typical of products of mature design.

2.2 MANUFACTURING

A manufacturing plant of 680,000 ft^2 is required to produce 50,000 Northrup II heliostats per year. In this plant glass is mirrored, mirror modules are fabricated and assembled, castings and bar stock are machined and assembled into drive units, controls are assembled, and the structural parts are fabricated, welded into subassemblies and painted. The initial investment required to put this plant in operation has been estimated to be $93,000,000 with about 75% of this amount relating to the manufacture of the drive unit.

The plant is a significant user of materials with the 50,000 heliostats per year requiring the following commodity purchases:

Commodity	Tons per Year
Steel - sheet	99,000
Steel - Bar Stock	6,000
Iron - Castings	29,000
Glass	18,000

The cost of these commodities comprise over one half of the manufacturing cost of the heliostat so sound material procurement practices are especially critical for these items.

Sites throughout the southwest U.S. were considered for the manufacturing plant. A detailed analysis of eight cities indicated that siting was not a major cost consideration. A combination of quantitative and subjective comparisons led to the selection of Albuquerque, New Mexico as the specific site for detailed analysis.

2.3 TRANSPORTATION

The heliostats will be transported from the manufacturing site to the power plant site by conventional trucks utilizing open flat bed trailers. The major components to be shipped are mirror modules, trusses, torque tubes, drive units, and pedestals. They will be shipped in full trailer-loads of each component since all component parts are interchangeable. Throughout the design phase, shipping

cubage has been a constant consideration and as a result the shipment of one heliostat requires only about 1/5 of a truckload, or conversely about 5 heliostats per truckload. To handle the 200 heliostats/day production rate requires a fleet of 80 tractors and 240 flat bed trailers.

2.4 FIELD ASSEMBLY AND INSTALLATION

The first step in the installation process is the planting of the pedestal in the heliostat field. Truckloads of pedestals will be delivered directly to the site. Options for insertion in the ground include driving by a vibratory hammer or setting in a pre-augered and grouted hole.

The other major components are delivered to an on-site assembly building where the mirror support rack consisting of two trusses and a torque tube are joined by welding. Six mirror modules are then mounted on each support rack. Two racks with mirror modules attached are then coupled to a drive unit and the mirrors are aligned to a prescribed cant. The completed assembly is then transported to the pedestals, hoisted in place, and bolted down to complete the mechanical assembly of the heliostat. Finally, the control components are mounted within the pedestal and coupled with factory-built cables to the drive unit and the field wiring junction boxes.

2.5 MAINTENANCE

The Northrup II heliostat has been designed to require very low maintenance. The control system is simplified compared to previous heliostat designs and premium grade electronic components are used throughout. In the event of malfunction, on-site correction is usually accomplished by PC board replacement. The drive unit is sealed and the gearing is bathed in oil. Since normal operating stresses are extremely low, the only significant planned maintenance on this component is oil replacement on a ten-year cycle. The support structure and the mirror module substrate are appropriately finished

to provide long-term weather protection. When impending corrosion is evident, cleaning and touch-up with paint is advised. In the event of mirror deterioration or breakage the module is replaced.

One area of maintenance is extremely site dependent - that is maintaining a high level of mirror reflectivity. Due to operating and stow positions the heliostat is always in a favorable position to receive the natural washing action of periodic rains. In some locations this will maintain the reflectivity at near-original levels. In other areas with sparse rainfall for extended periods of time an artificial washing system is needed. A semi-automatic washing procedure has been developed for this function.

2.6 COST ESTIMATES

Summarizing the costs of all events required to provide an installed heliostat yields a cost of $6711 per heliostat. This includes the cost of the land for the collector field, the field wiring, and an allocated portion of the cost of a Heliostat Controller. At 52.8 square meters and a net mirror reflectivity of 0.91 this is a cost of $139.67/$m^2$R. Based on a 90% experience curve our program goal of $116.85/$m^2$R will be achieved somewhere between the second and fourth year of production.

The annual cost of a 50MW_e collector subsystem ranges from $5.9 million/year to $4.5 million/year for the first through eighth year of production. On a cost per delivered energy basis, the cost ranges from 4.8¢/KWH to 3.7¢/KWH.

2.7 FUTURE DEVELOPMENT REQUIRED

The Northrup II heliostat can be produced with known processes, equipment and techniques. While new procedures are desirable they are not essential to initiating production. Some of the areas where evolutionary improvements seem most probable are:

- o Mirrors of higher net reflectivity by using very thin, low-iron glass. This is practical from a materials standpoint, but

manufacturing and material handling processes must be developed.

- o Lower cost mirror module substrates. Alternate forms or materials are easily introduced into the product since the silicone grease interface overcomes temperature-induced stress and distortion problems. Innovative substrates that exhibit low weight, rigidity, corrosion resistance and low cost are desired.
- o Improved production methods for relatively large precision gears and worms. The projected annual requirement for this type of gearing system creates a demand that should stimulate the development of improved gear and worm cutting processes.

2.8 DESIGN AND PRODUCTION PHILOSOPHY

The Northrup II heliostat has been designed to facilitate moving from low volume production to high volume production while maintaining the same design concepts. A review of the manufacturing processes involved for the major components is as follows:

- o Mirrors - Standard mirroring processes are used. Special glass is desirable for best performance, but not essential.
- o Mirror Substrates - Involves basic sheet metal processes - blanking, shearing, roll forming, etc.
- o Trusses - Derived from standard building trusses - a proven, high volume component.
- o Torque Tubes and Pedestals - Any of the many processes for manufacturing steel pipe can be applied to these parts.
- o Drive Units - A self contained gear drive that can be produced by a number of specialists.
- o Motor and Controls - Assemblies of existing hardware.

For each of these areas there exists a number of suppliers who can supply the needed components. This permits the solicitation of competitive quotations which could be influenced by ability to produce and the supplier's location relative to the market area being served. As volume develops, requirements for heliostats could outstrip the

supplier's existing productive capacity. A large market for their output in "heliostat" country could influence a supplier's plans for expanding productive capability. This could ultimately lead to all major components being produced in the southwestern part of the United States. The next step of integration would be to have all suppliers located in the same industrial complex service the needs of the heliostat industry and also supplying other customers with their specialty. The final step of integration would be to process all materials under one roof and one management.

How far this integration process proceeds will depend heavily on the interest and ability of component suppliers to make the commitments needed to provide the needed hardware. In those areas where suppliers do not maintain the needed pace in productive capacity or product costs, the components would have to be moved in-house for manufacture by the heliostat designer and marketer. The study presented here details the cost levels which can be achieved by producing all parts within a captive facility. During the early years of heliostat production these costs estimated for in-house production can be used as a benchmark for evaluating component supplier quotations.

2.9 SUMMARY OF FINDINGS

This study has shown that heliostats can be produced in volume at an installed cost level approaching $\$100/m^2R$. The annual cost of owning, operating, and maintaining a collector subsystem for an electric power plant is approximately $100 per KW of peak capacity. On a delivered energy basis, the cost of the collector subsystem is about 4¢/KWH.

SECTION 3.0

NORTHRUP HELIOSTAT DESCRIPTION

The Northrup heliostat is a dual axis unit having a central support pedestal and drive mount. Twelve mirror modules are mounted to a primary structure consisting of four truss purlins, cross bracing and two torque tubes. Except for clearance spaces between mirror modules, the heliostat presents a continuous mirrored face with no central slot or void regions. The total envelope face area is 54.9 m^2 (590.7 ft^2). The small clearance spaces between mirror modules and the mirror edge protective moulding reduce this total to a net reflective area of 52.8 m^2 (568 ft^2). Each of the twelve mirror modules has two pre-canted flat mirror facets, so this total reflective area is achieved by an array of twenty-four individual mirror elements. Figures 3-1 and 3-2 present a perspective view of the front and back of the Northrup heliostat. Figure 3-3 shows actual photographs of a Northrup heliostat.

3.1 DESCRIPTION

The following discussion presents a detailed description of the Northrup heliostat, the major component elements, and the rationale for the approach selected.

3.1.1 GENERAL CHARACTERISTICS

The Northrup heliostat has a face envelope which measures 7.44 m (24.42 ft) high and 7.37 m (24.19 ft) wide. The minimum ground clearance is 0.24 m (0.8 ft) when the heliostat is in the vertical position. The Northrup heliostat is designed to be stowed in any position from vertical to face-up horizontal, and as such provides maximum power outage/storm protection. The normal stow position is vertical for the purpose of natural rain washing. The normal stow position is vertical for the purpose of natural rain washing and to minimize dust accumulation. The alternate face-up horizontal stow will be employed to avoid sand abrasion and to reduce structural stress levels if high winds are encountered or forecast.

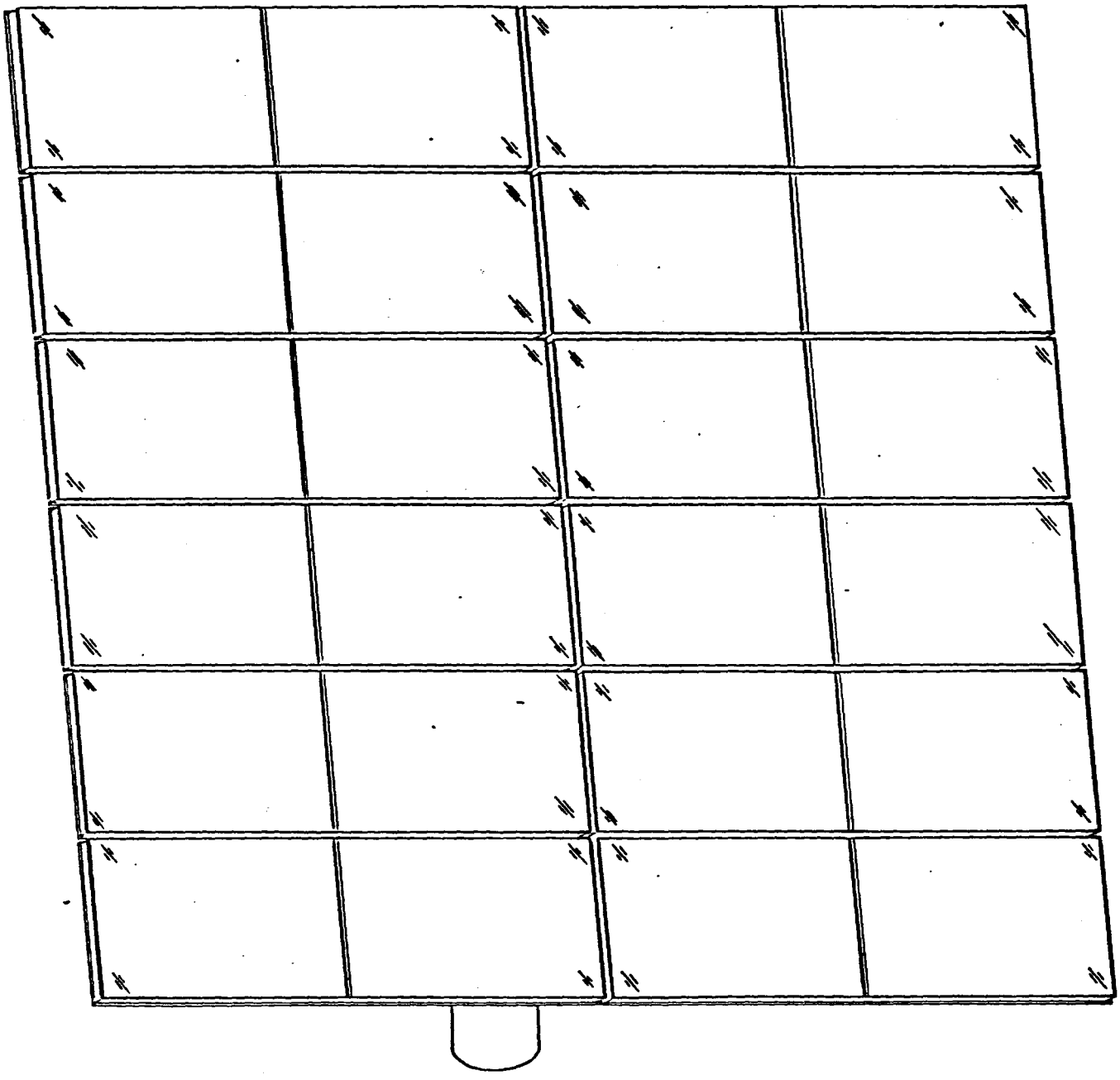

Fig. 3-1 Northrup II Heliostat Front View

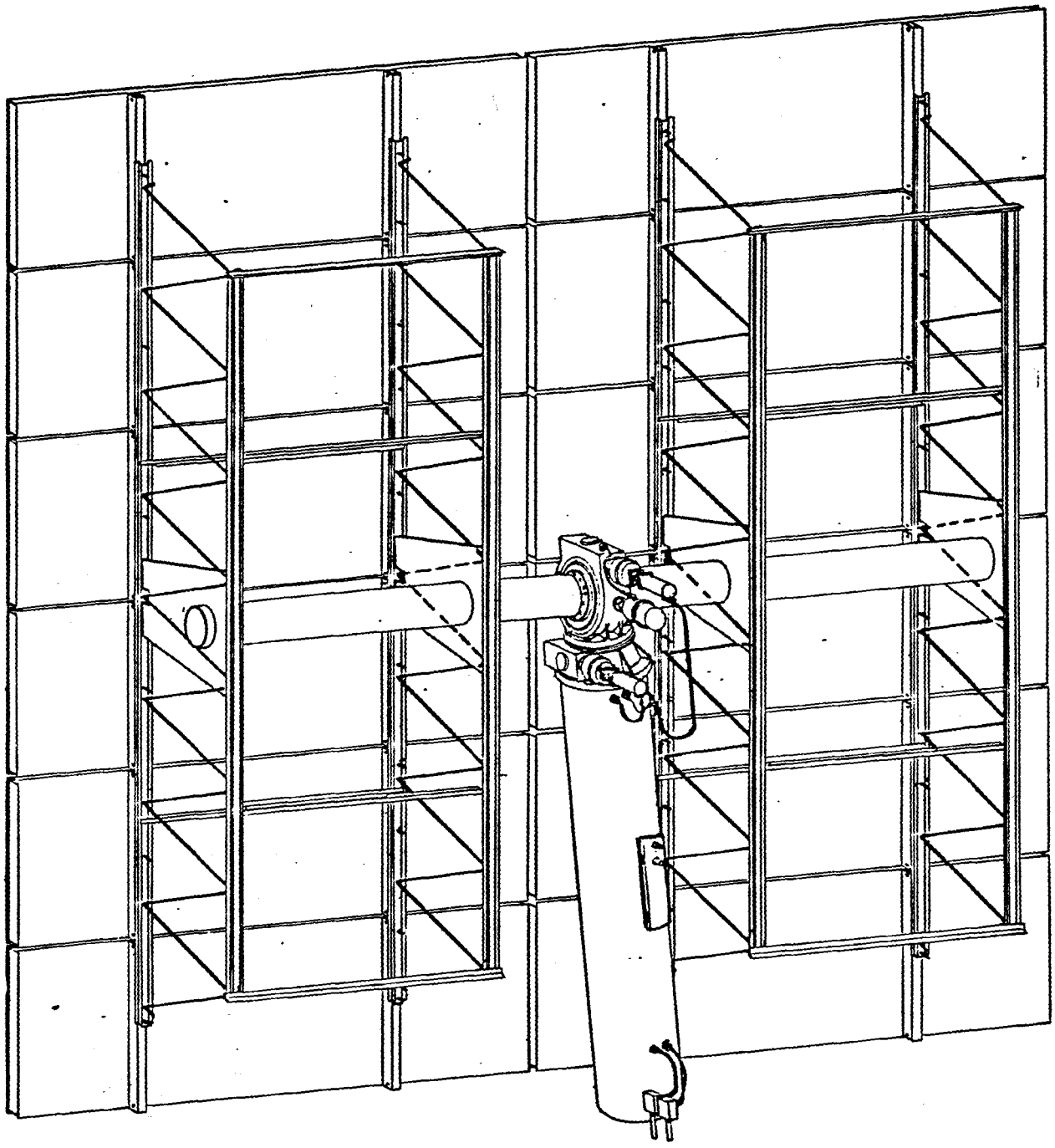

Fig. 3-2 Northrup II Heliostat - Back View

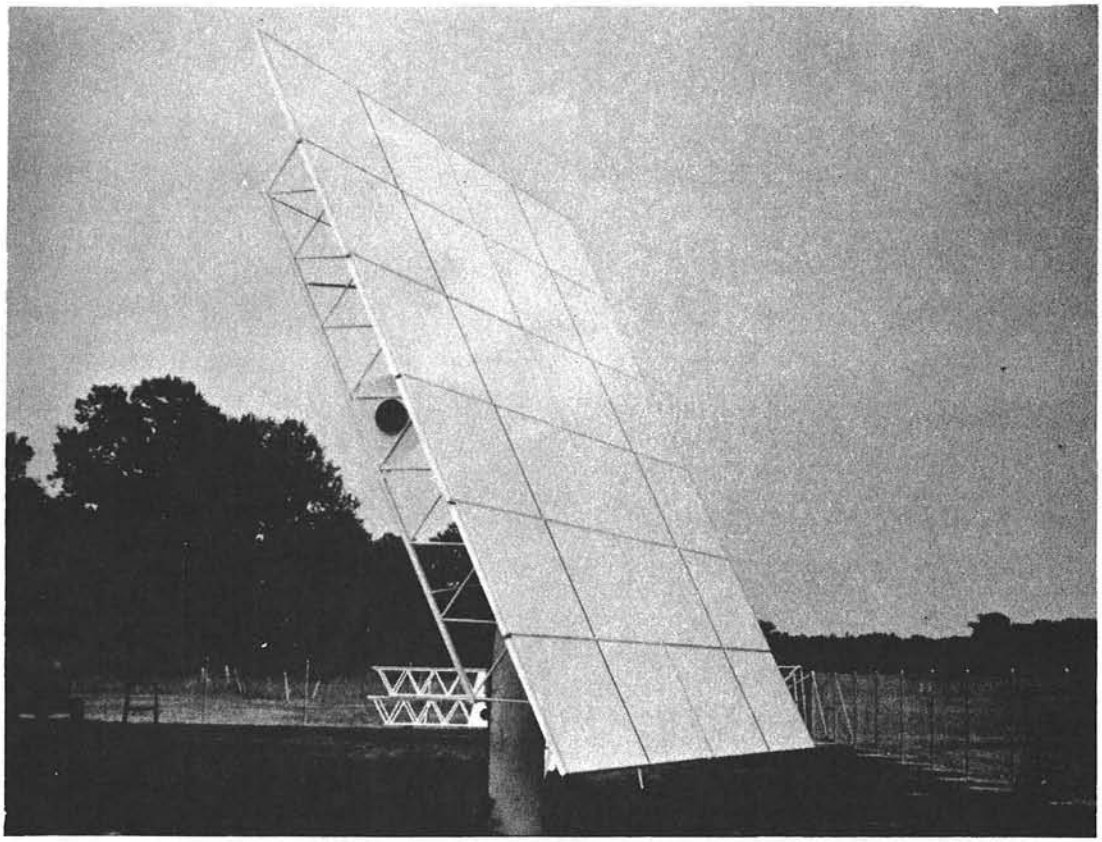

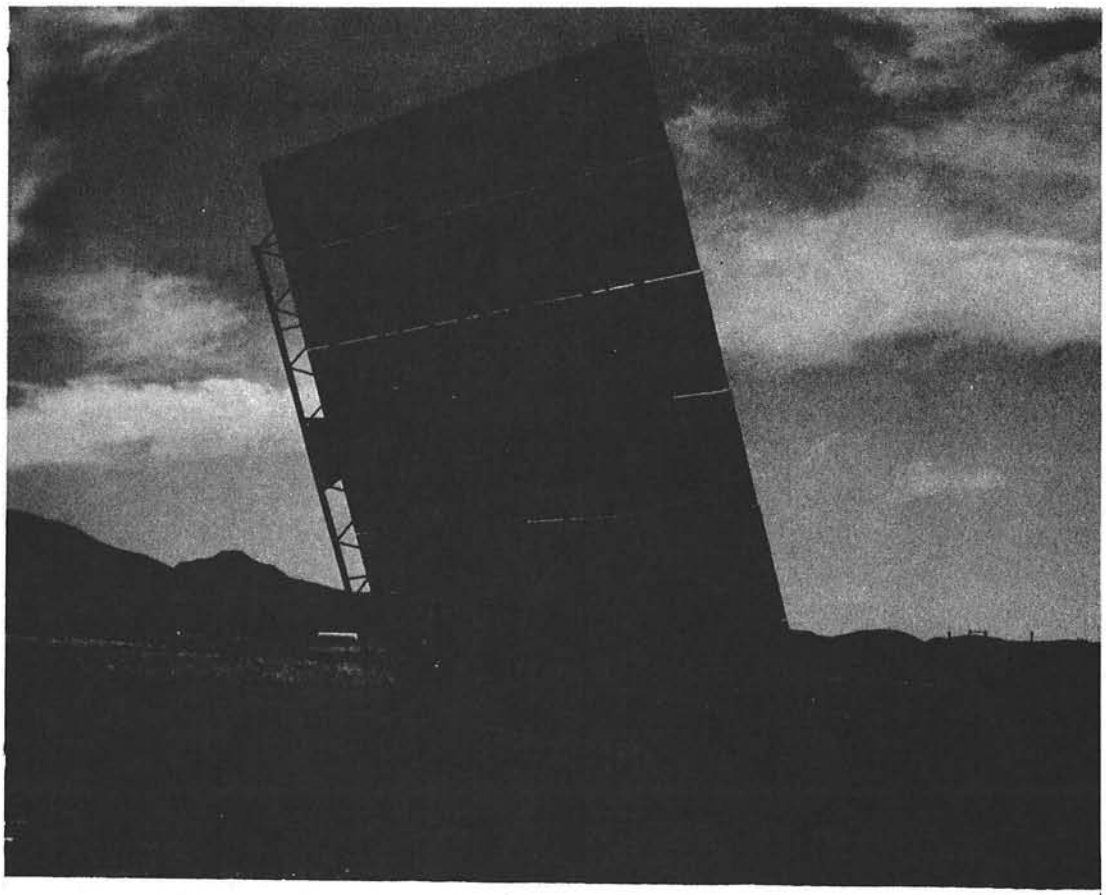

Figure 3-3 NORTHRUP HELIOSTAT, FRONT & REAR VIEW

The reflecting surface is comprised of twelve mirror modules each 1.22 m (4.01 ft) high and 3.67 m (12.03 ft) wide arranged in a 2-module wide x 6-module high pattern on the heliostat. All mirror modules are identical; i.e., there are no position-unique differences. Each mirror module is faced with two 1.22 m (4.0 ft) x 1.83 m (6.0 ft) mirrors which are pre-canted to minimize image size. A frontal view of the Northrup heliostat, therefore, exhibits a 24 facet appearance.

The mirror modules are attached to four main vertical beams, each of which is 0.75 m (2.46 ft) deep and 6.40 m (21.0 ft) long. The beam depth was governed by drive clearance considerations with the exceptional bending stiffness being a desirable side benefit. These four main beams interface with the drive unit by means of two transverse torque tubes. The heliostat assembly thus achieved may be visualized as identical left and right-hand subassemblies, each consisting of two beams, one torque tube, and six mirror modules. Such a left or right subassembly can in fact be physically removed from or installed on a heliostat as an integral unit.

The Northrup drive unit incorporates independent azimuth and elevation sections which are bolted together to form a one-piece drive unit. Both of these drive elements are identical in terms of motor, input-stage, and output stage gearing. The basic drive concept is keyed to the use of D-C stepper motors which provide both motive power (torque) and position control (precise incremental rotation); i.e., no encoders or other continuous position sensors are required. Stepper motors interface well with digital minicomputers and microprocessors, and are able to deliver an accurate rotation of 1.8 angular degrees per motor step. An intermediate, printed circuit board device known as a translator provides the sequencing and switching logic which converts pulses from a minicomputer or microprocessor into motor steps, therefore allowing step rate, direction, and number of steps to be controlled by external logic. With proper translator selection, stepping rates as high as 10,000 steps/second can be accurately achieved.

The Northrup drive unit employs a planetary type speed reducing first stage, and a worm-gear type speed reducing output stage. The total over-all speed reduction is 18,400:1, so a single motor pulse step of 1.8 angular degrees is reduced to approximately 0.0001 angular degrees of heliostat motion. The planetary first stage was selected because it provides a high reduction ratio and high torque capability in a compact sized unit. The output worm-gear stage was selected because of its self-locking/no back-drive capability (the worm can drive the gear, but the gear cannot back-drive the worm), moderately high ratio reduction, and high torque capability.

The drive unit is mounted to a flanged steel pile. The pile is a straight-cylinder, hollow pipe shape which is driven into place or grouted in an augered hole. Any misalignment of the pile flange relative to true horizontal is removed by rotational adjustment of a matched pair of tapered shims. For production units, it is planned to eliminate these shims, and to utilize the computer software to correct for any measured out-of-plane condition.

3.1.2 MIRROR MODULES

The mirror module design for the Northrup heliostat is based on using an all-steel mirror support structure fabricated from 26 gage galvannealed sheet metal. The substrate structure is composed of a face sheet upon which the mirrors are attached, 7 longitudinal and 2 transverse C-webs (ribs) which form the 7.62 cm (3.0 inch) high substrate core, and a backing sheet. These structural elements are adhesively bonded together to form a slab-like substrate measuring approximately 1.22 m (4.0 ft) high x 3.66 m (12.0 ft) wide and 7.62 cm (3.0 inches) thick. A problem was encountered with the 26 gage galvannealed material having ripples at the edges or center; i.e., the sheet stock was seldom available with adequate flatness. As a result, the prototype units were built with 24 gage material for the mirror backing sheet.

Figure 3-4 illustrates the forming operation on the longitudinal C-webs which provides the cant between the two mirror facets.

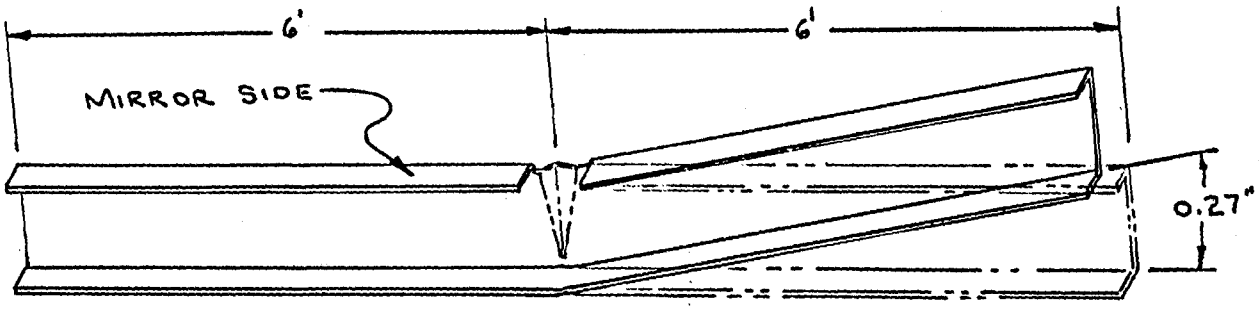

WEB BENDING

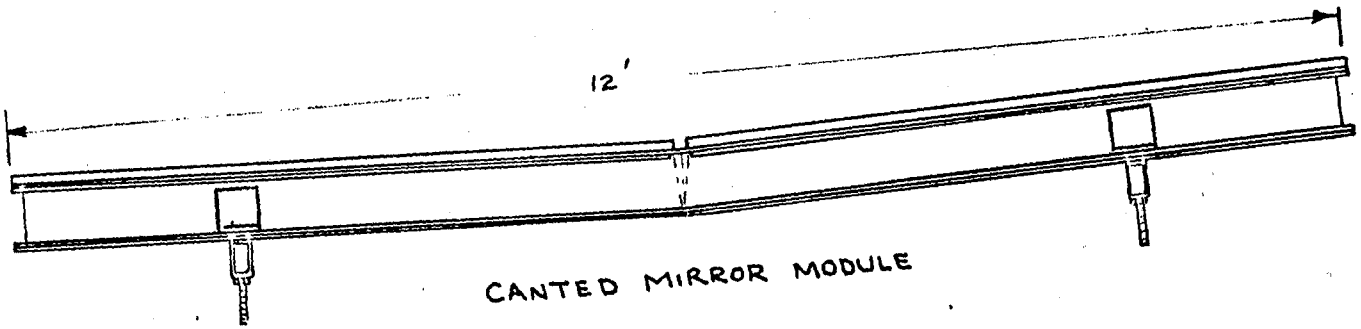

CANTED MIRROR MODULE

LONGITUDINAL WEB BENDING FOR FACET CANTING

Figure 3-4

The glass mirror is not bonded to the substrate, but adheres to it via a thin layer of silicone grease. The silicone grease is highly water repellent, non-volatile, and extremely inert. It provides a high degree of adhesion, but still permits relative differential thermal expansion and contraction between the mirror and steel substrate. Of equal importance is the fact that the silicone grease also provides an added measure of protection of the mirror silvering against humidity-condensation or rain water damage. A metal edge seal is bonded around the entire module glass-substrate edge with silicone rubber to preclude water penetration. This edge seal also serves as a compliant attachment to maintain the glass mirror position on the substrate. A pictorial representation of the mirror module construction is shown in Figure 3-5.

The fabrication sequence for assembling prototype modules is as follows: The unit is built-up beginning with the mirror. A flat, smooth set of two granite surface blocks are used to establish the required cant of the mirror facets. The mirror facets are laid face down on the canted granite surfaces and positioned by means of alignment stops attached to the blocks. The backside of the mirrors are then coated with a thin film (.002") of silicone grease using a rubber roller. The mirror backing sheet (26 gage galvannealed steel) is similarly coated with grease on an adjacent table. The backing sheet is applied to the glass mirrors so the two greased faces contact each other. The backing sheet is very flexible and is progressively laid-down and simultaneously rolled to minimize air entrapment during this mirror-grease-sheet assembly operation. The flatness of this initial assembly is maintained by the underlying surface blocks.

The 7 longitudinal C-webs and the 2 transverse C-web end pieces are assembled in a special magnetic holding fixture, and joined together with rivets and adhesive. The backing sheet is next bonded to this C-web subassembly to form a complete "substrate assembly". This substrate assembly is then primed and painted (for production, pre-painted sheet metal would be used). The completed, painted substrate is then adhesively bonded to the mirror backing sheet. During this operation, the flatness and cant is again maintained by the underlying surface blocks. The adhesive cure time is very rapid (approximately 10-15 minutes), so the unit can be removed from the surface blocks in a relatively short time.

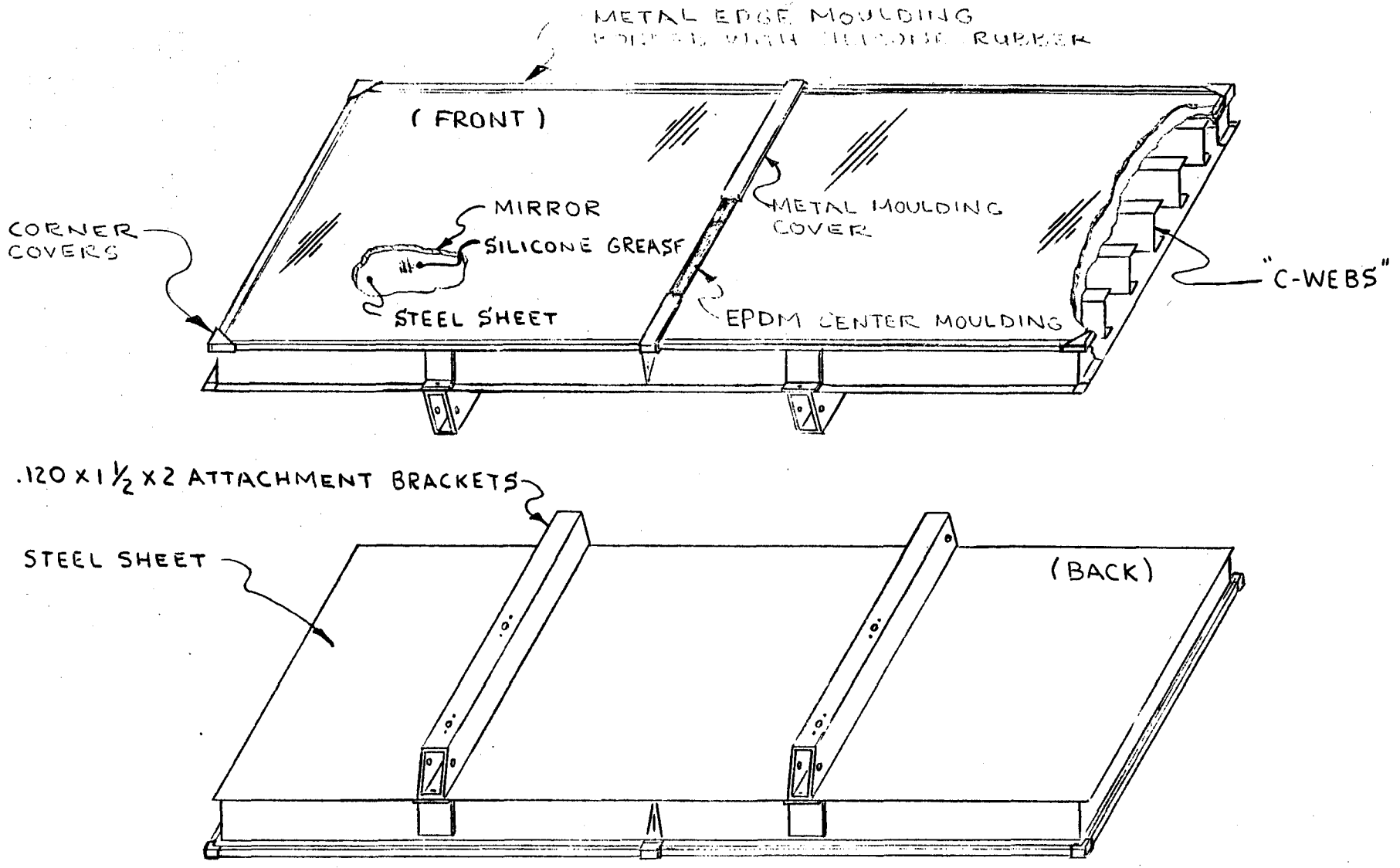

NORTHRUP MIRROR MODULE CONSTRUCTION

FIGURE 3-5

The final assembly operations include adhesively bonding and riveting the rectangular supports on the backside, and adhesively bonding the metal edge seal to the mirror and substrate lip. Figure 3-6 shows an exploded representation of the mirror module assembly.

The mirror facets to be used on the production heliostats will be 1.22 m (4.0 ft) x 1.83 m (6.0 ft) x 2.39 mm (0.094 inch) thick. The material will be low iron, soda lime float glass having a reflectivity of 0.91. Due to the unavailability of low iron glass, the prototype modules used standard float glass mirrors which have a reflectivity of 0.83. The second surface silvered layer is protected by a layer of copper, commercial mirror backing paint, plus the silicone grease coating which serves as additional protective layer.

The grease compound selected is Dow Corning #4 Silicone Compound. It is a grease-like compound similar in consistency to Vaseline. The material contains an inert silica filler in combination with poly-dimethyl silicone fluid. It has excellent dielectric properties, is highly water repellent, resistant to oxidation, essentially non-toxic and non-melting, and has shown little tendency to dry out in service. Silicone 4 Compound will retain much of its room temperature consistency from -40 C to 204 C (-40 F to 400 F). Practically non-volatile, it is odorless and resistant to a wide range of metals and chemicals, and is often used to lubricate plastic and rubber components.

Dow Corning Silicone 4 Compound is used in a wide variety of applications requiring the unique combination of inertness, moisture resistance, high dielectric, lubricity, and sealing properties. In many instances where the desirable properties of silicone fluids are required, the thicker silicone compounds are preferred, since the compound filler immobilizes the silicone fluid and maintains the silicone in a confined area. Such is the case on the Northrup mirror module design.

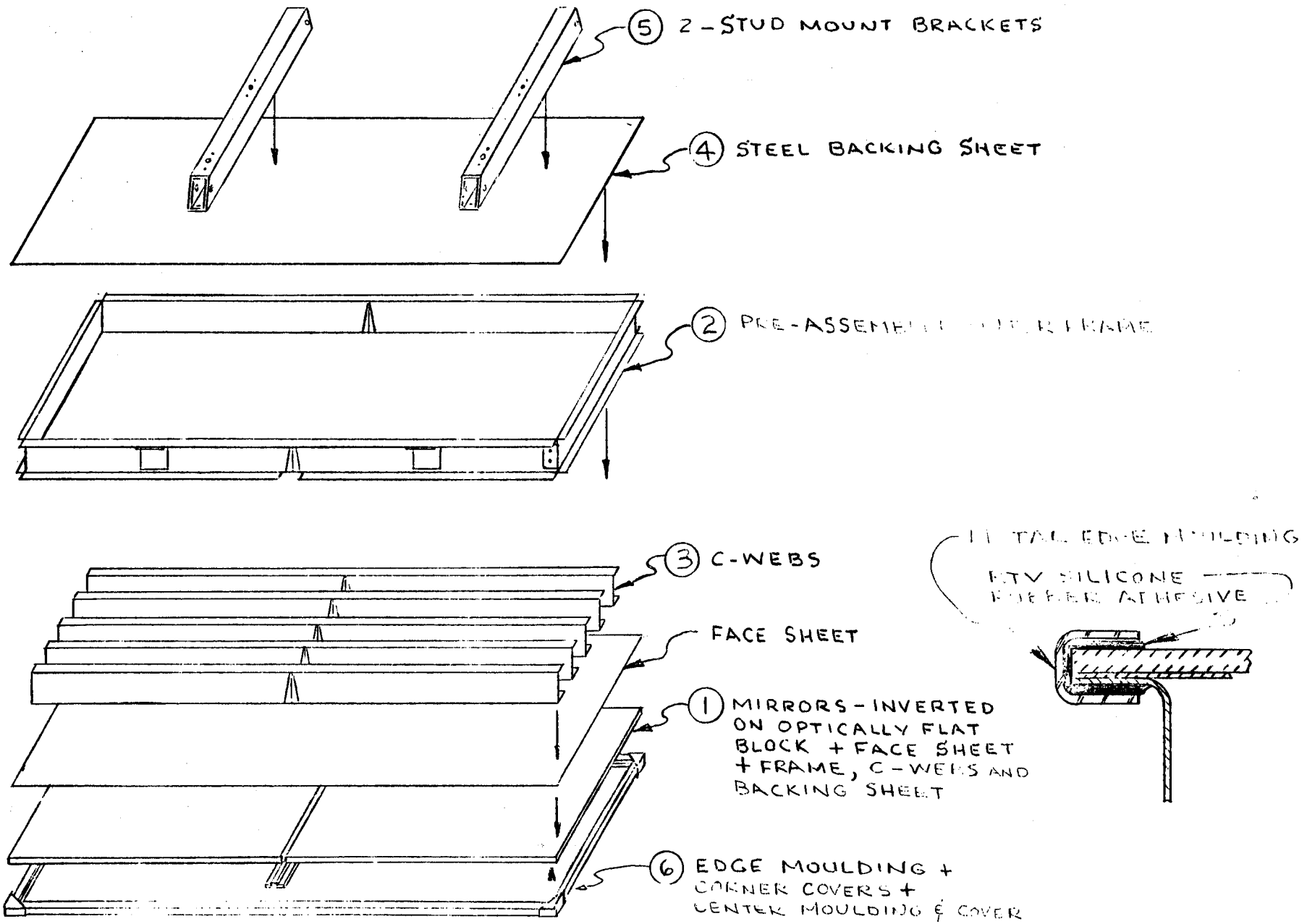

Figure 3-6 MIRROR MODULE EXPLODED VIEW

Dow Corning Silicone 4 Compound is not affected by air, dilute acids or alkalines, or by most aqueous solutions. It can be applied by hand or specially designed automated equipment using brushing, wiping, or rolling techniques. It can also be dispersed in a solvent (xylene, mineral spirits, perchloroethylene, or methyl ethyl ketone) and applied by brushing, dipping or spraying. It is formulated to meet the requirements of MIL-S-8660B. It readily adheres to dry metals, glass, ceramics, rubber, plastics, and insulating resins. It is commonly used as a moisture-proof seal for aircraft, automotive, and marine ignition systems and spark plug connections. Table 3-1 provides typical properties for Silicone 4 Compound along with its lighter and heavier counterparts, Silicone 7 and Silicone 111 compounds.

The silicone grease compound is applied to both the mirror back and the steel support sheet prior to rolling these members together. The steel support sheet is 26 gage (0.022 inch thick) and is zinc-coated galvannealed. Galvannealed sheets are heat treated after coating to produce a smooth surface of iron-zinc alloy. The heat treatment eliminates the normal zinc spangle pattern found on hot-dipped galvanized sheets. The smooth surface characteristic of galvannealed sheet enables good glass-to-support sheet adhesion to be achieved with less silicone compound (approximately 0.004" silicone grease thickness is required). The zinc coating weight is "light commercial" and averages .60-.80 ounce/square foot (approximately .0006 inch zinc thickness on each side).

The remaining sheet metal members of the mirror module are also fabricated from 26 gage (0.022 inch thick) galvannealed steel. These members include the longitudinal C-webs, the box frame, and the backing sheet. All of these members are adhesively bonded together using an acrylic structural adhesive, Versilok-201, manufactured by Hughson Chemicals (Lord Corporation; Erie, PA.). This adhesive provides a practical method for accomplishing the required build-up of glass-sheet-stringers-sheet with surface block support for flatness control. Versilok-201 adhesive is relatively insensitive to surface cleanliness, and can even be applied to oily metal surfaces with little loss of bond strength. The shear strength of the bonded joint

TABLE 3-1

TYPICAL PROPERTIES FOR SILICONE GREASE COMPOUNDS

		DOW CORNING 7 Compound	DOW CORNING 4 Compound	DOW CORNING 111 Compound
Physical				
CTM† 0176	Color	White, translucent	White, translucent	White, translucent
CTM 0191	Consistency	Light	Medium	Heavy
	Penetration, unworked	240-300	200-260	175-210
	worked 60, max	350	310	260
CTM 0033A	Bleed, 24 hrs/392 F (200 C), % max	10.0	6.0	0.5
CTM 0033A	Evaporation, 24 hrs/352 F (200 C), % max	5.0	2.0	2.0
	Service Temperature Range			
	degrees F	-40 to 400	-70 to 400	-40 to 400
	degrees C	-40 to 204	-57 to 204	-40 to 204
	Melting Point	None	None	None
CTM 0022	Specific Gravity at 77 F (25 C)	1.0	1.0	1.0
Electrical				
CTM 0112	Dielectric Constant			
	at 100 Hz	2.79	2.90	2.82
	at 100 KHz	2.75	2.89	2.80
CTM 0112	Dissipation Factor			
	at 100 Hz	.0006	.0006	.0006
	at 100 KHz	.0006	.0006	.0006
CTM 0114	Dielectric Strength, volts/mil			
	50 mil gap	400	400	400
	Volume Resistivity, ohm-cm			
	at 73 F (23 C)	1×10^{15}	1×10^{15}	1×10^{15}
	at 350 F (177 C)	—	1×10^{12}	—
CTM 0171	Arc Resistance, seconds	120	120	120

varies from 9 MPa (1300 psi) for galvanized steel to 42 MPa (6000 psi) for SAE 1010 cold rolled steel. This adhesive is a two-component system. The components may be mixed together and applied, or a no-mix method may be employed. With the no-mix method the activator can be applied to one or both of the surfaces to be bonded. The activator-coated surface can be used immediately or stored for several months. In either case, nothing happens until the second component, an adhesive resin, is applied to the bond interface and the coated surfaces are mated. The gel time after contact is 6-8 minutes, and the unit can be safely handled in 15 minutes i.e., 1000 psi shear strength is attained in this time period).

3.1.3 Rack Structure

The rack structure is assembled from conventional building truss purlins (main beams), pipe (torque tubes) and steel angle (cross bracing). The truss purlins selected are of a standard, commercial design, and are in fact being mass produced by the Butler Manufacturing Co. (Kansas City, Mo.). Their design is a very material-efficient one; a 6.4 m (21.0 ft) truss having a depth of 0.75 m (2.46 ft) weighs only 51 kg (113 lb). The complete beam is fabricated from 2.0 mm (0.078") sheet metal. The sheet stock is received in a 1.22 m (4.0 ft) width in coils. The coils are slit into two widths, one for forming the chord members, and the other for forming the web tubing. The chord stock is roll-formed to produce the shape shown in Figure 3-7. This shape offers good compression chord stability. The compression flanges of beams must resist buckling horizontally sideways. An additional advantage of this chord shape is that the beams can be nested together to minimize shipping volume; the nested shipping width is only 103 mm (4.05 inches) versus the true width of 142 mm (5.60 inches).

The tube stock is roll-formed into a 25.4 mm (1.0 inch) diameter tube shape, and is seam-welded to form a continuous tube. The tubes are then zig-zag bent to form the tubing into the triangular web pattern. The final operation is to resistance-weld the tubing to the top and bottom chord members. Only 17 resistance welds are required to assemble the tubing web and chords for a Northrup truss, all of which are

FIGURE 3-7

BUTLER TRUSS PURLIN - CHORD DETAIL

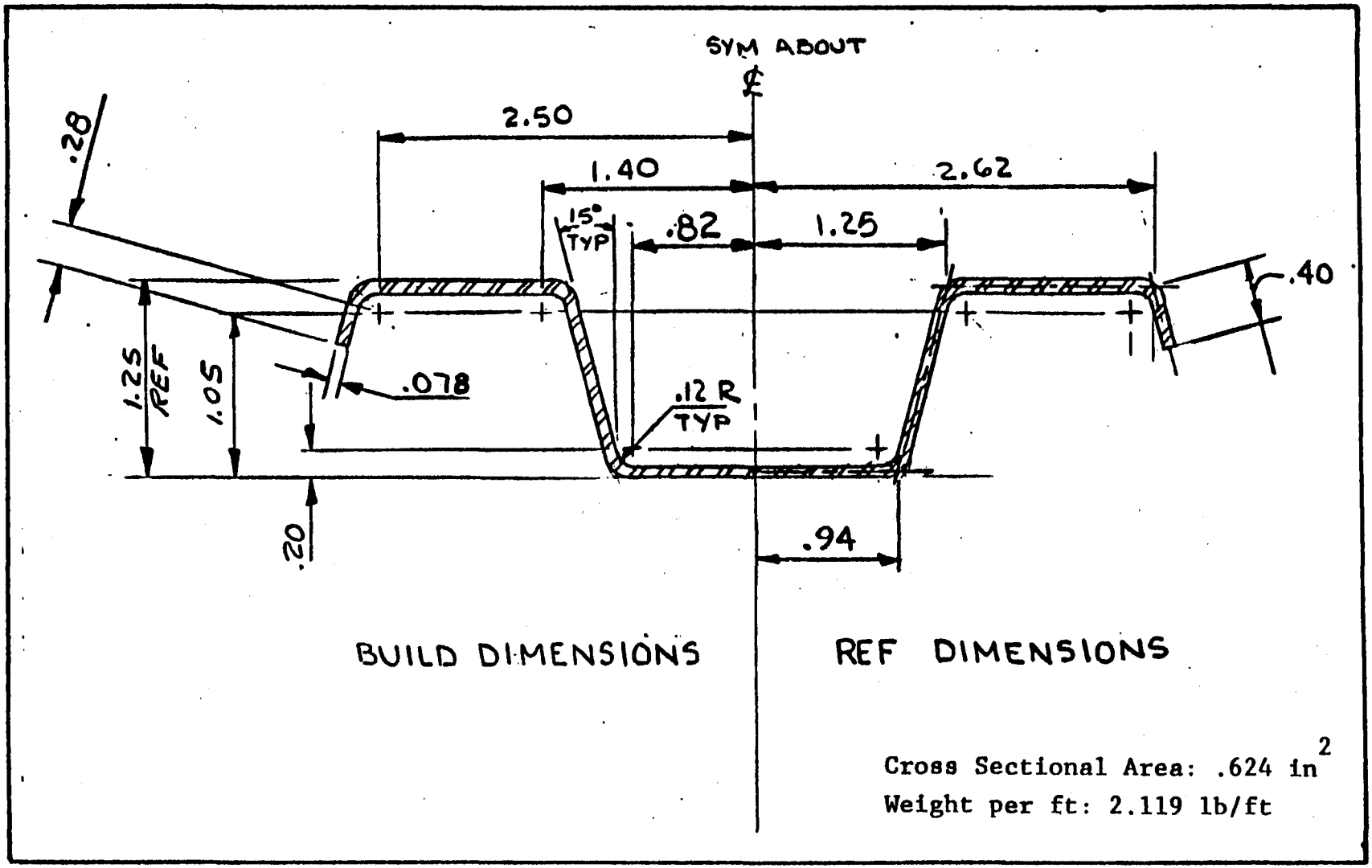

accomplished in a single, one-shot, operation. After welding, the trusses are processed through a finishing operation which includes both a primer and a final coating.

The torque tube is fabricated from a piece of 12-inch, Schedule 20 steel pipe. The true dimensions of this pipe are 0.324 m (12.75 inch) O.D. and 0.311 m (12.25 inch) I.D. A trade-off study was performed early in the program which showed that an economic optimum tube (inertia per unit weight/cost) should be on the order of 0.406 m (16 inch O.D.) and 2.3 mm (0.090 inch) wall thickness. However, physical constraints governed by the interface with the drive unit forced this diameter down to the present size; i.e., the added cost of the current, heavier torque tube is more than compensated for by a lower cost drive unit.

Each torque tube is flanged at the end which interfaces with the drive unit, and is attached to the drive with twelve 5/8-11 UNC bolts. Two trapezoidal shaped plates are welded to the torque tube, one at the non-flanged end and the other approximately 2.13 m (7.0 ft) toward the flanged end. These plates form the interface with the truss members, and are welded to the truss top and bottom chords at the field site. Since these plates serve to rigidize the truss chords relative to each other, shear deflections are virtually eliminated. Although the shipping volume is penalized with this design (versus the alternate approach of making these shear plates a part of the truss), it was believed that better perpendicularity and position location could be achieved by welding the plates to the torque tube in the factory, and then performing a final straightening and machining cut after welding. Figure 3-8 shows a pictorial representation of the torque tube. Figure 3-9 shows a photograph of the truss and torque tube subassembly being mated to a drive unit at the Northrup test facility.

The 2.13 m (7.0 ft) spacing between truss members was governed by mirror module gravity sag considerations; i.e., the 3.66 m (12.0 ft) mirror modules with supports located $\pm$ 1.07 m ($\pm$ 3.5 ft) from the module center line will always exhibit a desirable concave gravity sag. With the support spacing any significant amount less than this, an undesirable convex shape would result. With a greater support

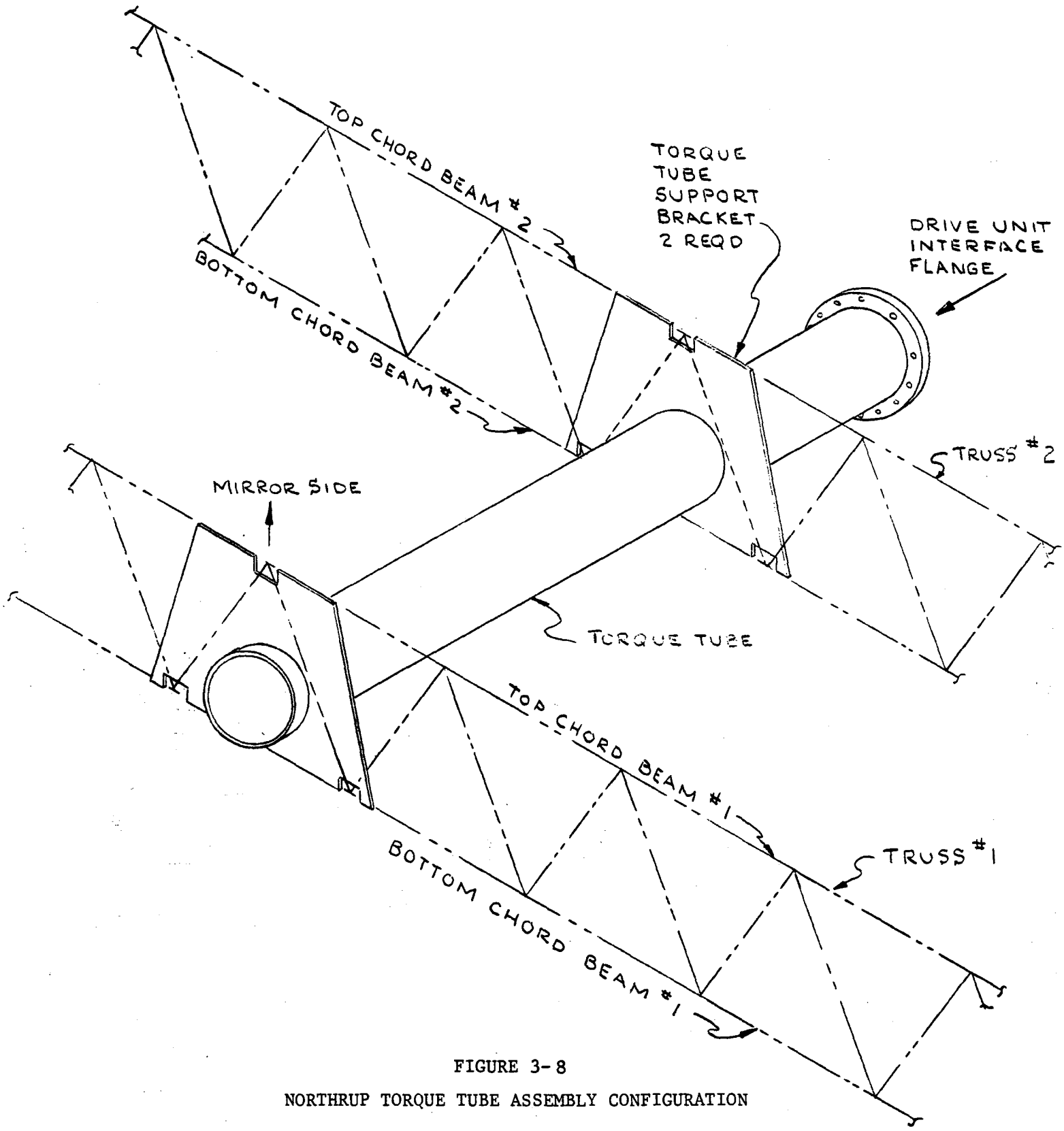

FIGURE 3-8

NORTHRUP TORQUE TUBE ASSEMBLY CONFIGURATION

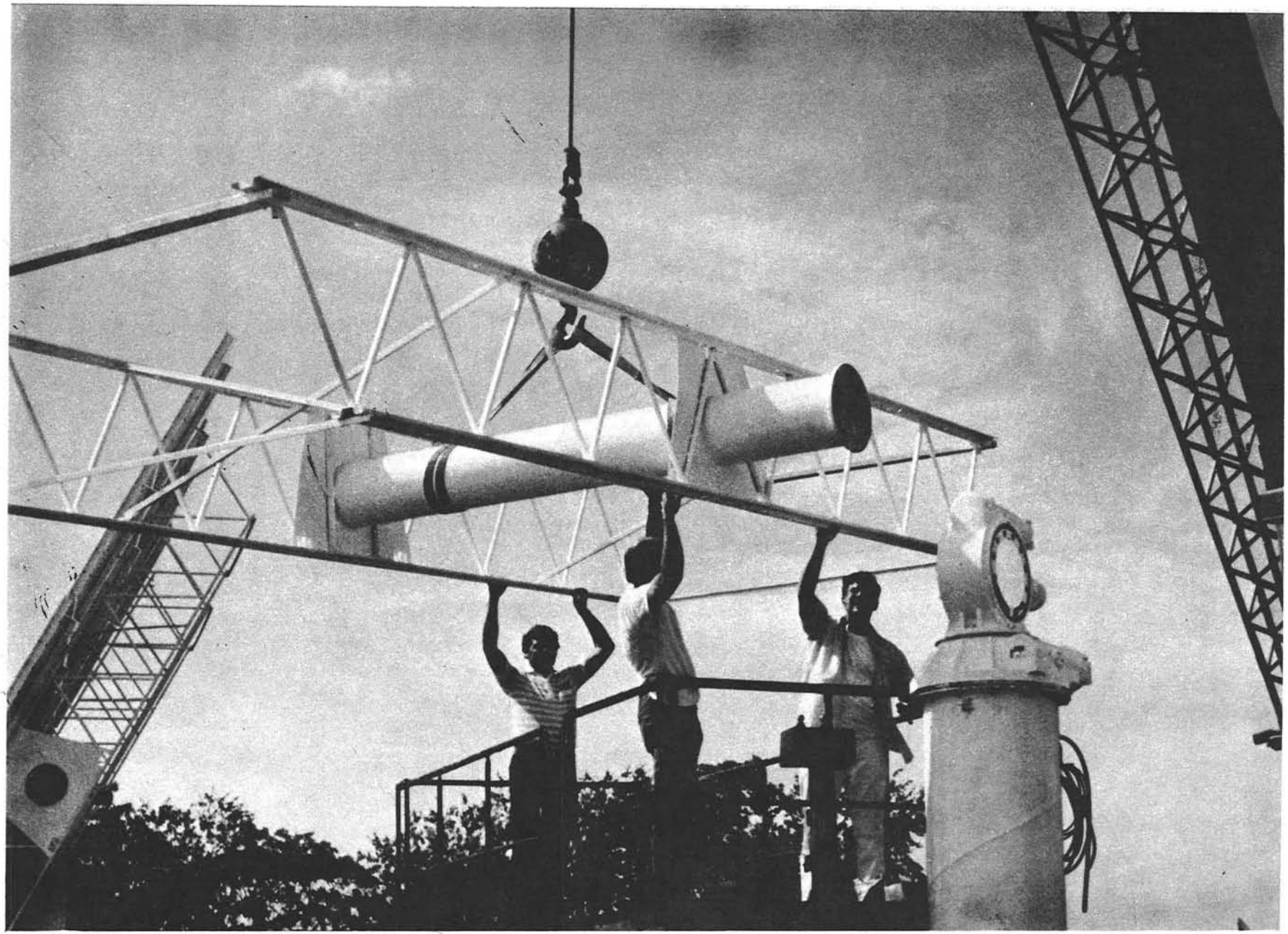

Figure 3-9 Torque Tube and Truss Assembly Being Mounted to Drive Unit

spacing than this, the torque tube bending becomes unnecessarily large due to the greater torque tube length.

The final elements of the rack structure are 12 cross-brace members, six of which are located between the left-side truss members, and six between the right-side truss members. The primary function of the cross-braces is to minimize differential torsion between the truss members, and to minimize torsion (twisting) of any individual truss. The cross-braces are installed during the field assembly by means of rivets.

After assembling the trusses, torque tubes, and cross brace members in the site assembly building, the mirror modules are next installed and pre-canted using mechanical means. The attachment method and canting adjustment is accomplished by three 3/8-24 UNF studs and nuts. Mirror module-to truss misalignment of the studs and holes is accomodated by the floating nut plates which permit $\pm$ 0.76 mm ($\pm$ 0.030 inch) lateral float. Stud angular misalignment introduced by module canting is accommodated by the use of spherically shaped nuts and washers (commercially available items). Figure 3-10 illustrates the mirror module attachments.

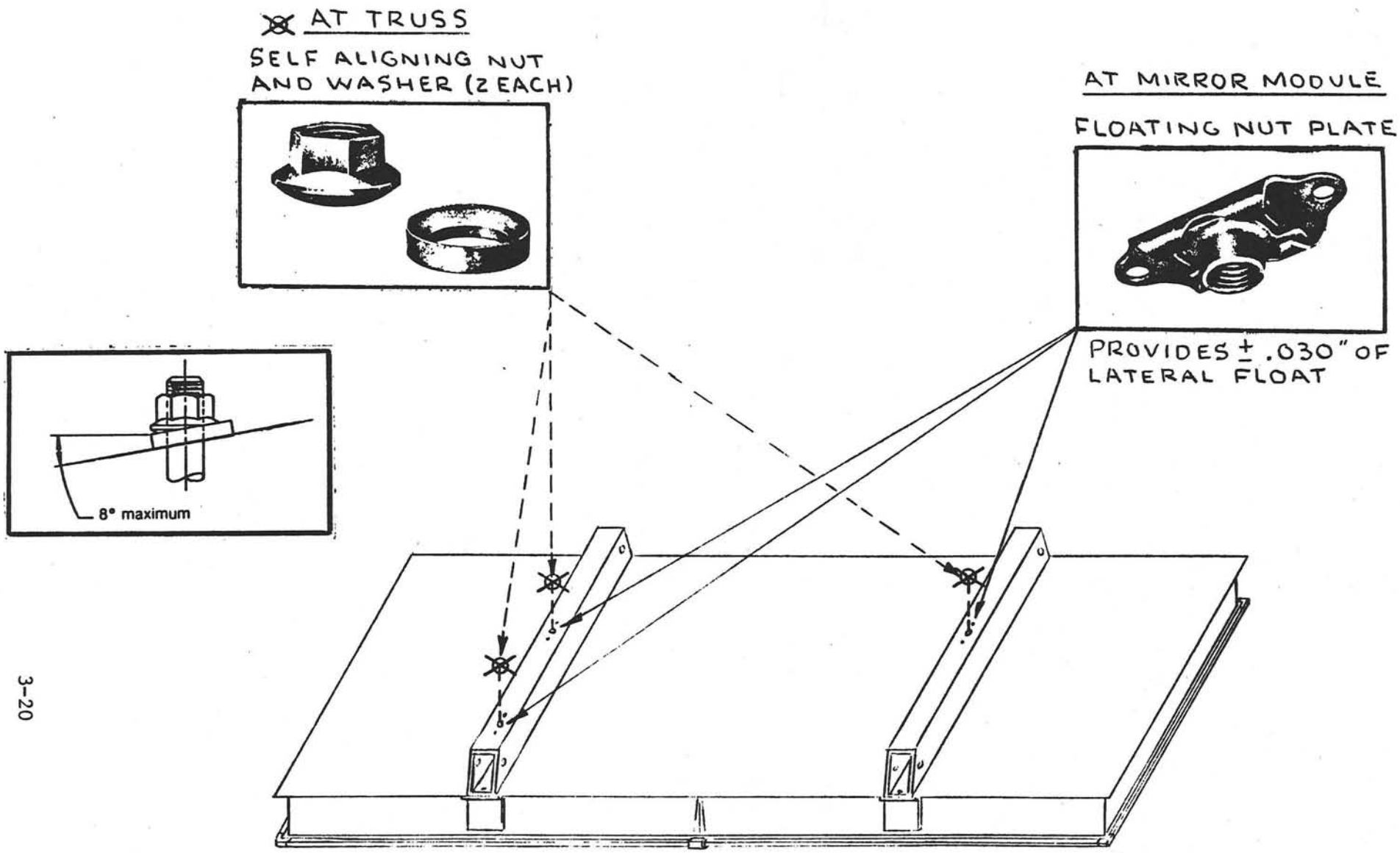

FIGURE 10 MIRROR MODULE ATTACHMENT METHOD

3.1.4 Drive Unit

The heliostat drive unit was designed and fabricated by the Winsmith Division of UMC Industries, Inc. of Springville N. Y. Separate azimuth and elevation drive systems are provided in cast iron housings. The azimuth and elevation motions are independent and are individually driven. Figure 3-11 shows a photograph of the drive unit being hoisted into position for assembly to the pedestal.

The motive input power for the azimuth and elevation drive section is a pair of permanent magnet D-C stepper motors manufactured by the Superior Electric Co, Bristol, Connecticut. The motors selected are Model M112-FJ327 units. Stepper motors offer precise incremental rotation in 1.8 angular degree step increments, variable speed (via the number of steps or pulse exitations per second), and high torque output. Although a stepper motor does not carry a horsepower rating per se (because it is a variable with stepping rate), the motor selected delivers 0.13 hp at a stepping rate of 500 steps/sec (150 rpm). Using position switches to "baseline" the heliostat starting position, any subsequent position can be determined by a simple pulse count. Therefore, position encoders are not required.

The azimuth and elevation drive gears are all identical to each other in terms of type, tooth form, and ratio. However, there are physical differences between the azimuth and elevation output gears since they have structural functions and interface requirements which are different. The first speed reduction stage is a planetary gear system, and the second stage (output stage) is a worm and gear type. The basic logic for selecting this drive concept is based on several key criteria:

1. The planetary type of drive stage provides a very high speed reduction ratio in a small package. Because this ratio is dictated by a function which is inversely proportional to a small difference in the number of teeth between two internal ring gears, both high ratios and a wide variety of ratios can be achieved with a small change in the number of teeth. Likewise, this wide range of ratios can be achieved in the same compact package.

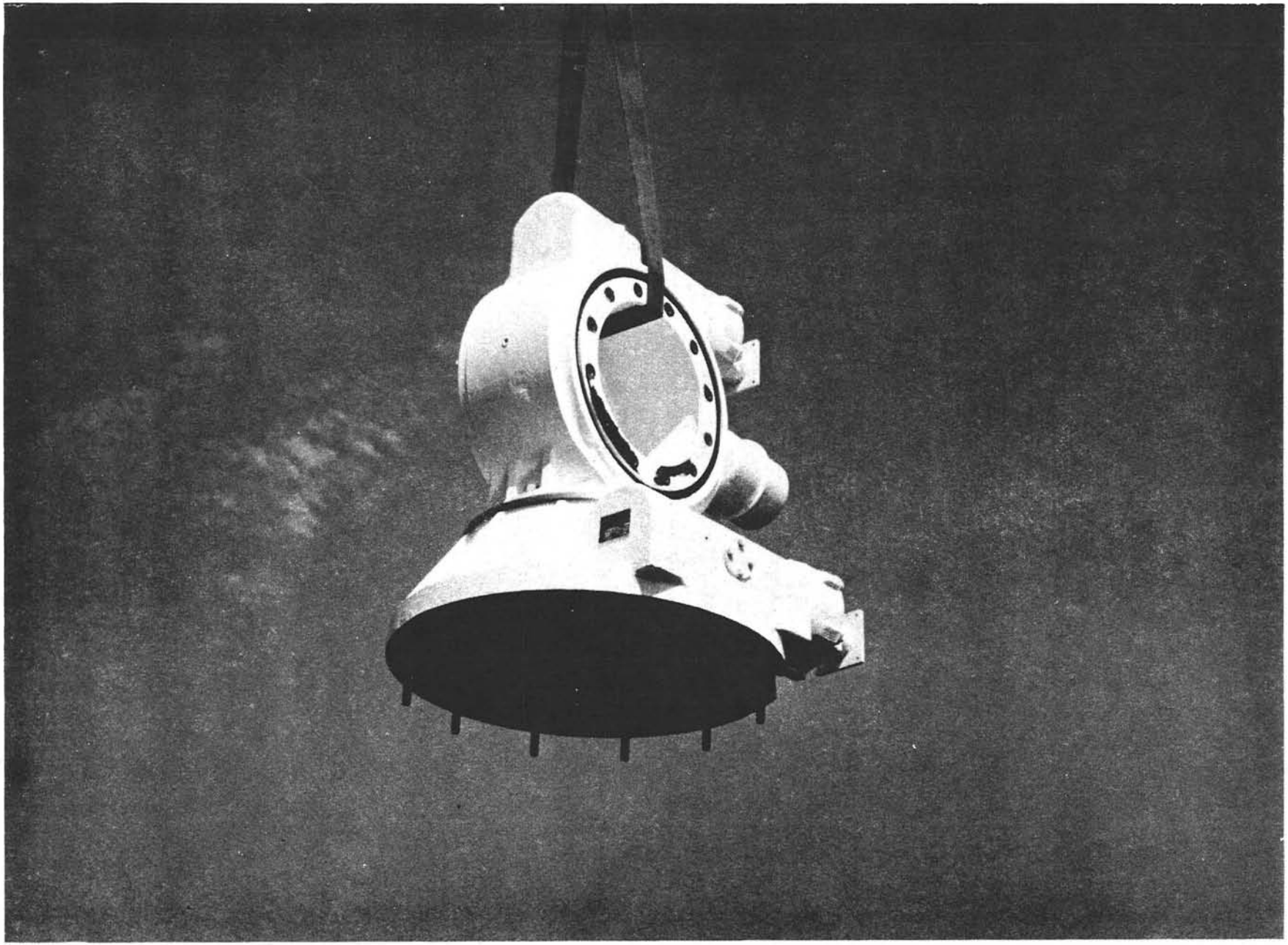

Figure 3-11 NORTHRUP DRIVE UNIT READY TO MOUNT ON PEDESTAL

2. The planetary type of drive stage with 2 load transmitting planet gears offers greater load carrying capacity than other gearing systems because more teeth are in action to distribute the total load. The Winsmith design is unique in that the planet gears are made integral with a planetary frame of ductile iron. This design acts to preserve tooth alignment because the frame and gears are not connected to the housing, and very little load is carried by the frame. The power is transmitted and most of the load is carried solely through the gears.

3. The element driven by the motor is a small sun gear (drive pinion) which has a likewise small inertia. Stepper motors "prefer" to drive small inertia loads, so the planetary drive is ideally suited to a stepper motor driver. Even though the downstream inertia increases as larger and larger gears are encountered, the motor "sees" these inertias reduced by the square of each ratio encountered. The small pinion gear and rapid ratio rise of the planetary system, therefore, is a desirable benefit to the stepper motor.

4. The output worm and gear also provides a high speed reduction ratio and high torque capacity, but with a considerably lower efficiency than the planetary stage due to high sliding friction forces. However, these frictional forces provide the main benefit of the worm/gear stage - - - - the unit is self-locking. Stated another way, the worm-thread can drive the gear, but the gear cannot back-drive the worm-thread. A worm and gear is considered non-back driving (locking) if the friction angle (which is equal to the arctan of the coefficient of friction) between the worm thread and tooth materials is greater than the lead angle. For a cast iron gear and steel worm, the static coefficient of friction will be 0.15 to 0.20, so the friction angle will be 8.5° to 11.3°. The Winsmith worm and gear is designed with a 7.7° lead angle, so the unit is self-locking.

The planetary stage has a speed reduction ratio of 460:1. Figure 3-12 shows a schematic representation of the planetary system and the speed reduction computation. It should be noted that the planet gears (denoted by P1 and P2) represent a set of two gears which revolve around the sun gear S1. The internal ring gear denoted R1 is stationary, and the ring gear R2 is the output stage.

The worm and gear output stage provides an additional 40:1 speed reduction. The worm has a 79.3 mm (3.121 inch) pitch diameter and 7.7 degree lead angle, and is fabricated from C1117 carbon steel, carburized and ground. The gear pitch diameter is 0.429 m (16.879 inches), the face width is 60.0 mm (2.362 inches), and is fabricated from SP-80 cast iron (nodular cast iron, 80 ksi yield strength, 100 ksi ultimate strength). The normal pressure angle for this gear set is 28^{o}, and the diametral pitch is 2.37 (teeth per inch of gear pitch diameter).

A single support bearing is used in each the azimuth and elevation portions of the drive. The bearing selected is a ball unit, Type "X", 4 point contact manufactured by the Keene Corp. (Kaydon Bearing Division, Muskegon, Mich.). The azimuth and elevation bearings are identical. The Kaydon part number is KG160XP0, and is 0.457 m (18.0 inch) OD x 0.406 m (16.0 inch) ID. Since these bearings are quite expensive, a Northrup-funded effort is currently underway to develop an integral bearing in which the races are machined into the castings. The ball bearings are then loaded into these races via a port which is subsequently sealed.

The drive unit is oil-filled and completely sealed to prevent moisture penetration and condensation. A diaphragm type of expansion chamber is included in the elevation portion of the drive to accomodate expansion and/or contraction of the elevation lubricant and case. The azimuth portion does not contain an expansion chamber, but does contain approximately 1100 in^3 of trapped air which serves to minimize the differential pressure between the inside and outside of the azimuth drive cavity. The drive unit case is a gray cast iron for production economy. Figure 3-13 provides a perspective view of the Northrup-Winsmith drive unit.

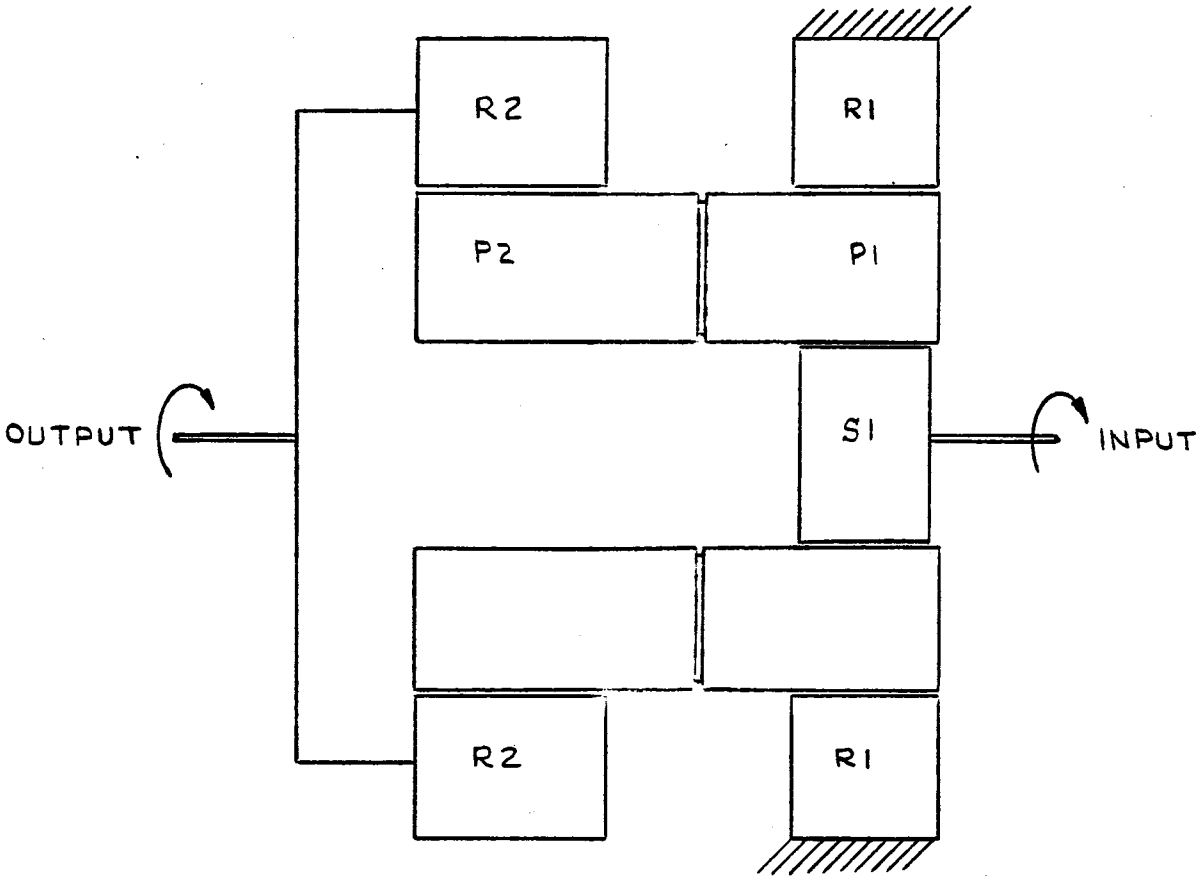

NUMBER OF TEETH

GEAR	NO.
S1	10
P1	40
R1	90
P2	40
R2	92

$$\text{RATIO} = \frac{1 + R1/S1}{1-\left(\frac{R1}{P1} \times \frac{P2}{R2}\right)} = \frac{1+90/10}{1-\left(\frac{90}{40} \times \frac{40}{92}\right)} = 460$$

Figure 3-12

Northrup Heliostat Drive Unit

Planetary Speed Reduction Stage

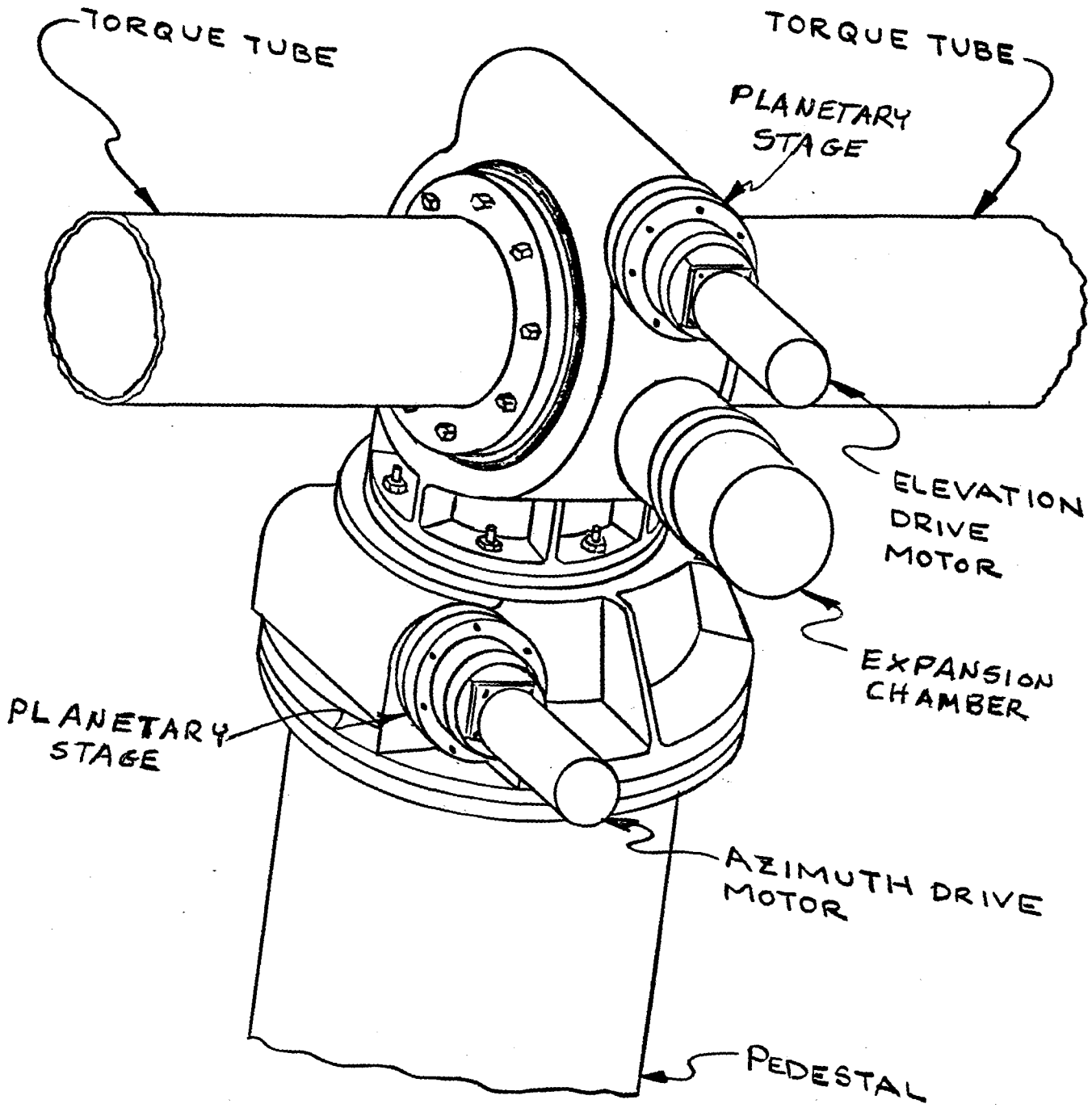

Figure 3-13

Perspective View of Northrup Drive Unit

3.1.5 Drive Motor and Controls Description

The heliostat controls consist of a control electronics unit, translators, and stepper motors.

The control electronics (CE) consist of a microprocessor controller that communicates with a central computer, receives serial data commands and outputs step sequences to a stepper motor translator. The CE also interfaces with limit or position switches to obtain reference positions and limit warnings. A manual control capability is provided to run the heliostat manually. The interface to the central controller is a differential current line driver/receiver pair. Data rate is software controllable from 300 to 9600 baud. A block diagram of the controls is shown in Figure 3-14. The processor is a 6502 that communicates to RAM, ROM, I/O, and a serial communications unit through an 8 bit data bus, 16 bit address bus and appropriate control lines. The firmware is contained in a 2048 by 8 bit EROM (part no. 2716).

The communications is accomplished with a 6850 Asynchronous Communications Interface Adapter (ACIA). This unit includes select, enable, read/write, interrupt and bus interface logic to allow data transfer over the bus. Serial data is transmitted and received by the asynchronous data interface and converted to parallel data that is handled by the processor. The functional configuration of the ACIA is programmed via the data bus during system initialization.

The 6532 chip provides the RAM, I/O, and timing. It is comprised of a 128 x 8 static RAM, two software controlled 8 bit bi-directional data ports, and a software programmable interval timer with interrupt, capable of timing in various intervals from 1 to 263,144 clock periods. One 8 bit data port interfaces with the translators (4 bits total), and limit switches (4 bits total). The other bit port is reserved for the heliostat address input. The timer gives the appropriate delays for acceleration, deceleration and stepping of the motors. A 555 timer provides about 20 ms power-up reset to the processor.

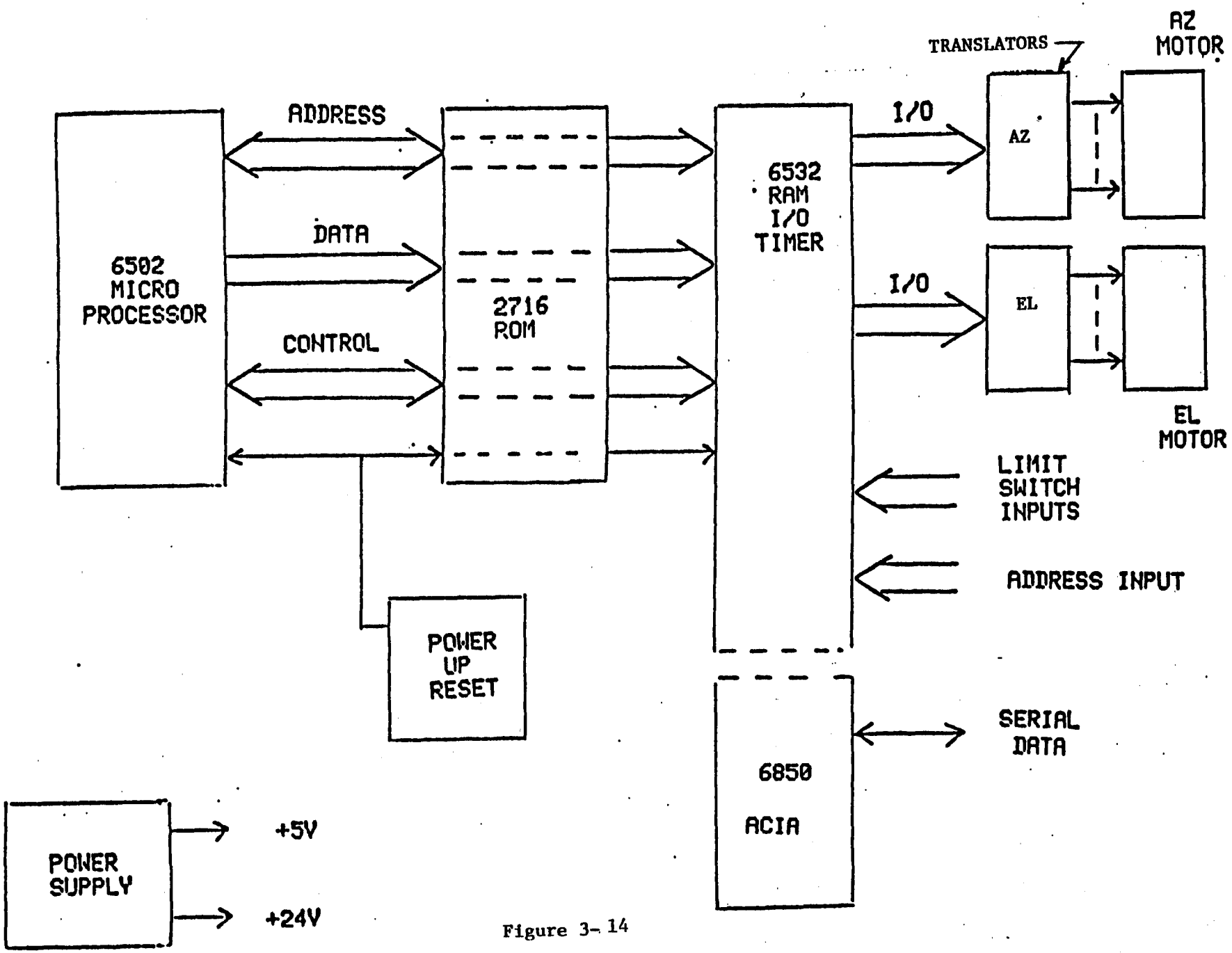

Figure 3-14

BREAD BOARD CONTROL ELECTRONICS

The translator used in the design is a Superior Electric TBM 105-1218. Two translators are required, one for azimuth and one for elevation. The translator receives either CW or CCW pulses from the microprocessor support chip (6532). The pulses are converted to four logic levels by the translator and supplied to the motor windings per the table below.

STEPPER MOTOR WINDING EXITATION

STEP	SWI	SW2	SW3	SW4
1	on	off	on	off
2	on	off	off	on
3	off	on	off	on
4	off	on	on	off

To reverse motor direction the windings are sequenced in reverse order, i.e., steps 4,3,2,1. The block diagram of the translator is shown in Figure 3-15.

The actual circuits in the translator consist of logic translation, power switches to apply current to the motor windings and a current source. The logic translation is accomplished by three or four chips consisting of a counter, gates, and ROM. The counter keeps track of the input pulses from the processor, the gates steer the counter output to the ROM, and the ROM converts the counter states to the logic shown in the above table. The power switching is accomplished by NPN silicon power transistors. The current source is the most complex part of the translator. It consists of a power switching inverter that converts a DC supply to stored energy in an inductor which is applied to the motor windings when a step signal is received from the logic.

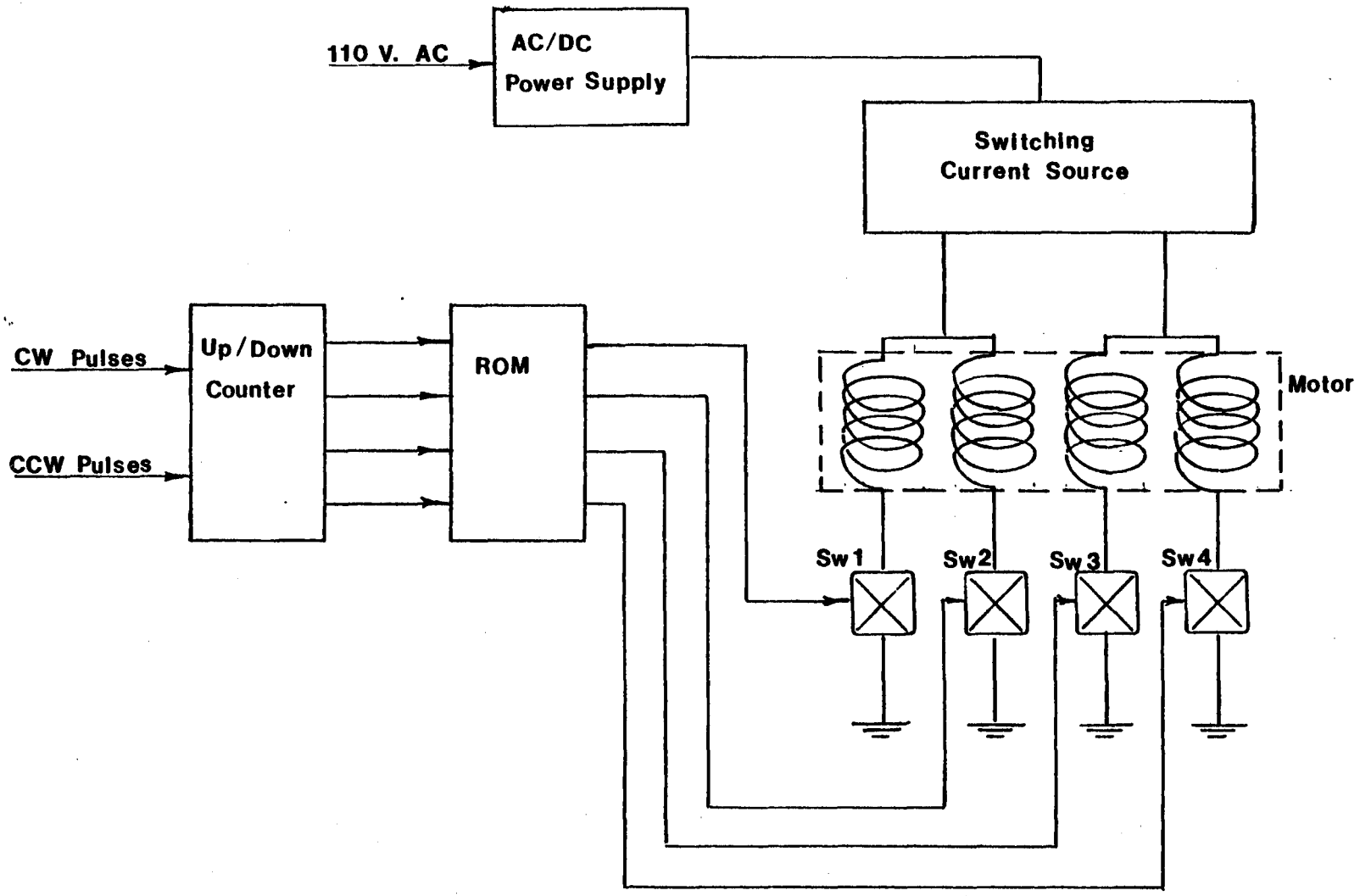

Figure 3- 15 Translator Block Diagram

3.1.6 Pedestal

Design of the combination foundation and support pedestal was performed under subcontract by Bechtel National Inc.

The heliostat support pedestal concept has evolved from poured concrete and steel to the current approach which uses a straight, pipe-like pile. The pedestal (pipe) unit is a welded steel hollow cylinder 0.61 m (24 inches) outside diameter having a wall thickness of 3.18 mm (0.125 inch). The total length (excluding the flange) is 6.52 m (21.37 ft) of which 3.47 m (11.37 ft) is above grade.

The steel pile is driven in place under suitable soil conditions. It is estimated that a 7-man crew can drive approximately 40 piles per day. An alternate installation method is to use an augered hole and to set the pile using a grout technique.

The pile can be driven with an angular plumbness of 1.1 angular degrees and a depth tolerance of $\pm$.05 m ($\pm$2 inches). To adjust for the out-of-plumb condition on the prototype heliostats a pair of tapered, gasket-like, shims were installed on top of the pile flange. These were rotated relative to each other to achieve a true-horizontal interface for the drive unit. For production units the out-of-plumb error will be removed using the computer software. The pile flange is factory-welded to the pipe and is 0.72 m (28.50 inches) in diameter x 12.7 mm (0.5 inch thick), and has a 12-hole pattern which accepts the 5/8-11 UNC studs which protrude from the drive unit bottom flange (the drive unit studs being pre-installed during the heliostat assembly in the field assembly building).

Figure 3-16 illustrates the Bechtel pedestal-pile concept for the prototype Northrup II heliostat.

Additional information relative to the pedestal and foundation design is found in Section 6.0. This section also includes results of trade studies which explored pedestal design alternatives, and which shows the cost differential between the driven-pile approach and the alternate auger-and-grout method.

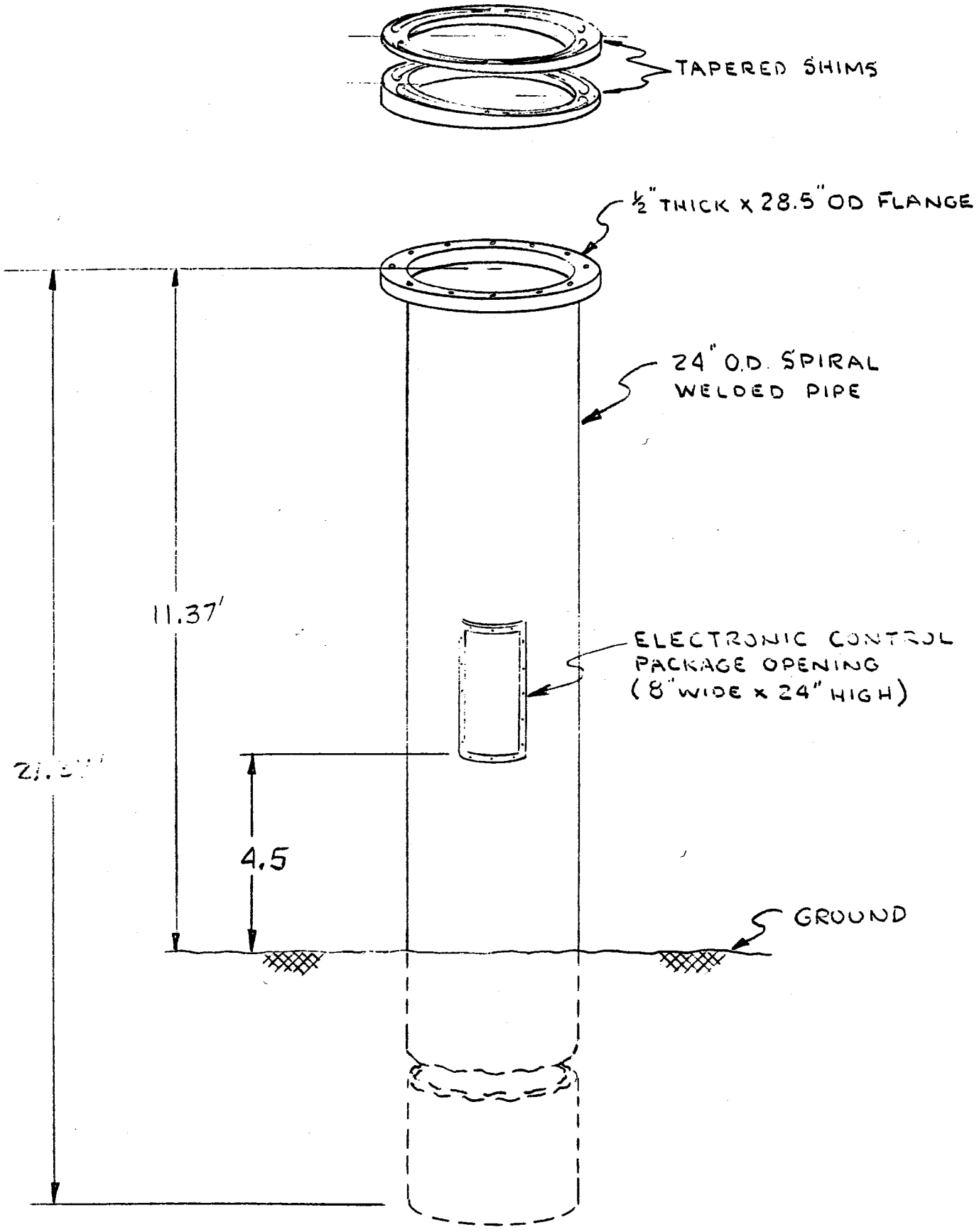

Figure 3-16 Bechtel Pile-Pedestal Concept for the Prototype Northrup Heliostat

3.2 PERFORMANCE

The following discussion presents the performance evaluation results for the Northrup heliostat. The performance evaluation includes weight, deflections, stress levels, and in the case of the drive unit, torque, speed, and efficiency performance.

3.2.1 Mirror Modules

The mirror modules for the Northrup heliostat are essentially an all-steel construction except for the reflecting mirrors. Steel, although somewhat heavier than other material alternatives results in the minimum cost for the Northrup design concept.

3.2.1.1 Weight

Table 3-2 provides a complete weight breakdown for the Northrup mirror module. Each module provides a net reflective area of 4.4 m^2 (47.33 ft^2), so the total weight of 90.5 kg (199.2 lb) may be normalized to a unit area weight of 20.6 kg/m^2 (4.21 lb/ft^2).

3.2.1.2 Thermal Curvature and Stress

Even though the silicone grease permits differential thermal expansion between the glass and the steel substrate, some thermal curvature does occur because the steel facing sheet adjacent to the mirror will be warmer than the backside substrate sheet. Actual measurements indicate this differential is on the order of 2.3°C (4.2°F). An analysis of the mirror module was performed in which the substrate was treated as a 3-layer composite consisting of a top sheet, web members, and bottom sheet. The computer simulation includes a thermal analysis in addition to the compression, tension, flexure, curvature, and stress effects.

Tables 3-3, 3-4, and 3-5 provide the results for windspeeds of 0, 8, and 12 m/s (0, 16, and 27 mph). The front-to-back temperature differential for the 8 m/sec case is very close to the actual measurement and wind condition (i.e.: 4.25°F theoretical vs 4.2°F actual). For all three cases, the radius of curvature was slightly convex, and varied from approximately 16 km (10 miles) to 20 km (12.6 miles). As will be noted later, these are generally negated by the concave gravity sag effects of the mirror modules.

TABLE 3-2

MIRROR MODULE WEIGHT

PIECE PART DESCRIPTION	SIZE OR QTY PER MODULE	WEIGHT, Kg (Lb)	
		MODULE	HELIOSTAT
Mirrors - Glass	2 each, .094 x 48 x 72"	26.9 (59.1)	322.4 (709.2)
Silicone Grease	14 ounces per module, .004" thk.	0.4 (0.8)	3.2 (7.1)
Face Sheet - Galvannealed	1 - .022 x 48 x 144.25"	19.8 (43.6)	237.6 (522.8)
Back Sheet - Galvannealed	1 - .022 x 48 x 144.25"	19.8 (43.6)	237.6 (522.8)
Horiz. " C" - Webs-Galvannealed	5 - .022 x 4 x 143.25"	8.1 (17.9)	98.2 (215.9)
Torque Box - Galvannealed	1 - .022 x 4 x 380.5"	4.4 (9.6)	52.1 (114.7)
Rectangular Members	2 - .120 x 2 x 1½ x 48"	9.7 (21.3)	116.1 (255.4)
Center Seal - EPDM	Extruded x 48"	0.05 (0.1)	0.5 (1.0)
Center Strip - Steel	3/4 x 50 x .022"	0.1 (0.2)	1.3 (2.8)
Edge Moulding - Steel	3/4 x 384 x .022"	0.8 (1.8)	9.9 (21.7)
Center Seal Adhesive	0.5 ounces per module	0.01 (0.03)	0.2 (0.4)
Edge Moulding Adhesive	6 ounces per module	0.2 (0.4)	2.0 (4.5)
Acrylic Adhesive	9 ounces per module	0.3 (0.6)	3.1 (6.8)
Rivets - Monel	14 - 1/8 D x 3/16 grip length	0.04 (0.1)	0.2 (0.5)
Nut Plates	4 - 3/8" D	0.04 (0.1)	0.4 (0.8)
TOTAL, kg (lb)		90.5 (199.2)	1084.7 (2386.4)
NET MIRROR AREA, m^2 (ft^2)		4.40 (47.3)	52.77 (568)
WEIGHT/AREA, kg/m^2 (lb/ft^2)		20.56 (4.21)	20.56 (4.21)

TABLE 3-3

0 M/S (0 MPH) WIND SPEED CASE

4' X 12' MIRROR MODULE THERMAL CURVATURE & STRESS

INPUT 48 OR 144 INCH DIMENSION, IN = 144

INPUT R1, CONVECTION RESISTANCE, DEG-F-SQ-FT-HR/BTU = 1

INPUT R5, CORE THERMAL RESISTANCE, DEG-F-SQ-FT-HR/BTU = 2

INPUT FACET PRE-DEFLECTION, INCHES = 0

INPUT GLASS SOLAR ABSORPTIVITY = .05

INPUT TAMB, DEG-F = 70

INPUT Q*COS(THETA), BTU/SQ-FT-HR = 300

OUTPUT

DEFLECTION CHANGE, INCHES=-4.08647139E-03

NET DEFLECTION, INCHES=-4.08647139E-03

FRONT SHEET TEMPERATURE = 76.7654888 DEG-F

BACK SHEET TEMPERATURE = 72.2550276 DEG-F

RADIUS OF CURVATURE =-52857.3384 FEET

STRESS SUMMARY & LOADS

SUBSTRATE LAYER #	TOPSIDE STRESS,PSI	BOTTOMSIDE STRESS,PSI	LOAD LB/IN
#1	-393	-394	-9
#2	-17	33	8
#3	0	0	0

NOTE: +VALUES INDICATE TENSION
-VALUES INDICATE COMPRESSION

TABLE 3-4

8 M/S (15 MPH) WIND SPEED CASE

4' X 12' MIRROR MODULE THERMAL CURVATURE & STRESS

INPUT 48 OR 144 INCH DIMENSION, IN = 144

INPUT R1, CONVECTION RESISTANCE, DEG-F-SQ-FT-HR/BTU = .6

INPUT R5, CORE THERMAL RESISTANCE, DEG-F-SQ-FT-HR/BTU = 2

INPUT FACET PRE-DEFLECTION, INCHES = 0

INPUT GLASS SOLAR ABSORPTIVITY = .05

INPUT TAMB, DEG-F = 70

INPUT Q*COS(THETA), BTU/SQ-FT-HR = 300

OUTPUT

DEFLECTION CHANGE, INCHES=-3.56678007E-03

NET DEFLECTION, INCHES=-3.56678007E-03

FRONT SHEET TEMPERATURE = 75.1177503 DEG-F

BACK SHEET TEMPERATURE = 71.1809013 DEG-F

RADIUS OF CURVATURE =-60558.8223 FEET

STRESS SUMMARY & LOADS

SUBSTRATE LAYER #	TOPSIDE STRESS,PSI	BOTTOMSIDE STRESS,PSI	LOAD LB/IN
#1	-343	-344	-8
#2	-15	28	7
#3	0	0	0

NOTE: +VALUES INDICATE TENSION
-VALUES INDICATE COMPRESSION

TABLE 3-5

12 M/S (27 MPH) WIND SPEED CASE

4′ X 12′ MIRROR MODULE THERMAL CURVATURE & STRESS

INPUT 48 OR 144 INCH DIMENSION, IN = 144

INPUT R1, CONVECTION RESISTANCE, DEG-F-SQ-FT-HR/BTU = .48

INPUT R5, CORE THERMAL RESISTANCE, DEG-F-SQ-FT-HR/BTU = 2

INPUT FACET PRE-DEFLECTION, INCHES = 0

INPUT GLASS SOLAR ABSORPTIVITY = .05

INPUT TAMB, DEG-F = 70

INPUT Q*COS(THETA), BTU/SQ-FT-HR = 300

OUTPUT

DEFLECTION CHANGE, INCHES=-3.25742474E-03

NET DEFLECTION, INCHES=-3.25742474E-03

FRONT SHEET TEMPERATURE = 74.4581588 DEG-F

BACK SHEET TEMPERATURE = 70.8627616 DEG-F

RADIUS OF CURVATURE =-66310.051 FEET

STRESS SUMMARY & LOADS

SUBSTRATE LAYER #	TOPSIDE STRESS,PSI	BOTTOMSIDE STRESS,PSI	LOAD LB/IN
#1	-313	-314	-7
#2	-14	26	6
#3	0	0	0

NOTE: +VALUES INDICATE TENSION
-VALUES INDICATE COMPRESSION

These tables also show that the sheet and web stress levels are very low.

It will be noted that the thermal curvature was only determined for the 3.66 m (12.0 ft) mirror module direction. In the transverse 1.22 m (4.0 ft) direction, there is no curvature effect because the stiffener for this direction is located externally on the backside and has no temperature gradient. Stated another way, the temperature difference between the mirror facing sheet and the backside sheet does not cause curvature because these sheets are connected only intermittently by the crossing stringers, and free differential thermal expansion or contraction of one of the sheets can occur without influencing the other sheet.

Appendix section 9.5.3 presents a derivation of the equations used in this analysis.

As a part of the Northrup test program, a mirror module was thermal cycled between -9C (15^{o}F) and +49C (120^{o}F) a total of 10 times, and water sprayed at each extreme. A "zebra-board" (a flat panel with a grid matrix) was used to visually observe the mirror surface for any temperature induced distortions or curvatures. Although the front-to-back temperature differentials caused by solar heating were not simulated, the fact that no distortion or curvatures were noted confirms the basic free-floating mirror concept using the silicone grease attachment method.

The details of the thermal cycling test are provided in Appendix G, paragraph 9.7.2.1.2.

3.2.1.3 Deflections - Gravity and Wind

The mirror module deflections and resultant milliradian errors were determined for both the gravity-only case, and for the case where gravity plus an additive 12 m/s (27 mph) wind are acting on a mirror module. The effects analyzed included bending and shear in both the longitudinal 3.66 m (12.0 ft) and transverse 1.22 m (4.0 ft) direction, and the effect of the 3-point attachment on the bending. It should be noted that the stiffness in the longitudinal direction is derived from the module internal "C"-stringers, whereas, the transverse stiffness is derived from the external rectangular structural tubing members. The computer analysis shows that shear deflection effects are negligible, longitudinal bending effects are small, and the transverse bending and attachment effects are dominant.

The computer model divides the module into 168 "mini-facets" and determines the vector error for each. The total or resultant error is then calculated as the RMS of these 168 elements. Table 3-6 tabulates the RMS values versus elevation angle for the no-wind and 12 m/s (27 mph) wind speed cases.

The worst gravity-only RMS error occurs when the heliostat is horizontal and is 0.359 mrad. The worst gravity plus wind error occurs when the heliostat is 30° from horizontal and is 0.441 mrad. If it is assumed that a field of heliostats has a uniform distribution of elevation angles from 0° to 90°, the field-average RMS error is 0.25 mrad for gravity-only, and 0.35 mrad for gravity plus wind.

Appendix paragraph 9.5.2.1 presents a derivation of the equations used in this analysis and several sample computer print-outs.

Another deflection parameter of interest for the mirror module is the local gravity sag which occurs between the longitudinal "C"-webs. These stringers are spaced 0.20m (8 inches) apart, and will sag under the influence of gravity and face-on winds. Backside winds probably do not cause any effect because the module backside sheet and vented interior serve as a deflection buffer.

Table 3-7 presents the between-stringer sag for gravity-only, and

TABLE 3-6

MIRROR MODULE DEFLECTIONS

GRAVITY AND WIND INDUCED MRAD ERRORS

Heliostat Elevation Angles	No - Wind Gravity Only		Gravity Plus 12 m/s Wind	
	Load	RMS Error	Load	RMS Error
0^{o} (vertical)	0 lb/ft^2	0 mrad	1.591 lb/ft^2	.136 mrad
10	.731	.062	2.322	.198
20	1.440	.123	3.042	.260
30	2.105	.179	3.719	.318
40	2.706	.231	4.332	.370
50	3.225	.275	4.847	.414
60	3.646	.311	5.164	.441 ← max
70	3.956	.337	5.155	.440
80	4.146	.353	4.675	.399
90 (horiz)	4.21	.359 ← max	4.21	.360
Field Average		.25 mrad RMS		.35 mrad RMS

TABLE 3-7

GRAVITY AND FACE WIND SAG BETWEEN STRINGERS

ANGLE	GRAVITY LOAD	GRAVITY INDUCED IMPERFECTIONS, MRAD, RMS	27 MPH WIND + GRAVITY	GRAVITY PLUS WIND INDUCED IMPERFECTIONS, MRAD, RMS
0 (vert)	0 lbs/ft^2	0 mrad	1.591 lbs/ft^2	.041 mrad
10	.371	.010	1.962	.051
20	.731	.019	2.333	.060
30	1.068	.028	2.682	.069
40	1.373	.035	2.999	.077
50	1.636	.042	3.258	.084
60	1.850	.048	3.368	.087 ← max
70	2.007	.052	3.206	.083
80	2.104	.054	2.633	.068
90 (horiz)	2.136	.055 ← max	2.136	.055
Field Average		.039 mrad RMS		.069 mrad RMS

gravity plus a 12 m/s (27 mph) versus heliostat elevation angle. The worst gravity-only RMS error due to between-stringer sag occurs when the heliostat is horizontal and is 0.055 mrad. The worst gravity plus wind error occurs when the heliostat is 30^{o} from horizontal and is 0.087 mrad. If it is assumed that a field of heliostats has a uniform distribution of elevation angles from 0^{o} to 90^{o}, the field-average RMS error for between-stringer sag is 0.039 mrad due to gravity-only, and 0.069 mrad for gravity plus a face-on 12 m/s (27 mph) wind.

Appendix section 9.5.2.1 (page E-10) presents a derivation of the equations used in this analysis plus a sample calculation.

Ideally, the module deflections and slopes, and the between stringer sag effects should be analyzed together as an integrated problem with the milliradian angles vectorially added. However, for computational simplicity two separate analyses were performed, and the results algebraically added together. Table 3-8 presents the resultant combined effects. The worst gravity-only combined error occurs when the heliostat is horizontal and is 0.414 mrad. The worst gravity plus wind error occurs when the heliostat is 30^{o} from horizontal and is 0.528 mrad.

A laser ray trace test of two mirror modules was performed on two mirror modules by Sandia-Albuquerque, and a mirror-only imperfection test was performed by Northrup-Hutchins (see Appendix E, para. 9.7.2.1.4). An interesting comparison can be made between these test data and the analytical results for the gravity-only case described above. The analytical RMS error for a horizontal mirror module was determined to be 0.414 mrad. This value does not include any provision for mirror glass imperfections. However, the Northrup glass imperfection measurements indicate an RMS error of 0.771 mrad in the 144-inch mirror dimension, and 0.706 mrad in the 48-inch mirror dimension. If these two values are combined by the RMS method to give a random direction average, the RMS-average glass imperfection error would be 0.739 mrad. Treating the analytical bending deflection/gravity sag effects and this glass imperfection value as arithmetically combineable effects, the total error is 1.153 mrad. The laser ray trace data showed an RMS error of 0.863 mrad in the 144 inch direction, and 1.233 mrad in the 48 inch direction. If these values are combined by the RMS method to give a random-direction average, the laser ray RMS error would be 1.064 mrad which compares well with the analytical prediction of module bending and sag with a glass imperfection adjustment.

TABLE 3-8

MODULE BENDING AND MIRROR SAG COMBINED EFFECTS

GRAVITY AND WIND INDUCED RMS ERRORS

Heliostat Elevation Angle	No - Wind Gravity Only		Gravity Plus 12 m/s Wind	
	Load	RMS Error	Load	RMS Error
0 (Vert)	0 lb/ft^2	0 mrad	1.591 lb/ft^2	.177 mrad
10	.731	.072	2.332	.249
20	1.440	.142	3.042	.320
30	2.105	.207	3.719	.387
40	2.706	.266	4.332	.447
50	3.225	.317	4.847	.498
60	3.646	.359	5.164	.528 ← max
70	3.956	.389	5.155	.523
80	4.146	.407	4.675	.467
90	4.21	.414 ← max	4.21	.415
Field Average		.293 mrad		.417 mrad

3.2.1.4 Stress - 40 m/s (90 mph) Wind

A stress analysis of the mirror module and its attachments was performed for the 40 m/s (90 mph) wind case. Although the heliostat would normally be stowed face-up horizontal in a high wind to minimize sand erosion of the mirror, the Northrup heliostat is designed to be stowed in any position from vertical to face-up horizontal. Therefore, the stress analysis was performed for loads encompassing all stow position possibilities

For conservatism, a drag coefficient of 2.38 was used in the mirror module stress analysis. This corresponds to the local peak load at the heliostat center of 1.79 kPa (37.4 lb/ft^2) for a 40 m/s (90 mph) wind speed, corrected to the heliostat-center height of 3.87 m (12.7 ft).

The results of the stress analysis are summarized on Table 3-9, and detailed in Appendix section 9.5.4.

A detailed analysis of the localized stresses at the attachments was performed. It was found that the adhesive tensile and peeling stresses were the primary area of concern for the 40 m/s (90 mph) wind loads; the adhesive in question being the Versilok-201 which is used to bond the stringers to the face sheets and the attachment members to the backside of the mirror module. With either a "C"-channel or a "Z"-member being used as the backside attachment member, the off-set of the nut-plate and the bond footprint centerline from the shear center of the member resulted in a high moment and high local stress in the adhesive. The resolution of the problem was achieved by changing to an enclosed rectangular box-section member.

The important conclusion is that the mirror modules can withstand a 40 m/s (90 mph) wind in any orientation. The design was analytically confirmed for the peak local pressure which occurs in the heliostat center with a vertical stow. The actual practice, the heliostat would be stowed in a horizontal position if a high wind were forecast.

A mirror module survival load test was performed to confirm these analytical findings. A detailed discussion of these tests is provided

TABLE 3-9

MIRROR MODULE STRENGTH SUMMARY

40 m/s (90 mph) WIND

0^{o} Elevation - Facing Wind

STRUCTURAL ITEM	CRITICAL FAILURE MODE	LOAD OR STRESS	ALLOWABLE LOAD OR STRESS	MARGIN OF SAFETY
STRINGER/FACE SHEETS (BENDING)	YIELD	33.4 mPa (4850 psi)	248.2 mPa (36000 psi)	LARGE
(SHEAR)	BUCKLING	10.5 mPa (1530 psi)	67.4 mPa (9770 psi)	LARGE
LOCAL STRINGER CLIPS	BENDING	137.6 mPa (19,950 psi)	248.2 mPa (26000 psi)	+.80
CROSS MEMBER (BEAM BENDING)	BENDING	86.2 mPa (12500 psi)	248.2 mPa (36000 psi)	LARGE
(LOCAL ATTACHMENT AT NUT PLATE)	BENDING	408 kg (897.6 lb)	545 kg (1200 lb)	+.34
ADHESIVE - CROSS MEMBER TO STRINGER	BOND TENSION	340 kg (748 lb)	455 kg (1000 lb)	+.34
GLASS MIRROR (HORIZONTAL STOW)	BENDING	4.5 mPa* (660 psi)	6.9 mPa (1000 psi)	+.52

*For infrequent overload conditions of a vertically stowed heliostat and a 40 meter/second (90 mph) wind, the stress would be 9.4 mPa (1360 psi) maximum.

in Appendix G, paragraph 9.7.2.1.3. The mirror module was attached to a support structure by the 3-support studs in a face-down position. One half of the module was loaded with wet sand on the backside to a unit load of 1.79 kPa (37.4 lb/ft^2) to simulate a 40 m/s (90 mph) wind load with the heliostat in a vertical stow position. Dial indicator readings were taken at 7 key locations to determine if any adhesive bond failures occurred. The module successfully passed the test with no incident or anomalies. The load was increased to 3.0 kPa (62.3 lb/ft^2) in an attempt to cause failure, and was repeated on the other one half of the mirror module, again without any problem. The conclusion is that the mirror module strength is adequate for windspeeds considerably in excess of 40 m/s (90 mph) in either a vertical or horizontal stow position.

One additional stress topic which deserves discussion at this point is hail resistance. Extensive mirror module hail tests have been performed through-out the contract period to verify the adequacy of the mirror-silicone grease-steel substrate to resist breakage. Some initial tests were performed with "specification" ice balls of 0.75 inch diameter at speeds of 65 ft/sec. However, breakage was virtually non-existent, so subsequent tests were all performed with "margin" ice balls of 1.0 inch diameter.

A pneumatically-powered hail gun was constructed at the Northrup-Hutchins facility. Photoelectric sensors were employed to measure the time interval over a fixed, known distance which enabled the velocity to be computed. Various velocities were achieved by adjusting the chamber pressure which propelled the hail balls. The firing of an ice ball was accomplished by an electrical switch which in turn would trigger a solenoid valve to release the high pressure air into the barrel. Spherical ice balls of 1.0 inch diameter were made in a 2-piece aluminum mold which was fabricated specifically for this purpose. To insure adequate hardness, the ice balls were frozen and chilled to $20^{\circ}F$ maximum.

For ice balls fired into the mirror interior area (away from the edges), velocities as high as 140 ft/sec could be tolerated without breakage. Edge hits would generally pass velocities up to 100 ft/sec. Infrequent breaks would occur at or near the edges at velocities near 75 ft/sec. It is believed that these were generally caused by an existing edge defect such as a

minute crack or chip, or a backing sheet imperfection, and an impact in the near vicinity would cause the defect to propagate from the defect to the impact zone. Generally, breakage was very infrequent even with the "margin" ice balls of 1.0 inch diameter, and velocities well above 75 ft/sec. Hence, the mirror module design is felt to be very adequate from the hail impact standpoint.

3.2.2 Rack Structure

The rack structure for the Northrup heliostat is an all-steel unit based on employing standard Butler Mfg. Co. truss purlins, standard pipe torque tubes, and angle iron cross braces. All of the major elements of the rack structure are commercially available items, and are currently being produced in large scale quantities using mass-production facilities and techniques.

3.2.2.1 Weight

Table 3-10 provides a complete weight breakdown for the Northrup rack structure. Since the net reflective area of the heliostat is 52.8 m^2 (568 ft^2), the total weight of 621.9 kg (1368.2 lb) corresponds to a rack structure weight per unit area of mirror of 11.79 kg/m^2 (2.41 lb/ft^2).

3.2.2.2 Deflections - Gravity and 12 m/s (27 mph) Wind

A computer code named "WINDBEND" was developed to evaluate the effect of gravity and wind loads on mirror module pointing errors. Figure 3-17 pictorially illustrates the analysis method used in the "WINDBEND" program. Figures 3-18 and 3-19 provide sample input and output tabulations. Some of the key points associated with the "WINDBEND" illustration shown in Figure 3-17 are:

a. The gravity load on the torque tube may be resolved into two component forces. The component which is normal to the mirror plane is the only component which causes any pointing error; the parallel component causes planar rotation, but no error.

b. The wind and gravity-induced torsions of the torque tube are always additive regardless of whether the wind is impacting the heliostat from the front or backside.

c. Torque tube torsionally-induced errors, truss gravity bending errors, and truss wind bending errors are in the same plane, and are arithmetically combined. However, depending on whether the wind is approaching from the front or back, and depending on whether the mirror modules are located on the upper or lower-half of the heliostat, some of these effects are additive, but some are also subtractive.

TABLE 3-10

RACK STRUCTURE WEIGHT

PIECE PART DESCRIPTION	SIZE OR QTY PER HELIOSTAT	WEIGHT, kg (lb)	
		UNIT	HELIOSTAT
Truss - Top Chord	4 - .078 x 8 x 252"	20.2 (44.5)	80.9 (178.0)
Truss - Bottom Chord	4 - .078 x 8 x 210"	16.9 (37.1)	67.4 (148.3)
Truss - Web Tubing	4 - .078 x 1.0 OD x 500"	14.5 (32.0)	58.2 (128.0)
Torque Tube Pipe	2 - 12.75 OD x .25 Wall x 111.5" L	141.0 (310.2)	282.0 (620.3)
Torque Tube Flange	2 - 15.75 OD x .69 average thk.	17.5 (38.4)	35.0 (76.9)
Torque - Truss Plate	4 - .090 x 27 x 38 x 24"	7.7 (17.0)	30.9 (68.0)
Cross - Brace Diagonal	8 - 1 x 1 x ¼ x 90"	5.1 (11.2)	40.6 (89.4)
Cross - Brace Lateral	4 - 1 x 1 x ¼ x 86"	4.9 (10.7)	19.4 (42.7)
Rivets - Monel	32 - ¼D x 3/8" grip length	0.0 (0.0)	0.1 (0.2)
Rivets - Monel	4 - ¼D x 5/8" grip length	0.0 (0.0)	0.0 (0.0)
Bolts - Drive Attachment	24 - 5/8 - 11 UNC x 1.75" L	0.1 (0.2)	2.1 (4.7)
Studs - Module Attachment	36 - 3/8 - 24 UNF x 6" L	0.1 (0.2)	3.1 (6.8)
Nuts - Module Attachment	108 - 3/8 - 24 UNF	0.0 (0.0)	1.1 (2.4)
Washers-Module Attachment	72 - 3/8 - Spherical Well	0.0 (0.0)	1.1 (2.5)
TOTAL, kg (lb)			621.9 (1368.2)
NET MIRROR AREA, m^2 (ft^2)			52.77 (568)
WEIGHT/AREA, kg/m^2 (lb/ft^2)			11.79 (2.41)

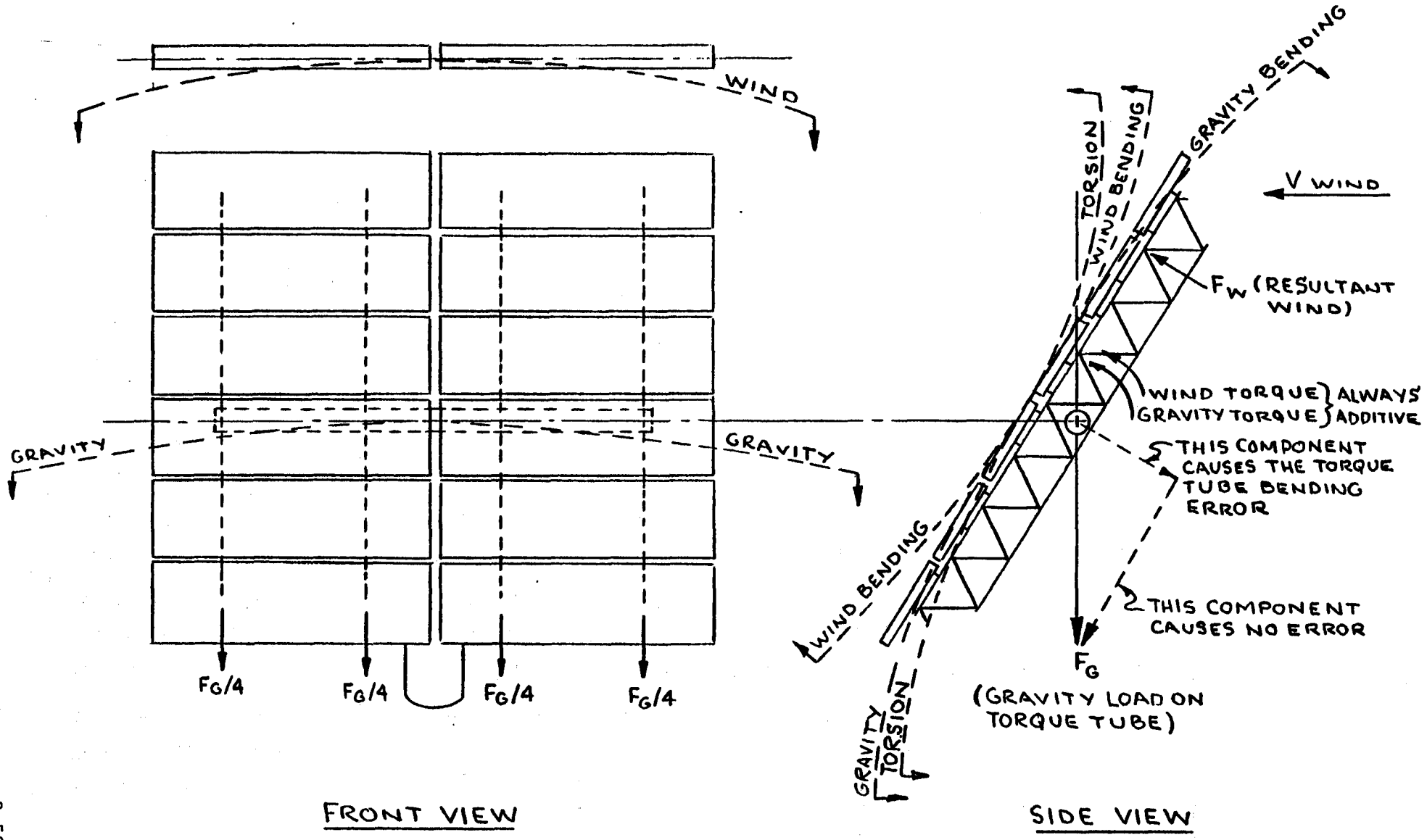

Figure 3-17

"WINDBEND" ANALYSIS METHOD

Figure 3-18

WIND & GRAVITY MRAD ERROR ANALYSIS

INPUT WIND SPEED AT 30', MPH = 27

INPUT MIRROR MODULE WEIGHT, EACH, LB = 199.2

INPUT BEAM INERTIA, IN↑4 = 249

INPUT BEAM WEIGHT, LB/FT = 6.65

INPUT TORQUE TUBE LENGTH, INCHES = 110.38

INPUT TORQUE TUBE O.D., INCHES = 12.75

INPUT TORQUE TUBE WALL THICKNESS, INCHES = .25

TORQUE TUBE I.D., INCHES = 12.25

TORQUE TUBE BENDING INERTIA, INCHES↑4 = 191.82

TORQUE TUBE + FLANGE EQUIV BENDING INERTIA, INCHES↑4 = 168.43

TORQUE TUBE POLAR INERTIA, INCHES↑4 = 383.64

TORQUE TUBE WEIGHT LB/FT = 33.34

Figure 3-19

WIND ANGLE, = 40 DEG, WIND SPEED = 27 MPH

(1).BEAM BENDING EFFECT (GRAVITY & WIND):

MODULE	DEF1,IN*10↑4	DEF2,IN*10↑4	MRAD ERROR
#1	150	116	.172
#2	101	69	.161
#3	29	9	.098
#4	23	8	.079
#5	81	55	.129
#6	121	93	.138
HELIOSTAT-AVERAGE MRAD ERROR:			.129

(2).TORQUE TUBE - WIND AND GRAVITY TORSIONAL LOADING

TORSION FROM	END TORSION	MID TORSION	EFF MRAD TORSION
WIND	.148	.057	.057
GRAVITY	.383	.148	.148
ARITHMETIC-SUM MRAD TORSIONAL ERROR:			.205

(3).TORQUE TUBE + FLANGE - WIND AND GRAVITY LOAD BENDING:

TORQUE TUBE	DEF1,IN*10↑4	DEF2,IN*10↑4	MRAD BEND
WIND	233	20	.254
GRAVITY	803	70	.873
VECTOR-SUM MRAD BENDING ERROR:			.815

(4).VECTOR-COMBINED BEAM & TORQUE TUBE BENDING & TORSION EFFECTS:

MIRROR MODULE	BEAM DEFLECTION MRAD ERROR	TORQUE TUBE TORSIONAL MRAD ERROR	TORQUE TUBE BENDING MRAD ERROR	VECTOR-SUM MRAD ERROR
#1	.172	.205	.815	.897
#2	.161	.205	.815	.893
#3	.098	.205	.815	.869
#4	.079	.205	.815	.824
#5	.129	.205	.815	.818
#6	.138	.205	.815	.817
TOTAL HELIOSTAT RMS MRAD ERROR:				.853

d. Gravity-induced torque tube bending; wind-induced torque-tube bending; and the arithmetically summed torsion and truss bending are, generally, error effects which occur in different planes, and must, therefore, be vectorially combined to derive the total effect. An added-complication is that some of the error sources affect the pointing error, and some affect the beam quality. Also, some of the errors can be partially compensated by software computation (such as gravity-induced torsion versus elevation angle), and some can be partially compensated by "smart-canting" (such as gravity-induced bending of the trusses and torque tube).

The "WINDBEND" model was used to evaluate all of the bending and torsion effects for heliostat elevation angles from 0^{o} to 90^{o} for the gravity-only case, and the gravity plus 12 m/s (27 mph) wind case without any compensatory software or "smart-canting" included. The results of this analysis are tabulated in Table 3-11. Appendix 9.5.2.2 (pages E-42 through E-65) also provides a complete set of the "WINDBEND" computer tabulations for all of the cases analyzed. These non-compensated results show relatively large maximum RMS errors (1.766 mrad and 2.074 mrad error in the reflected beam for the gravity-only and gravity plus wind cases respectively).

These errors can be easily reduced without any hardware change by the software and canting operations as follows:

1. The gravity-induced torsion of the torque tube which varies with elevation angle can be removed from the error picture by including its effect in the software elevation vector computation.

2. The gravity-sag of the torque tube and the torque tube flange bending, the effect of which varies with elevation angle, can be partially removed from the error picture by biasing the mirror module canting such that the one-half of the maximum sag error is removed. This would be accomplished by a sag-adjusted canting fixture in the site assembly building. The remaining error (0.873 mrad maximum, and 0.626 mrad RMS field average) manifests itself as a beam quality (fringe) error only, and does not affect the pointing error.

TABLE 3-11

RACK STRUCTURE INDUCED REFLECTED BEAM ERRORS

WITH NO COMPENSATING SOFTWARE OR CANTING

WIND ANGLE OF ATTACK	GRAVITY ONLY RMS POINTING ERROR	GRAVITY PLUS 12 M/S (27 MPH) WIND RMS POINTING ERROR
0° (vert.)	0.386	0.632 mrad
10	0.486	0.920
20	0.702	1.202
30	0.942	1.468
40	1.172	1.706
50	1.376	1.910
60	1.542	2.046
70	1.664	2.074 ← max
80	1.740	1.922
90 (horz.)	1.766 ← max	1.766
RMS Field Average	1.278 mrad	1.634 mrad

3. The gravity-sag of the truss also varies with elevation angle, and can be partially compensated for by biasing the mirror module canting so one-half of the maximum error is removed. The remaining error (0.135 mrad maximum, and 0.097 mrad RMS field average) are beam quality (fringe) errors only which do not affect the pointing error.

4. The truss also experiences a gravity shear deflection which is a maximum when the heliostat is vertical and minimum when the heliostat is horizontal. Figure 3-20 pictorially illustrates the deflected shape caused by shear loading. The error which results can be partially compensated by adjusting the canting operation such that one-half of the maximum error is eliminated. The remaining error (0.055 mrad maximum, and 0.036 mrad RMS field average) would again manifest itself as a beam quality (fringe) error.

These non-correctable "remaining errors" for the gravity-sag of torque tube and all gravity-effects on the trusses are vectors which lie in planes which are normal to each other, so the resultant fringe effects are not additive. The gravity-sag of the torque tube primarily represents an azimuth-fringe effect, and the truss error deflections are primarily elevation-fringe effects.

It will be noted that all of the gravity deflection errors have been reduced by the canting and software correction technique, and all are now beam quality (fringe) errors: there are no gravity-induced pointing errors caused by structural deflections. The worst-case beam quality errors from gravity deflections occur when a heliostat is either horizontal or vertical and are:

Elevation Error = 0.19 mrad (reflected beam)
Azimuth Error = 0.87 mrad (reflected beam)

The RMS-average beam quality for a family of heliostats at elevation angles varying from 0^{o} to 90^{o} are:

Elevation Error = 0.13 mrad (reflected beam)
Azimuth Error = 0.63 mrad (reflected beam)

The wind bending effects cannot be removed by software or canting because they are variable in magnitude and direction. The "WINDBEND"

Figure 3-20

MRAD ERRORS FROM CHORD SHEAR LOADING

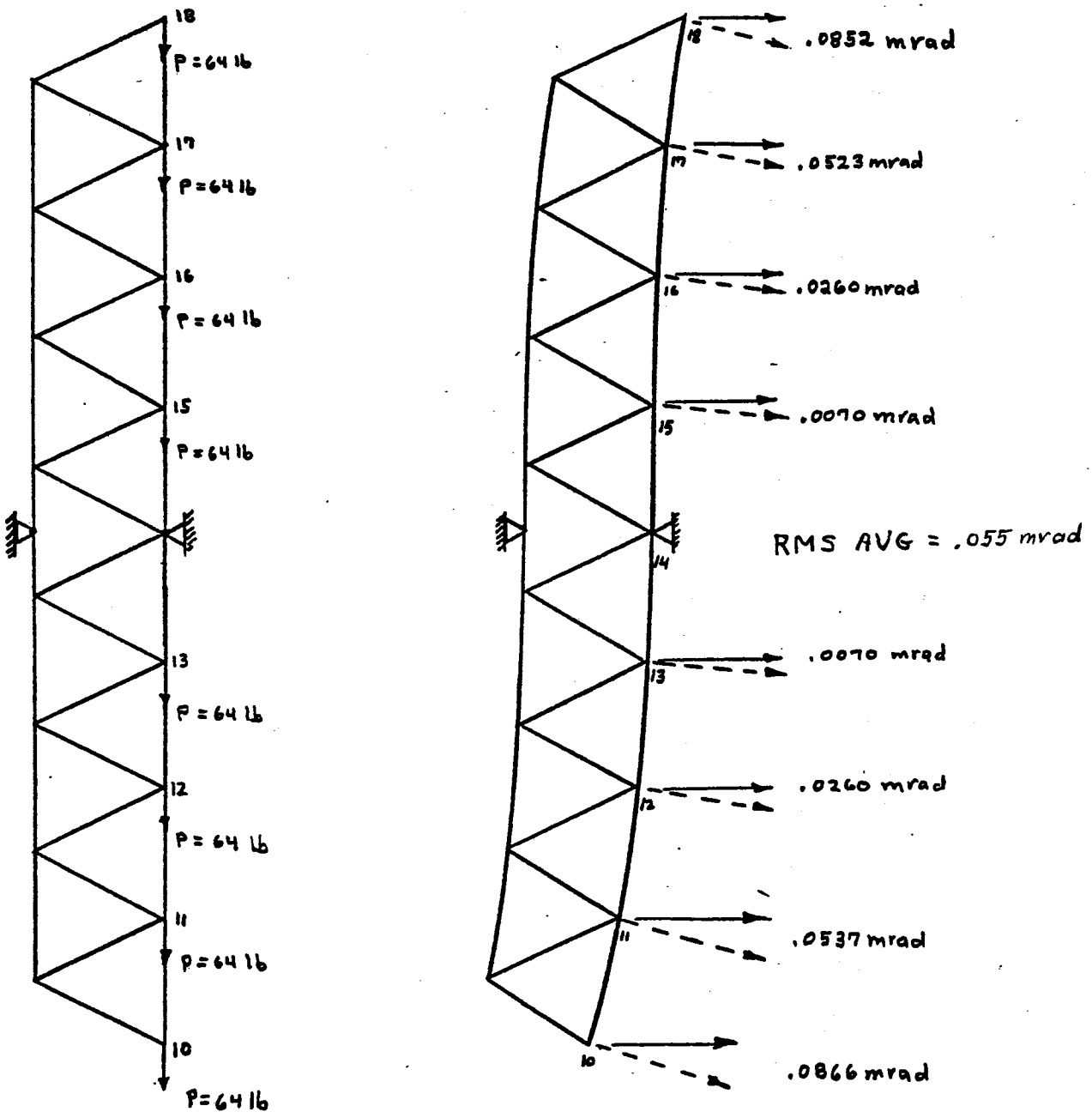

Analysis courtesy of Butler Mfg Co
Kansas City, Missouri

computer program was used to evaluate the effect of a 12 m/s (27 mph) wind as a function of angle of attack with all gravity loads removed. A complete set of output tabulations is provided in Appendix section 9.5.2.2. The wind effect may be conveniently divided into the following categories:

1. Wind induced torsion of the torque tube primarily causes an elevation pointing error. The worst-case error (at-target) occurs when the heliostat is within 20^{o} of horizontal and is 0.188 mrad. The RMS average for the family of elevation angles from 0^{o} to 90^{o} is 0.110 mrad at-target.

2. Wind-induced bending of the torque tube and torque tube flange primarily manifests itself as an azimuth-direction fringe increase; i.e., a beam quality degradation in the azimuth direction. The worst-case error (at-target) occurs when the heliostat is 50^{o} from horizontal and is 0.508 mrad. The RMS-average for the family of elevation angles from 0^{o} to 90^{o} is 0.436 mrad at target.

3. Wind-induced bending of the truss members causes an elevation-direction fringe increase or beam quality degradation. The worst-case error (at-target) occurs when the heliostat is 50^{o} from horizontal and is 0.084 mrad. The RMS-average error for the family of elevation angles from 0^{o} to 90^{o} is 0.073 mrad.

Table 3-12 summarizes the errors for the gravity-only, and for the wind-only cases.

TABLE 3-12

RACK STRUCTURE DEFLECTION ERRORS IN THE REFLECTED BEAM
WITH COMPENSATING SOFTWARE AND CANTING

	GRAVITY ONLY ERRORS mrad	12 m/s (27 mph) WIND ONLY ERRORS mrad
A. BEAM QUALITY		
1. WORST CASE		
a. ELEVATION	0.19	0.08
b. AZIMUTH	0.87	0.51
2. FIELD RMS AVERAGE		
a. ELEVATION	0.13	0.07
b. AZIMUTH	0.63	0.44
B. POINTING ERRORS		
1. WORST CASE		
a. ELEVATION	0	0.19
b. AZIMUTH	0	0
2. FIELD RMS AVERAGE		
a. ELEVATION	0	0.11
b. AZIMUTH	0	0

3.2.2.3 Rack Structure Stress - 40 m/s (90 mph) Wind

A stress analysis of the rack structure was performed for the 40m/s (90 mph) wind case. Although the heliostat would normally be stowed face-up horizontal in a high wind to minimize sand erosion of the mirrors, the Northrup heliostat is designed to be stowed in any position from vertical to face-up horizontal. Therefore, the stress analysis was performed for loads encompassing all stow position possibilities.

The results of the stress analysis are summarized on Table 3-13.

The bulk of the rack structure is critical for the heliostat positioned 40^{o} from vertical, when the wind normal force is maximum. This condition produces the highest bending and shear loads in the torque tube and in the trusses.

A primary area of concern during this high loading condition is the high bending stress produced in the torque tube root attachment flange. A 3/4 inch continuous plate was found to be the most economical means of providing the bolted flange for the prototype unit, as it provides sufficient strength with minimum material and cutting required. A thicker rolled ring might be the most economical for the production units.

The plates which attach the trusses to the torque tube were analyzed for a side wind condition. This condition produces the critical stresses in the plate as the entire lateral loading must be reacted by plate bending.

An important conclusion is that the structure is designed primarily for stiffness to minimize pointing errors and inherently has sufficient strength to withstand 40 m/s (90 mph) winds in any position. The only areas that become critical for this high loading are the local attachment points, which can be made to be adequate for strength quite inexpensively.

Appendix section 9.5.4.3 presents the details of the rack structure analysis for the 40 m/s (90 mph) wind speed loads.

Table 3-13
RACK STRUCTURE STRENGTH SUMMARY
40 m/s (90 mph) wind

STRUCTURAL ITEM	CRITICAL FAILURE MODE	STRESS OR LOAD	ALLOWABLE STRESS OR LOAD	MARGIN OF SAFETY
TORQUE TUBE & WELD	TENSION YIELD	101.1 mPa (14,670 psi)	248.2 mPa (36,000 psi)	+1.45
TORQUE TUBE FLANGE PLATE	BENDING YIELD	310.2 mPa (44,990 psi)	322.7 mPa (46,800 psi)	+ .04
TORQUE TUBE BOLTS	TENSION YIELD	4,709 kg (10,360 lbs)	7,273 kg (16,000 lbs	+ .54
TRUSS CHORD	COMPRESSION YIELD	43.0 mPa (6,230 psi)	248.2 mPa (36,000 psi)	LARGE
	BENDING	157.9 mPa (22,900 psi)	248.2 mPa (36,000 psi)	+ .57
TRUSS DIAGONALS (MAIN)	BUCKLING	962 kg (2117 lbs)	3441 kg (7570 lbs)	LARGE
(WELD-TO-PLATE)	SHEAR YIELD	64.9 mPa (9408 psi)	137.9 mPa (20,000 psi)	+1.13
	BENDING	106.7 mPa (15470 psi)	248.2 mPa (36,000 psi)	+1.32
TRUSS-TO-TORQUE TUBE (WELD) ATTACHMENT PLATE	SHEAR YIELD	39.4 mPa (5720 psi)	137.9 mPa (20,000 psi)	LARGE
(PLATE)	SHEAR BUCKLING	39.4 mPa (5720 psi)	137.9 mPa (20,000 psi)	LARGE
(PLATE)	FLATWISE BENDING	308.5mPa (44,740 psi)	322.7mPa (46,800 psi)	+ .05

3.2.3 Drive Unit

The following discussion presents the performance evaluation for the Northrup-Winsmith drive unit. The performance evaluation includes weight, input and output torque versus motor speed, efficiency, deflections, and stress levels.

3.2.3.1 Weight

Table 3-14 provides a detailed weight breakdown for the drive unit. The total weight of 559 kg (1231 lb) may be normalized to a weight per unit area of reflecting mirror of 10.6 kg/m^2 (2.2 lb/ft^2). This computed weight checks very well with the actual measurement of 556.8 kg (1225 lb).

3.2.3.2 Input Torque and Horsepower

The motive power for both the azimuth and elevation drive subassemblies is a permanent magnet D-C stepper motor, Model M112-FJ327, manufactured by Superior Electric. The driver unit is a Model TBM-105-1218 translator. It should be noted that the motor torque output is dependent on the mating translator; i.e., the switching method and pulse acceleration rate differs with translator logic, so different motor performance accompanies different translators. Table 3-15 provides the motor torque and horsepower versus stepping rate for the M112-FJ327 motor and TBM-105-1218 translator combination. At the planned control and slew speed of 500 steps/second, the torque and power will be 62 kg-cm (862 oz-in) and 0.095 kw (0.128 hp) respectively. At a singularity-resolution rate of 1000 steps/second, the torque and power will be 38.1 kg-cm (529 oz-in) and 0.117 kw (0.157 hp).

It should be noted that the M112-FJ327 motor selection is a recent event caused by a lower-than-anticipated drive unit efficiency (14-15% vs a predicted 20-21%) which was discovered during the Northrup test program. The M112-FJ327 motor replaces a very similar M112-FJ326 stepper motor (similar in size, weight, and cost). The new motor provides about 40% more torque, but must be operated at approximately one-half of the original speed to achieve this benefit. As a result, the slew rates are considerably lower than desired. A complete discussion of this problem is provided in Appendix G paragraph 9.7.2.5.

Table 3-14

DRIVE UNIT WEIGHT

	PIECE PART DESCRIPTION	WEIGHT, kg (lb)	
A.	Azimuth Subassembly		
	1. Cast Body	120.3	(264.6)
	2. Worm Gear	80.3	(176.6)
	3. Worm and Shaft	16.8	(36.9)
	4. Worm Bearings	3.7	(8.2)
	5. Planetary Unit	28.6	(63.0)
	6. Main Bearing	3.5	(7.8)
	7. Bearing Retainers	12.3	(27.1)
	8. Oil, 12 quarts	9.5	(21.0)
	9. Nuts, bolts, seals, misc.	4.5	(10.0)
	Total Azimuth Subassembly	279.6	(615.2)
B.	Elevation Subassembly		
	1. Cast Body	109.3	(240.5)
	2. Worm Gear	76.6	(168.5)
	3. Worm and Shaft	16.8	(36.9)
	4. Worm Bearings	3.7	(8.2)
	5. Planetary Unit	28.6	(63.0)
	6. Main Bearing	3.5	(7.8)
	7. Bearing Retainer	13.9	(30.5)
	8. Oil, 12 quarts	9.5	(21.0)
	9. Nuts, bolts, seals, misc.	4.5	(10.0)
	Total Elevation Subassembly	266.5	(586.4)
C.	Total Drive Unit Less Motors	546.2	(1201.6)
D.	Stepper Motors, M112FJ327 (2)	13.2	(29.0)
	Total Drive Unit Weight	559.4	(1230.6)

TABLE 3-15

DRIVE MOTOR TORQUE AND POWER, M112-FJ327

MOTOR RATE, STEPS/SEC	MOTOR SPEED, RPM	MOTOR TORQUE, kg-cm (oz-in)	MOTOR POWER kw (hp)
250	75	61.2 (850)	.047 (.063)
500	150	62.0 (862)	.095 (.128)
750	225	50.4 (700)	.116 (.156)
1000	300	38.1 (529)	.117 (.157)
1250	375	31.0 (431)	.119 (.160)
1500	450	26.6 (370)	.123 (.165)

3.2.3.3 Output Torque and Horsepower

The drive unit output torque and horsepower vary with stepping rate (motor speed) due primarily to the input torque variation, but also due to frictional variations in the worm and gear set. A computer program known as "NORTHWIN" was created to evaluate the theoretical efficiency, torque, and power characteristics. Figures 3-21 and 3-22 show sample outputs for the normal control and slew speed of 500 steps/sec, and for a singularity resolution speed of 1500 steps/sec based on these theoretical calculations.

Actual test data were obtained during the Northrup test program which indicated that the planetary stage efficiency was lower than anticipated (39% versus 55% theoretical). As a result, the "NORTHWIN" computer model was modified to incorporate this actual efficiency. Figures 3-23 and 3-24 show sample computer outputs for the normal control and slew speed of 500 steps/sec, and for a singularity resolution speed of 1500 steps/sec based on the test-data-matched version of the "NORTHWIN" program. A complete set of performance tabulations for both the theoretical and test-data-matched versions of the "NORTHWIN" program are provided in Appendix E, paragraph 9.5.5. Table 3-16 provides a summary of the key performance parameters versus stepping rate for the test-data-matched computer analysis.

The torque requirement for the stow condition is governed by the requirement to reach a face-up horizontal position in a 22 m/s (50 mph) wind. The worst-case combined wind and gravity moment for this maneuver is 1607 kg-m (11600 ft-lb), so the 1657 kg-m (11963 lb-ft) torque output capability shown on Table 3-16 is adequate. The torque requirement for the singularity resolution condition is governed by the requirement to perform a large-angle azimuth maneuver with the heliostat in a near-horizontal elevation attitude. The worst-case azimuth wind moment for a near-horizontal heliostat is very low. Even if the heliostat elevation were 50^{o} from horizontal, the maximum azimuth moment would only be 379 kg-m (2731 ft-lb) with a 15.6 m/s (35 mph) wind, so the torque capability of 723 kg-m (5215 ft-lb) shown on Table 3-16 is very adequate.

Figure 3-21

THEORETICAL DRIVE PERFORMANCE

NORTHRUP-WINSMITH PLANETARY-WORM DRIVE UNIT

INPUT PLANETARY STAGE RATIO AT MOTOR 460

THEORETICAL PLANETARY STAGE EFFICIENCY,% 54.87

INPUT STEPPING RATE,STEPS/SEC 500

INPUT WORM/GEAR REDUCTION RATIO 40

INPUT WORM P.D. 3.121

INPUT WORM LEAD ANGLE 7.7

INPUT STAGE

MOTOR STEP RATE, STEPS/SEC = 500
MOTOR RPM = 150
MOTOR TORQUE,OZ-IN= 860.297872
MOTOR OUTPUT HP = .127969309
PLANETARY OUTPUT TORQUE,IN-LB= 13571.3
PLANETARY EFFICIENCY,%= 54.87

OUTPUT STAGE

INPUT TORQUE,FT-LB= 1130.94
EFFICIENCY,%= 37.2
OUTPUT TORQUE,FT-LB= 16830.62
WORM RPM= .326

TOTAL DRIVE UNIT

INPUT TORQUE,OZ-IN= 860.29
EFFICIENCY,%= 20.41
OUTPUT TORQUE,FT-LB= 16830.62
DRIVE OUTPUT HP = .026
COMBINED RATIO= 18400
SLEW RATE, DEG/MIN = 2.934

Figure 3-22

THEORETICAL DRIVE PERFORMANCE

NORTHRUP-WINSMITH PLANETARY-WORM DRIVE UNIT

INPUT PLANETARY STAGE RATIO AT MOTOR 460

THEORETICAL PLANETARY STAGE EFFICIENCY,% 54.87

INPUT STEPPING RATE,STEPS/SEC 1500

INPUT WORM/GEAR REDUCTION RATIO 40

INPUT WORM P.D. 3.121

INPUT WORM LEAD ANGLE 7.7

INPUT STAGE

MOTOR STEP RATE, STEPS/SEC = 1500
MOTOR RPM = 450
MOTOR TORQUE,OZ-IN= 370
MOTOR OUTPUT HP = .1651125
PLANETARY OUTPUT TORQUE,IN-LB= 5836.7
PLANETARY EFFICIENCY,%= 54.87

OUTPUT STAGE

INPUT TORQUE,FT-LB= 486.39
EFFICIENCY,%= 37.71
OUTPUT TORQUE,FT-LB= 7337.61
WORM RPM= .978

TOTAL DRIVE UNIT

INPUT TORQUE,OZ-IN= 370
EFFICIENCY,%= 20.69
OUTPUT TORQUE,FT-LB= 7337.61
DRIVE OUTPUT HP = .034
COMBINED RATIO= 18400
SLEW RATE, DEG/MIN = 8.804

Figure 3-23

TEST DATA MATCHED DRIVE PERFORMANCE

NORTHRUP-WINSMITH PLANETARY-WORM DRIVE UNIT

```
 INPUT PLANETARY STAGE RATIO AT MOTOR 460

 PROBABLE ACTUAL PLANETARY STAGE EFFICIENCY,% 39

 INPUT STEPPING RATE,STEPS/SEC 500

 INPUT WORM/GEAR REDUCTION RATIO 40

 INPUT WORM P.D. 3.121

 INPUT WORM LEAD ANGLE 7.7


INPUT STAGE
-----------
  MOTOR STEP RATE, STEPS/SEC = 500
  MOTOR RPM = 150
  MOTOR TORQUE,OZ-IN= 860.297872
  MOTOR OUTPUT HP = .127969309
  PLANETARY OUTPUT TORQUE,IN-LB= 9646
  PLANETARY EFFICIENCY,%= 39


OUTPUT STAGE
------------
  INPUT TORQUE,FT-LB= 803.84
  EFFICIENCY,%= 37.2
  OUTPUT TORQUE,FT-LB= 11962.71
  WORM RPM= .326


TOTAL DRIVE UNIT
----------------
  INPUT TORQUE,OZ-IN= 860.29
  EFFICIENCY,%= 14.5
  OUTPUT TORQUE,FT-LB= 11962.71
  DRIVE OUTPUT HP = .019
  COMBINED RATIO= 18400
  SLEW RATE, DEG/MIN = 2.934
```

Figure 3-24

TEST DATA MATCHED DRIVE PERFORMANCE

NORTHRUP-WINSMITH PLANETARY-WORM DRIVE UNIT

INPUT PLANETARY STAGE RATIO AT MOTOR 460

PROBABLE ACTUAL PLANETARY STAGE EFFICIENCY,% 39

INPUT STEPPING RATE,STEPS/SEC 1500

INPUT WORM/GEAR REDUCTION RATIO 40

INPUT WORM P.D. 3.121

INPUT WORM LEAD ANGLE 7.7

INPUT STAGE

MOTOR STEP RATE, STEPS/SEC = 1500
MOTOR RPM = 450
MOTOR TORQUE,OZ-IN= 370
MOTOR OUTPUT HP = .1651125
PLANETARY OUTPUT TORQUE,IN-LB= 4148.6
PLANETARY EFFICIENCY,%= 39

OUTPUT STAGE

INPUT TORQUE,FT-LB= 345.71
EFFICIENCY,%= 37.71
OUTPUT TORQUE,FT-LB= 5215.36
WORM RPM= .978

TOTAL DRIVE UNIT

INPUT TORQUE,OZ-IN= 370
EFFICIENCY,%= 14.7
OUTPUT TORQUE,FT-LB= 5215.36
DRIVE OUTPUT HP = .024
COMBINED RATIO= 18400
SLEW RATE, DEG/MIN = 8.804

TABLE 3-16

DRIVE UNIT PERFORMANCE CHARACTERISTICS

BASED ON TEST - DATA - MATCHED "NORTHWIN" COMPUTER PROGRAM

MOTOR SPEED STEPS/SEC.	MOTOR SPEED RPM	DRIVE UNIT EFFICIENCY, %	DRIVE OUTPUT TORQUE kg-m, (lb-ft)	OUTPUT POWER kw (hp)	SLEW RATE, DEG/MIN
250	75	14.46	1632 (11780)	.007 (.009)	1.467
500	150	14.50	1657 (11963)	.014 (.019)	2.934
750	225	14.55	1353 (9767)	.017 (.023)	4.402
1000	300	14.60	1018 (7350)	.017 (.023)	5.869
1250	375	14.65	827 (5970)	.017 (.023)	7.336
1500	450	14.70	723 (5215)	.018 (.024)	8.804

3.2.3.4 Deflections-Gravity and 27 mph Wind

Drive unit deflections were determined for the gravity case and for the case where both gravity and a 12 m/s (27 mph) wind are acting on the heliostat. The results of the analysis are in terms of angular pointing misalignments. The effects of the deflection of the elevation and azimuth bearings and the housings are included.

The bearing deflection analysis was performed by the methods in the "New Departure Engineering Data, Analysis of Stresses and Deflections," Copyright 1946, New Departure, Division of General Motors Corp., Bristol, Connecticut. The deflections due to moment and radial loads were analyzed separately and added, which is slightly conservative due to the non-linear nature of the deflections. Also the thrust loading was neglected which has the same conservative effect.

The drive housings were broken down into 3 sub-parts and the stiffness was computed for each sub-part. The sub-parts are (a) the azimuth drive housing "ring", (b) the azimuth gear housing, and (c) the elevation drive outer housing. Items (b) and (c) were treated as equivalent cylinder beams and item (a) was treated as a ring with circumferential moment loading. The effect of local bolt-flange bending was neglected which is unconservative, but the resulting deflection is sufficiently small to justify this omission.

The critical loading conditions selected for the misalignment analysis of the bearings are (a) the heliostat 60° from vertical with a 12 m/s (27 mph) backwind, and (b) the heliostat 0° (vertical) with a 12 m/s (27 mph) backwind at a 70°azimuth angle of attack. The critical loading condition for the drive housing deflection is a vertical heliostat with a 12 m/s (27 mph) backwind.

The worst case deflections due to gravity effects are 0.68 mrad for azimuth and 1.73 mrad for the elevation axis. For the 12 m/s (27 mph) wind case (no gravity), the worst case deflections are 1.31 mrad azimuth, and 0.46 mrad for elevation. The deflections due to gravity are generally compensated for in the software or by the mirror module canting operation, thus reducing the error. A summary of the drive unit deflection contributions is presented in Table 3-17. Note that the values shown are drive deflections and must be multiplied by 2 to obtain comparable pointing errors on-target.

TABLE 3-17

(a) DRIVE ANGULAR MISALIGNMENT FOR HELIOSTAT 60° FROM VERTICAL, WIND AT α = 0° AZIMUTH

	GRAVITY		12 m/s (27 mph) WIND	
DUE TO	AZIMUTH	ELEVATION	AZIMUTH	ELEVATION
BEARINGS	.68 mrad.	1.55 mrad	.10 mrad	.31 mrad
HOUSING	0	.06	0	.05
BACKLASH	0	0	.38	0
MISCELLANEOUS *	0	.12	0	.10
TOTAL	.68	1.73	.48	.46

(b) DRIVE ANGULAR MISALIGNMENT FOR HELIOSTAT VERTICAL, WIND AT α = 0° TO 70° AZIMUTH

	GRAVITY		12 m/s (27 mph) WIND	
DUE TO	AZIMUTH	ELEVATION	AZIMUTH	ELEVATION
BEARINGS	0	1.04	.73	.14
HOUSING	0	.11	.08	.02
BACKLASH	0	0	.38	0
MISCELLANEOUS *	0	.24	.12	.01
TOTAL	0	1.39	1.31	.17

* Miscellaneous errors include gear tooth bending, worm bearing deflections, and flange bending.

3.2.3.5 Stress - 40 m/s (90 mph) Wind

The primary mechanical elements of the drive units, the gears and bearings, were analyzed to verify their strength to withstand 40 m/s (90 mph) wind loads. Tooth bending and shear stresses were calculated by the methods in "Design of Worm and Spiral Gears" by Earle Buckingham and Henry Ryffel. Bending stress at the root of the gear teeth were calculated, as these were suggested as the critical points by this reference. The results of the analysis showed that the worm thread bending stress is 133,766 psi in a 40 m/s (90 mph) wind and 41,326 psi in a 22 m/s (50 mph) wind for vertical stow. The corresponding gear tooth shear stress is 42,359 psi and 13,086 psi, respectively. In addition, the gear tooth bending stress was calculated by beam formulas including stress concentration factors, and the results showed 117,773 psi in a 40 m/s (90 mph) wind and 36,350 psi in a 22 m/s (50 mph) wind. These are all acceptable for the Winsmith gear tooth design.

The loads in the main drive bearings were calculated in terms of radial, thrust, and moment loads, and compared to the static load ratings of bearings. The results are shown in Appendix E, page E-150. The radial and thrust loads were well below the static load capacity, but the moment was slightly over the catalog rating of the bearing static load capacity when stowed horizontally in a 40 m/s (90 mph) wind, and well over the rated static load capacity when stowed vertically. Both conditions are considered acceptable by the bearing manufacturer (Keene Corp.) for the infrequent occurrence of 40 m/s (90 mph) wind conditions.

3.2.4 Drive Motor and Controls Performance

3.2.4.1 Control Hardware Performance

The heliostat controller (HC) requires serial data in the format of address, azimuth, elevation, and mode words. The azimuth and elevation position commands consist of two bytes each (most significant and least significant respectively). Each byte consists of one start bit, two stop bits, 8 data bits, and no parity bits. The HC times out after 1.5 bytes if data transmission is lost.

The HC keeps track of the total number of step commands and transmits its current position based on the reference position established upon power up. Upon receiving an absolute position command, the HC subtracts its commanded position from its current position and outputs the appropriate number of steps.

The heliostat mode is controlled by the mode byte which determines track, slew, request for status, and clear malfunction.

The HC checks limit switch status upon power up and sets a status bit if the switches are in a stow condition.

The HC returns position and status information upon request. The status word consists of limit switch indications, motor movement, wake-up malfunction and power drop-out information.

The stepper motors require acceleration and deceleration in order to reach slewing speeds. This is a normal requirement of stepper motors and is needed to overcome inertia without losing steps. The profile for acceleration and deceleration for azimuth and elevation stepper motors is shown in Figure 3-25 For simplification of software, it was determined that if two motors were required to move to a position simultaneously, they accelerate in parallel and both decelerate when either motor is required to stop. After both motors stop, the motor requiring additional position movement resumes normal operation (see Figure 3-25)

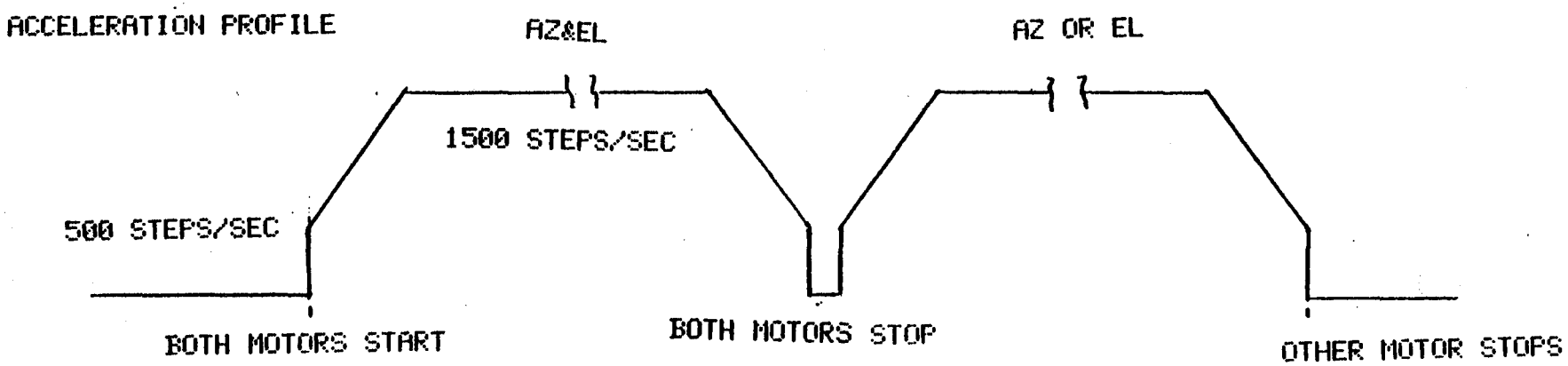

- ACCELERATION/DEACCELERATION NEEDED
- NEED TO COUNT CYCLES
- DELAY ADJUSTMENT REQUIRED FOR DIFFERENT BRANCHES

Figure 3-25

Stepper Motor Sequence Profile

3.2.4.2 Software Performance

Software for the Northrup II heliostats consists of two packages, one handling the external data processing, communication and control (the Mini Heliostat Array Controller) and one handling the internal data processing, communication, and direct motor control (the Heliostat Control).

Functions of the Mini-HAC software are those generally associated with the Master Control, Heliostat Array Controller, and Field Controller. The "Master Control" features of the software include providing the system time reference, the corresponding solar vector definition, and the target coordinates as a function of the operating mode. Figure 3-26 shows these major software elements and their schematic linkage. For the two-heliostat system of this program, the Mini-HAC program is being written for the Hewlett Packard 9825 "Desktop Computer" and compatible peripherals. (Clock, CRT, RS 232 Serial I/O, IEEE 488-1975 Parallel I/O, Plotter, Printer, and Disk Storage)

The HP 9825 is the system controller. In the initializing sequence, the controller interogates the clock for month, day, and time, computes the solar vector cosines, and establishes the subroutine to be processed for the assigned mode.

The operating segment of the software, shown schematically in Figure 3-27 for the tracking mode subroutine "T-TRACK", computes the target vector cosines, the required heliostat angles, the magnitude of the motor operation sequences needed to reach the required position, and processes the operating mode data to the Heliostat Control Electronics The operating software continuously cycles through an update and re-positi sequence until interrupted by the controller.

Status information is obtained directly from the Heliostat Control Electronics by the controller through a parallel communications bus and is recorded on a disk file, and displayed on both the CRT and hard copy plots.

The detail flow diagram for the Heliostat Control Electronics Motor Control software is included in Appendix 9.8.

Upon receipt of a six word message from the controller, the heliostats check the first word for being the applicable address and then either implement the control action defined in the remaining five words or stand by for the next message. Two words define the azimuth position requirement, two define the elevation position requirement and the last word sets the HCE mode. Motor speed and direction are controlled by bits in the mode word in addition to the basic mode action (operate motors or transmit status).

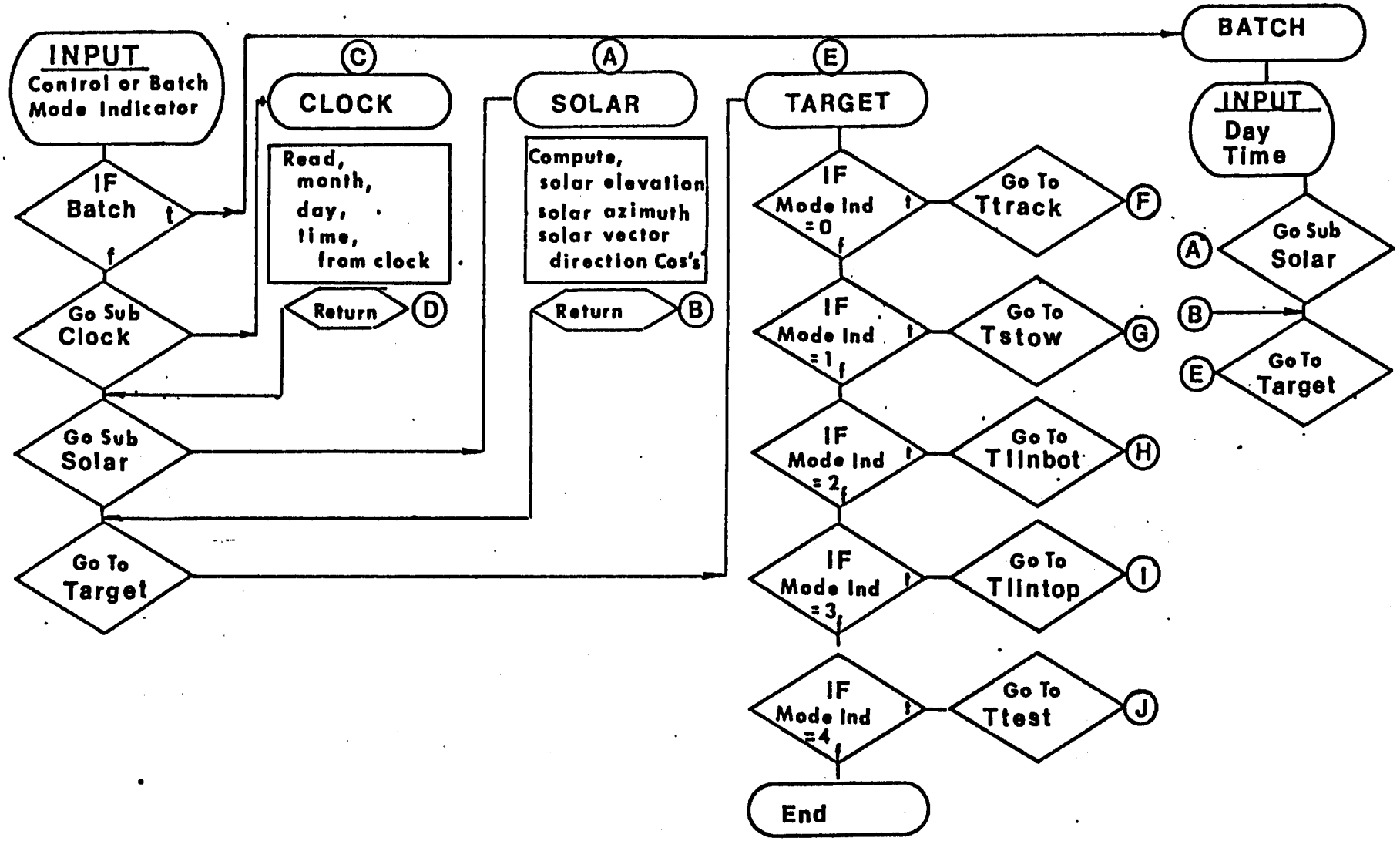

Figure 3-26 Mini HAC Software Schematic-Initializing Segment

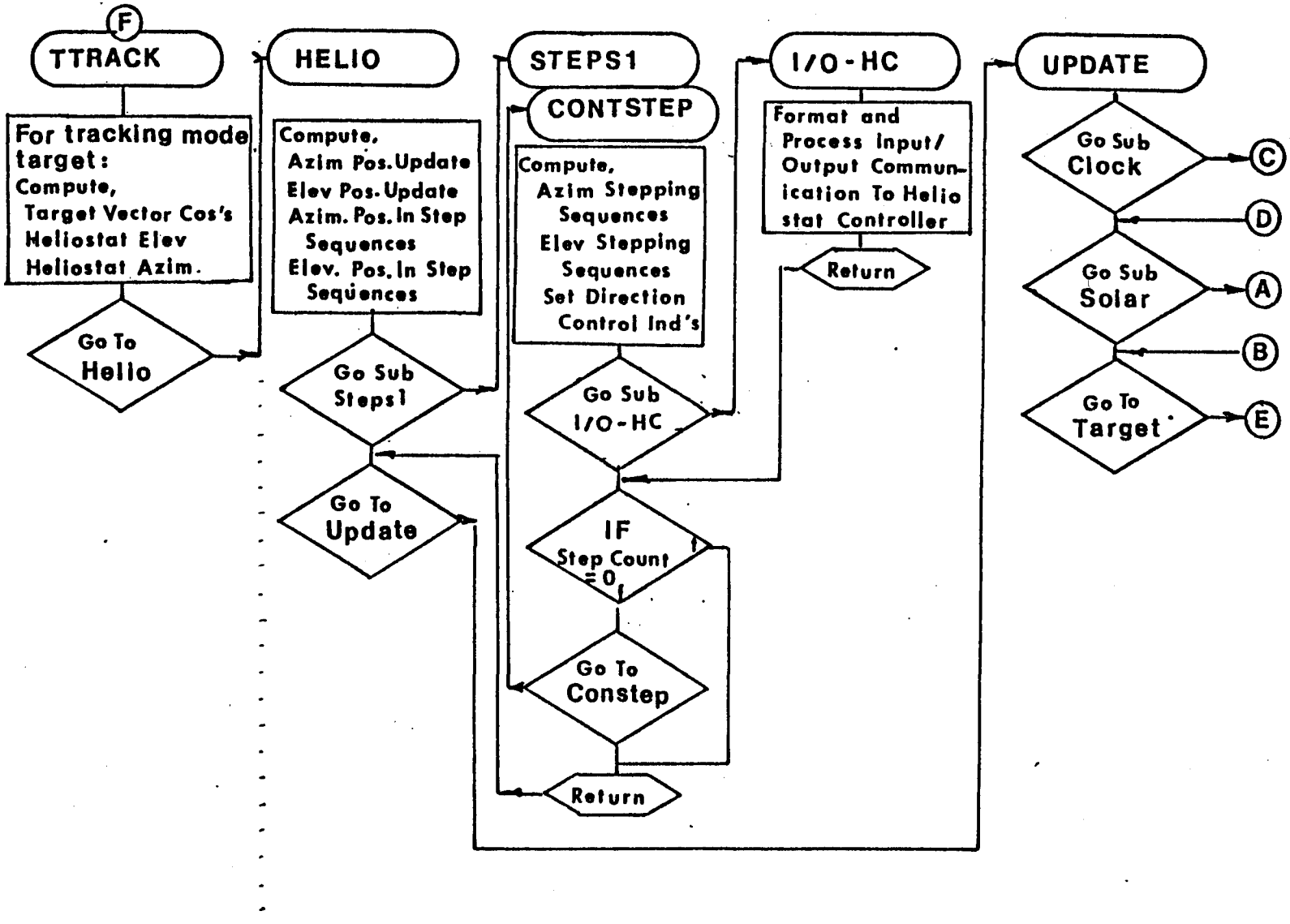

Figure 3-27 Mini HAC Software Schematic-Operating Segment

3.2.4.3 Power Consumption

One significant operating cost of a collector sub-system is the cost of the electrical energy which is consumed by the motors, translators, power supplies, and controls. Table 3-18 summarizes the average power consumption.

As shown on Table 3-18 the energy consumption amounts to 2.958 kwh per heliostat per day. A 50 MW_e plant would contain 5974 heliostats of the Northrup heliostat configuration. Hence, for 350 days of operation, the heliostat field would consume 6.18 x 10^6 Kwh/year.

Based on an equivalent of seven hours per day at peak output for 350 days of operation per year, a 50 MW_e plant will generate about 123 x 10^6 Kwh/year. The parasitic energy consumption for heliostat operation would, therefore, be approximately 5.0% of the plant output.

Another item of interest is the peak power demand placed on the system by the heliostat field. When the system is called upon to react to a slew command all heliostats will operate simultaneously. The power demand per heliostat is:

Azimuth Drive	200 watts
Elevation Drive	200 watts
Microprocessor	15 watts
Pedestal Fan	20 watts
Total Demand	435 watts

A 5974 collector field for a 50 MW_e power plant will draw 2.60 megawatts which is 5.2% of the peak plant output.

Table 3-18

Electrical Energy Consumption Per Day Per Heliostat

	Power Input In Watts	Hours Per Day	KWH Per Day
Azimuth Drive			
When motor is operating	200	1.36*	0.272
Standby	85	10.64*	0.904
Off	0	12.00	0
Elevation Drive			
When motor is operating	200	0.68*	0.136
Standby	85	11.32*	0.962
Off	0	12.00	0
Microprocessor			
On	15	12.00	0.180
Off	0	12.00	0
Pedestal Fan			
On	20	24	0.48
Off	0	0	0
TOTAL PER HELIOSTAT PER DAY			2.958

* Assumes 240° azimuth motion/day and 120° elevation motion/day.

3.2.5 Error Budget and Error Performance

In this section the error effects from the mirror module, rack structure, drive unit, controls, and pedestal are brought together, combined, and evaluated against the requirements of the "Collector Subsystem Requirements", Sandia No A10772.

3.2.5.1 Pointing Error (Tracking Accuracy)

The appropriate requirement is specified in paragraph 3.2.1.a of specification A10772 as follows:

> "Maximum beam pointing error (tracking accuracy) shall be limited to 1.5 mrad standard deviation for each gimbal axis under the following conditions:
>
> Wind - none
>
> Temperature - 0^{o} to 50^{o}C (32^{o} to 122^{o}F)
>
> Gravity Effects - at all elevation and azimuth angles that could occur in a heliostat field.
>
> Azimuth Angles - at all angles except during gimbal lock.
>
> Sun Location - at least .26 rad above horizon, any time of year.
>
> Heliostat Location - any position in the field.
>
> Pointing error is defined as the difference between the aim point and measured beam centroid for all of the above conditions for any tracking aim point (on target or at standby)."

Table 3-19 presents the beam pointing errors for the Northrup heliostat design. An explanation of each item is as follows:

1. Control Resolution and Accuracy (0.17 mrad) - This is caused by the software transmittal of pulse (motor steps) trains which always contain 100 steps. This represents a potential $\pm$ 50 step error. Since a motor step corresponds to 1.8 degrees angular rotation (31.4 mrad), and the gear ratio is 18400:1, this represents

a heliostat position error of 0.085 mrad and a pointing error of 0.17 mrad.

2. Computation and Sun Location (azimuth = 0.46 mrad, elevation = 0.23 mrad) - This is caused by the 10 second interval between computations; i.e., the heliostat position could be $\pm$ 5 seconds in error. At the maximum tracking rates this corresponds to a 0.22 mrad azimuth position error and 0.09 mrad elevation error. There is an additional error of 0.07 mrad compution code variance of the sun position versus the Ephemeras (each axis). These errors are RSS combined and doubled to obtain the total pointing errors of 0.46 mrad azimuth, and 0.23 mrad elevation.

3. Drive Backlash (0.76 mrad - azimuth only) - The backlash in the output gear causes a 0.38 mrad possible error in heliostat position; i.e., a 0.76 mrad pointing error. However, due to gravity forces, the elevation drive is always loaded in one direction, so no pointing error results. In the azimuth direction, friction will generally keep the loading in one direction. However, during some singularity resolution maneuvers, the azimuth drive reverses direction for a short time, and a backlash error could occur. The software could then take note of this reversal and introduce a backlash correction when this occurs. Ideally, all of the backlash error could, therefore, be eliminated. In actual practice, the ever-present winds will tend to blow the heliostat back and forth in the azimuth backlash band. Hence, the full backlash error is included in the analysis.

4. Mechanical Alignment-Initialization (0.17 mrad) - The true azimuth and elevation position of the heliostat will be established by a laser alignment system, and will be accounted for in the software. However, this position will be referenced to position switches and pulse count, and as such will be limited in accuracy to the control resolution (0.17 mrad).

5. Gravity Deflection (0.2 mrad azimuth, 0.2 mrad elevation) - As discussed in para. 3.2.2.2 and 3.2.3.4, gravity deflections, if uncorrected, would cause relatively large pointing errors. The Northrup design concept is to "remove" these errors by software computation and deflection - corrected mirror module canting. Not all of the error can

be eliminated, but what remains manifests itself as a beam quality effect (see para. 3.2.5.2). It is estimated that the computational error of correcting for gravity deflections is 0.2 mrad for each axis.

6. Foundation Movement (0.3 mrad) - The foundation (pedestal) is initially driven into the ground with a vertical alignment accuracy of 1.1 angular degrees. This angular misalignment is measured and corrected using the soft-ware. After installation it is anticipated that some pedestal movement would occur due to periodic high wind loads (estimated to be 1.0 mrad maximum). Again a measurement of the misalignment would be made on a spot-check basis, and an analytical adjustment made to the soft-ware to correct for this. In either case there exists an error in the ability to measure the misalignment. This measurement error is assummed to be 0.3 mrad maximum for each axis.

7. Non Orthogonal Axes (0.3 mrad) - it is estimated that the drive unit will be fabricated with the azimuth and elevation axes orthogonality of 1.0 mrad. This non-orthogonality will be compensated for soft-ware correction. It is estimated that the axes orthogonality can be measured with an accuracy of 0.3 mrad. The soft-ware will correct the measurable non-orthogonality, but the measurement error is an unknown which would remain.

These errors were assumed to be independent and random, and therefore, were combined by the root-sum-square (RSS) technique. The total resultant pointing error is 1.03 mrad for azimuth, and 0.58 mrad for elevation. For conservatism, these are assumed to be one-standard deviation values, even though they are based in some cases on maximum-estimated (3-standard deviation) individual errors. These total values are well within the 1.5 mrad allowable pointing error for each axis.

TABLE 3-19

REFLECTED BEAM POINTING ERROR SUMMARY

	Uncorrected		Correction	Net Pointing Error	
	AZIM	ELEV		AZIM	ELEV
1. Control Resolution	.17 mrad	.17 mrad	NONE	.17 mrad	.17 mrad
2. Analytics					
A. Computation	.44	.18	NONE	.46	.23
B. Sun Location	.14	.14	NONE		
3. Drive Unit Backlash	.76	0	NONE	.76	0
4. Alignment (Initialization)	.17	.17	NONE	.17	.17
5. Gravity Deflection					
A. Rack	0	1.766	Software + Canting	.2	.2
B. Drive (Test Data)	0.30	3.60			
6. Foundation Movement	1.0	1.0	Software	0.3	0.3
7. Non-Orthogonal Axes	1.0	1.0	Software	0.3	0.3
RSS TOTAL	1.71	4.27		1.03	0.58
REQUIREMENT	-	-		1.5	1.5

3.2.5.2 Beam Quality (Fringe Angle)

The appropriate requirement is specified in paragraph 3.2.1.b of specification A10772 as follows:

> "Beam quality shall be such that a minimum of 90% of the reflected energy at target slant range shall fall within the area defined by the theoretical beam shape plus a 1.4 mrad fringe width. Heliostat beam quality shall be met throughout 60 days without realignment. Beam quality requirements are applicable under the following conditions:
>
> Wind - none
>
> Temperature - 0° to $50^{\circ}C$ (32° to $122^{\circ}F$)
>
> Gravity Effects - at all elevation and azimuth angles that could occur in a heliostat field.
>
> Sun Location - at least .26 rad above horizon, any time of year.
>
> Heliostat location - any position in the field and any slant range.
>
> Operating Mode - tracking on plant receiver
>
> Facet Alignment - as planned for the plant
>
> Theoretical Beam Shape - the theoretical beam contour, determined by HELIOS, is the isoflux contour that contains 90% of the total power. This isoflux contour will be increased by 1.4 mrad fringe. The HELIOS computer code is available through Sandia."

Table 3-20 presents the beam quality errors for the Northrup heliostat design. A brief explanation of each contributing item is as follows:

1. Canting Alignment (0.36 mrad) - It is estimated that each mirror module can be canted with an accuracy of 1.2 mrad. Since there are twelve mirror modules (n) per heliostat, the statistical total error will be the individual error divided by the square root of (n-1); i.e., the resultant error is $1.2/(11)^{\frac{1}{2}} = 0.36$ mrad.

2. Out-of-Flat (0.5 mrad) = It is estimated that the combined surface block flatness, the glass flatness, the steel backing sheet flatness (ripple) and the silicone grease thickness variations will contribute 0.5 mrad to the fringe angle error.

3. Thermal De-Focusing (0.23 mrad azimuth, 0.0 mrad elevation) - As shown in para. 3.2.1.2, the temperature difference through the mirror module causes a 16 km (10 mile) radius of curvature in a convex direction. This corresponds to a fringe angle expansion of 0.23 mrad. This effect only occurs in the 3.66 m (12.0 ft) direction which corresponds to an azimuth - fringe. There is no thermal de-focusing in the transverse direction.

4. Rack Structure Gravity Deflections (0.87 mrad azimuth, 0.19 mrad elevation) - Paragraph 3.2.2.2 presented a discussion of the gravity deflection effects and the technique for minimizing errors from these deflections for the rack structure. The general approach is to utilize the software or to bias the mirror module canting to remove one half of the maximum error for each deflection mode. This process eliminates deflection-induced pointing errors, but introduces beam quality errors because all of the error is not eliminated. The fringe error thus introduced is 0.87 mrad in the azimuth direction, and 0.19 mrad in the elevation direction.

5. Mirror Module Gravity Deflections (0.36 mrad azimuth, 0.41 mrad elevation) - Paragraph 3.2.1.3 presented a discussion of the gravity deflection effects for the mirror modules. For the azimuth direction the fringe angle increase is 0.36 mrad. For the elevation direction, the fringe angle increase is somewhat higher due to the gravity sag of the mirror between the internal ribs, and is 0.41 mrad.

6. Mirror Specularity (0.5 mrad) - It is assumed that the mirror imperfections cause a fringe angle increase of 0.5 mrad. It should be noted that combining this mirror specularity variance of 0.5 mrad with the out-of-flat variance estimate of 0.5 mrad results in a total which is consistent with the Sandia laser-ray measurement at 1.06 mrad as discussed in paragraph 3.2.1.3.

These errors were assumed to be independent and random, and were combined by the root-sum-square method. The total RSS error for azimuth is 1.25 mrad, and for elevation is 0.91 mrad.

TABLE 3-20

REFLECTED BEAM QUALITY ERROR SUMMARY

	Uncorrected		Correction	Net Beam Quality	
	AZIM	ELEV		AZIM	ELEV
1. Alignment (canting)	.36 mrad	.36 mrad	None	.36 mrad	.36 mrad
2. Out-of-Flat	.5	.5	None	.5	.5
3. Thermal Defocusing	.23	0	None	.23	0
4. Gravity Deflections					
A. Rack Structure	1.75	.39	Canting + Software	.87	.19
B. Mirror Modules	.36	.41	None	.36	.41
5. Mirror Specularity	.5	.5	None	.5	.5
RSS TOTAL	1.97	0.97		1.25	0.91
REQUIREMENT	-	-		1.40	1.40

3.2.5.3 Wind-Induced Errors (Structural Deflections)

The appropriate requirement is specified in paragraph 3.2.1.c of specification A10772 as follows.

> "Overall structural support shall limit reflective surface static deflections to an effective 1.7 mrad standard deviation for a field of heliostats in a 12 m/s (27 mph) wind.
>
> Wind deflections of the foundation, pedestal, drive mechanism, torque tube, and mirror support members shall be included, but not the slope errors due to gravity and temperature effects. Wind deflection limits apply to the mirror normal (not reflected beam) for each axis fixed in the reflector plane. Both beam quality and beam pointing are affected.
>
> To assure that the net slope errors of a field of heliostats is less than 1.7 mrad, the rms value of the slope errors taken over the entire reflective surface of an individual heliostat, computed under the worst conditions of wind and heliostat orientation (but excluding foundation deflection), shall be limited to 3.6 mrad for a single heliostat. This limit represents a 3-sigma value for the field derived by subtracting foundation deflection (see 3.2.1.d) from the total surface slope error (1.7 -0.5=1.2 mrad standard deviation x 3 = 3.6 mrad 3-sigma). The conditions under which this requirement applies are:
>
> Wind, including gusts - 12 m/s (27 mph) at 10 m (33 ft) elevation
>
> Temperature 0^{o} to 50^{o}C (32^{o} to 122^{o}F)
>
> Heliostat Location - any position in the field at any time of year.
>
> Gravity Effects - not included
>
> Mirror Module Waviness - none
>
> Facet Alignment Error - none

Table 3-21 presents the structural deflection errors from a 12 m/s (27 mph) wind for the Northrup heliostat design. An explanation of each item is as follows:

1. Mirror Module (0.023 mrad azimuth, 0.302 mrad elevation, worst case) -

The "MODBEND" computer code was used to evaluate the mirror module bending in both the azimuth and elevation direction. Bending, shear, and attachment deflection effects are included in the analysis. The resultant worst-case errors are 0.023 mrad for azimuth and 0.302 mrad for elevation (at the worst elevation angles). For a field of heliostats having a uniform distribution of elevation angles, the RMS average error is 0.020 mrad for azimuth and 0.231 mrad for elevation.

2. Truss Bending (0 mrad azimuth, .041 mrad elevation, (worst case) - The "WINDBEND" computer model was used for this elevation. The resultant worst-elevation-angle errors were zero mrad for the azimuth direction, and 0.041 mrad for elevation. For a field of heliostats having a uniform distribution of elevation angles, the RMS average errors are 0 mrad for azimuth and .020 for the elevation direction.

3. Torque Tube Deflection (.254 mrad azimuth, .094 mrad elevation, worst-case) - The wind forces cause a torque tube torsion which introduces a elevation error, and a bending moment which causes an azimuth error. The "WINDBEND" computer model was used to evaluate these effects. The worst-case errors are .254 mrad for azimuth, and .094 mrad for elevation. For a family of heliostats, the RMS average errors are 0.218 mrad for azimuth and 0.055 mrad for elevation.

4. Drive Unit (1.85 mrad azimuth, 0.79 mrad elevation) - The drive unit deflections are due in large part to the bearing deflections. Other contributing factors are the housing bending and torsional effects, backlash, flange bending, and gear tooth deflection. The deflection values shown are based on test data. It is estimated that the worst case deflection values shown above would equate to RMS field-average values no greater than 1.27 mrad for azimuth and 0.54 mrad for elevation.

5. Pedestal (0.16 mrad azimuth, 0.28 mrad elevation) - The above-ground pedestal deflections from the wind consist of simple bending and torsion. The bending portion was assigned as an elevation error, and the torsion as an azimuth error. It is estimated that these deflections would equate to RMS field-average values no greater than 0.11 mrad for azimuth and 0.20 mrad for elevation.

Since these individual errors are not generally random or independent of each other with a given 12 m/s (27 mph) wind, the total error is determined as an arithmetic sum. Worst-case errors are 2.29 mrad for azimuth and 1.51 mrad for elevation. The field-average errors are 1.62 mrad for azimuth and 1.04 mrad for the elevation direction.

TABLE 3-21

STRUCTURAL DEFLECTION ERRORS

FROM A 12 m/s (27 mph) WIND

	Worst Case Elevation Angle Deflection Error, mrad		RMS Field Average Deflection Error, mrad	
	AZIM	ELEV	AZIM	ELEV
MIRROR MODULE	.023	.302	.020	.231
TRUSS PURLINS	0	.041	0	.020
TORQUE TUBE	.254	.094	.218	.055
DRIVE UNIT *	1.85	.79	1.27	.54
PEDESTAL	.16	.28	.113	.198
TOTAL (SUM)	2.287	1.507	1.621	1.044
REQUIREMENT	3.6	3.6	1.7	1.7

*Based on actual test data

3.3 SUMMARY OF SYSTEM STUDIES

The following discussion presents a summary of the system studies which have been performed in support of the Northrup heliostat design.

3.3.1 Wind Loads and Moments

The wind forces and resultant moments were computed in accordance with "Wind Forces on Structures", ASCE Paper No. 3269, Transactions, American Society of Civil Engineers, Vol. 126, Part II, 1961. The critical wind conditions analyzed were:

a. Requirements Wind - 12.1 m/s (27 mph)
b. Operating Wind - 15.6 m/s (35 mph)
c. Stowing Wind - 22.4 m/s (50 mph)
d. Survival Wind - 40.2 m/s (90 mph)

Since these wind conditions were specified at an elevation height of 9.1 m (30 ft), a reduction factor was applied to obtain the wind speed at the heliostat mid-point height of 3.89 m (12.75 ft). This reduction was performed in accordance with para. 3.1.1 of Sandia Specification A10772, Appendix 1.

The Northrup heliostat is symmetric in height and width, and presents a continuous face area with no major slots or voids. Hence, the forces and moments are the same for the azimuth and elevation directions when the wind angle of attack relative to these directions is the same. Also, due to the symmetry of the heliostat, the unit performs as a flat plate having an aspect ratio of unity. The gross envelope area of the mirrored plane, approximately 54.9 m^2 (590.7 ft^2), was used for all load computations, rather than the lower-value solid area.

Table 3-22 summarizes the lift, drag, and center of pressure coefficients for the Northrup heliostat, unity-aspect ratio configuration. Table 3-23 presents the wind speed, dynamic pressure, and lift and drag forces. Table 3-24 presents the azimuth and elevation moments, and Table 3-25 the pedestal base moments

Table 3-22

Wind Force Parameter Summary

Angle of Attack	C_L	C_D	C_{CP}
0	0	1.126	.500
10	.228	1.103	.470
20	.400	1.061	.451
30	.571	.989	.437
40	.730	.890	.430
50	.860	.761	.420
60	.898	.593	.398
70	.803	.274	.343
80	.361	.107	.263
90	0	0	0

Note: C_L = lift coefficient

C_D = drag coefficient

C_{CP} = center of pressure coefficient

Table 3-23

Wind Induced Pressures and Loads

	27 mph (reqmts)	35 mph (operating)	50 mph (stowing)	90 mph (survival)
1. Windspeed corrected to 12.75 ft height	23.748 mph	30.784 mph	43.977 mph	79.159 mph
2. Dynamic pressure, q, lb/ft^2	1.413	2.374	4.845	15.698
3. Dynamic pressure x Area, lb_f	848.2	1425.1	2908.5	9423.5
4. Drag Force, F_D, lb_f				
0^o	955	1605	3275	10611
10	936	1572	3208	10394
20	900	1512	3086	9998
30	839	1409	2877	9320
40	755	1268	2589	8387
50	645	1085	2213	7171
60	503	845	1725	5588
70	232	390	796	2582
80	91	152	311	1008
90	0	0	0	0
5. Lift Force, F_L lb_f				
0^o	0	0	0	0
10	193	325	663	2149
20	339	570	1163	3769
30	484	814	1661	5381
40	619	1040	2123	6879
50	729	1226	2501	8104
60	762	1280	2612	8462
70	681	1144	2336	7567
80	306	514	1050	3402
90	0	0	0	0

Table 3-24

Elevation and Azimuth Moments

Angle of Attack	Moment Arm d,ft	Windspeed at 30 ft Height			
		27 mph (reqmts)	35 mph (operating)	50 mph (stowing)	90 mph (survival)
0	0	0 ft-lb	0 ft-lb	0 ft-lb	0 ft-lb
10	.735	702	1179	2407	7799
20	1.201	1155	1941	3961	12832
30	1.544	1496	2513	5130	16620
40	1.715	1674	2813	5740	18598
50	1.960	1909	3207	6546	21209
60	2.499	2277	3826	7808	25297
70	3.847	2768	4651	9497	30752
80	5.807	1843	3097	6320	20476
90	12.25	0	0	0	0

Table 3-25

Ground-Level Column Base Moments

Angle of Attack	Windspeed at 30 ft Height			
	27 mph (reqmts)	35 mph (operate)	50 mph (stowing)	90 mph (survival)
0	12176 ft-lb	20460 ft-lb	41756 ft-lb	135290 ft-lb
10	12629	21222	43309	140323
20	12628	21219	43304	140307
30	12191	20485	41805	135450
40	11298	18985	38744	125532
50	10138	17035	34765	112639
60	8689	14601	29797	96544
70	5731	9630	19652	63673
80	3000	5040	10286	33328
90	0	0	0	0

(at ground level) for the requirements, operating, stowing, and survival wind conditions.

It should be noted that the elevation and azimuth wind moments shown in Table 3-24 are worst case conditions corresponding to either of the following situations:

1. Elevation Moments - The elevation angle may vary, but the wind vector is always directly into the front or back of the mirror module plane. In other words, the wind vector lies in the same plane, and is coincident with the azimuth pointing vector.

2. Azimuth Moments - The heliostat is vertical, and the wind vector is approaching the mirror module plane from a generally sideward direction. Stated another way, the wind vector lies in the same plane, and is coincident with the elevation pointing vector.

Since the heliostats are never vertical during operation (or during high wind speed conditions), the maximum azimuth moments are generally not experienced. Conversely, the maximum elevation moments for a given wind and elevation angle are commonly experienced. A cross-wind analysis was performed which illustrates how the azimuth and elevation moments vary when the heliostat is at various orientations other than those where the wind vector and pointing vector are coincident. Figure 3-28 and 3-29 show the moment variation with orientation for the four specified wind conditions. These calculations show that certain high moment conditions, such as might be experienced when stowing with a 22 m/s (50 mph) wind, may be avoided by choosing a proper azimuth-elevation path to the stow position which also must comply with beam safety considerations. Another advantageous phenomenon which can be utilized is the fact that the wind forces always act to return a heliostat to the vertical position, no matter whether the wind is approaching from the heliostat front or back side. The advantage to be gained from exploiting these wind characteristics is a smaller motor size and less electrical

Figure 3-28

AZIMUTH AND ELEVATION-AXIS MOMENTS FOR CROSS-WIND CONDITIONS

27 MPH WIND MOMENTS, FT-LB

	90°	70°	60°	40°	20°	0°
0°	AZ = 0 EL = 0	AZ = 2769 EL = 0	AZ = 2278 EL = 0	AZ = 1675 EL = 0	AZ = 1155 EL = 0	AZ = 0 EL = 0
20°	AZ = 0 EL = 0	AZ = 2445 EL = 135	AZ = 2012 EL = 289	AZ = 1479 EL = 678	AZ = 1020 EL = 1020	AZ = 0 EL = 1155
40°	AZ = 0 EL = 0	AZ = 1625 EL = 196	AZ = 1337 EL = 419	AZ = 983 EL = 983	AZ = 678 EL = 1479	AZ = 0 EL = 1675
60°	AZ = 0 EL = 0	AZ = 692 EL = 267	AZ = 570 EL = 570	AZ = 419 EL = 1337	AZ = 289 EL = 2012	AZ = 0 EL = 2278
70°	AZ = 0 EL = 0	AZ = 324 EL = 324	AZ = 267 EL = 692	AZ = 196 EL = 1625	AZ = 135 EL = 2445	AZ = 0 EL = 2769
90°	AZ = 0 EL = 0	AZ = 0 EL = 0	AZ = 0 EL = 0	AZ = 0 EL = 0	AZ = 0 EL = 0	AZ = 0 EL = 0

35 MPH WIND MOMENTS, FT-LB

	90°	70°	60°	40°	20°	0°
0°	AZ = 0 EL = 0	AZ = 4654 EL = 0	AZ = 3828 EL = 0	AZ = 2815 EL = 0	AZ = 1941 EL = 0	AZ = 0 EL = 0
20°	AZ = 0 EL = 0	AZ = 4109 EL = 227	AZ = 3381 EL = 485	AZ = 2486 EL = 1139	AZ = 1714 EL = 1714	AZ = 0 EL = 1941
40°	AZ = 0 EL = 0	AZ = 2731 EL = 329	AZ = 2247 EL = 704	AZ = 1652 EL = 1652	AZ = 1139 EL = 2486	AZ = 0 EL = 2815
60°	AZ = 0 EL = 0	AZ = 1163 EL = 448	AZ = 957 EL = 957	AZ = 704 EL = 2247	AZ = 485 EL = 3381	AZ = 0 EL = 3828
70°	AZ = 0 EL = 0	AZ = 544 EL = 544	AZ = 448 EL = 1163	AZ = 329 EL = 2731	AZ = 227 EL = 4109	AZ = 0 EL = 4654
90°	AZ = 0 EL = 0	AZ = 0 EL = 0	AZ = 0 EL = 0	AZ = 0 EL = 0	AZ = 0 EL = 0	AZ = 0 EL = 0

Figure 3-29

AZIMUTH AND ELEVATION-AXIS MOMENTS FOR CROSS-WIND CONDITIONS

50 MPH WIND MOMENTS, FT-LB

	90°	70°	60°	40°	20°	0°
0°	AZ = 0 EL = 0	AZ = 9497 EL = 0	AZ = 7813 EL = 0	AZ = 5745 EL = 0	AZ = 3962 EL = 0	AZ = 0 EL = 0
20°	AZ = 0 EL = 0	AZ = 8386 EL = 463	AZ = 6899 EL = 990	AZ = 5073 EL = 2325	AZ = 3498 EL = 3498	AZ = 0 EL = 3962
40°	AZ = 0 EL = 0	AZ = 5573 EL = 672	AZ = 4585 EL = 1436	AZ = 3372 EL = 3372	AZ = 2325 EL = 5073	AZ = 0 EL = 5745
60°	AZ = 0 EL = 0	AZ = 2374 EL = 914	AZ = 1953 EL = 1953	AZ = 1436 EL = 4585	AZ = 990 EL = 6899	AZ = 0 EL = 7813
70°	AZ = 0 EL = 0	AZ = 1111 EL = 1111	AZ = 914 EL = 2374	AZ = 672 EL = 5573	AZ = 463 EL = 8386	AZ = 0 EL = 9497
90°	AZ = 0 EL = 0	AZ = 0 EL = 0	AZ = 0 EL = 0	AZ = 0 EL = 0	AZ = 0 EL = 0	AZ = 0 EL = 0

90 MPH WIND MOMENTS, FT-LB

	90°	70°	60°	40°	20°	0°
0°	AZ = 0 EL = 0	AZ = 30771 EL = 0	AZ = 25315 EL = 0	AZ = 18615 EL = 0	AZ = 12836 EL = 0	AZ = 0 EL = 0
20°	AZ = 0 EL = 0	AZ = 27171 EL = 1502	AZ = 22354 EL = 3209	AZ = 16438 EL = 7532	AZ = 11334 EL = 11334	AZ = 0 EL = 12836
40°	AZ = 0 EL = 0	AZ = 18057 EL = 2178	AZ = 14855 EL = 4654	AZ = 10924 EL = 10924	AZ = 7532 EL = 16438	AZ = 0 EL = 18615
60°	AZ = 0 EL = 0	AZ = 7693 EL = 2961	AZ = 6329 EL = 6329	AZ = 4654 EL = 14855	AZ = 3209 EL = 22354	AZ = 0 EL = 25315
70°	AZ = 0 EL = 0	AZ = 3600 EL = 3600	AZ = 2962 EL = 7693	AZ = 2178 EL = 18057	AZ = 1502 EL = 27171	AZ = 0 EL = 30771
90°	AZ = 0 EL = 0	AZ = 0 EL = 0	AZ = 0 EL = 0	AZ = 0 EL = 0	AZ = 0 EL = 0	AZ = 0 EL = 0

power. Unfortunately, the Northrup heliostat design cannot capitalize on these effects in some environments because of a sand and dust mirror erosion concern; the heliostats must be stowed horizontally if high wind conditions are present or anticipated to preclude any possible mirror damage from blowing sand.

3.3.2 Mirror Module Trade Studies

The Northrup mirror module concept has evolved from an initial all-bonded mirror + Styrofoam + steel pan approach to the current all-steel stringer concept with many intermediate alternates in-between. Some of the intermediate configurations which were examined included:

1. Mirror + aluminum sheet + Styrofoam + aluminum sheet with the mirror bonded in the center and at the edges with a compliant adhesive.
2. Same as 1. except used fiberglass sheets.
3. Same as 1. except used galvanized steel sheets.
4. Same as 1., 2., and 3. except with polystyrene bead board in place of the Styrofoam.
5. Mirror + Styrofoam + glass sheet backing.
6. Mirror + tensioned panel.
7. Mirror + steel sheet + deep-formed polystyrene sheet (Nor-Core) + steel sheet.
8. Mirror + hollow steel pan + foamed-in-place polyurethane filler.
9. Mirror + steel sheet + steel egg-crate core + steel sheet.
10. Mirror + steel sheet + criss-cross corrugated steel panels + steel sheet.
11. Mirror + steel sheet + corrugated paper + steel sheet.
12. Mirror + fiberglass sheet + corrugated fiberglass panels (criss-crossed) + fiberglass sheet.

Although some of these alternate concepts were technically competitive with the current all-steel stringer approach, none were lower in material cost. For any mass produced product the key to a low finished product cost is the minimizing of material costs. The labor cost is seldom a major factor. The material costs varied from approximately $\$19.37/m^2$ ($\$1.80/ft^2$) to $\$29.60/m^2$ ($\$2.75/ft^2$) for the configurations analyzed with the lowest value being the selected approach, and the highest value being the fiberglass and Styrofoam configuration.

In addition to cost problems, some of the alternate concepts exhibited poor thermal performance; i.e., thermal de-focusing. For example, the mirror-polyurethane-steel pan configuration exhibits thermal curvature characteristics which vary from about 305 m (1000 ft) convex to 610 m (2000 ft) concave with no pre-curvature, or from flat to 213 m (700 ft) concave if a pre-curvature is built-in to avoid the convex cases. Even with thermally stabilized substrates such as the aluminum sheet-Styrofoam-aluminum sheet configuration, convex de-focusing would occur due to the frontside heating effect caused by the absorptivity of the mirror glass. The selected configuration is the best thermal performer because the silicone grease permits differential thermal expansion or contraction between the mirror and substrate, and also because the core stringers are non-compliant and restrict dimensional changes by their ability to carry compressive or tensile loads.

Perhaps the greatest objection to the selected mirror module configuration is weight. Compared to some of the lightweight alternates, the all-steel mirror modules are about twice as heavy which results in higher structural deflections and higher gravity moments which the drive unit must overcome. However, as discussed earlier, the gravity deflections can be largely eliminated by the software and the mirror module canting operation. The high gravity moment in reality is of little consequence to the drive unit because it is highest when the wind-induced moments are lowest (near-vertical heliostat elevation), and decreases greatly when the high wind moments are encountered (near-horizontal heliostat elevation).

3.3.3 Rack Structure Trades

The original Northrup heliostat rack structure utilized 6 tapered trusses, each of which was 8.5 m (28 ft) long, and weighed 80 kg (175 lb). The current configuration only uses 4 truss members, each of which is 6.4 m (21 ft) long, and weighs only 52 kg (114 lb). In terms of total truss weight a reduction from 477 kg (1050 lb) to 207 kg (454 lb) has been achieved.

The primary change in philosophy which enabled this reduction was to increase the size of the mirror modules. Initially, the modules were 1.22 m (4.0 ft) square, and a total of 34 modules were required for a heliostat. Currently, the module size is 1.22 x 3.66 m (4 x 12 ft), and only 12 modules are required for a heliostat. The larger mirror modules require less support structure. The module alignment process is simplified by the fewer number of modules, and the torque tube length is shortened because the span between the outer beams is lessened.

The truss design is a standard commercial configuration of the Butler Manufacturing Co. of Kansas City, Missouri. Alternate truss designs employing structural angles and solid bar web members were also examined before the Butler concept was selected. It was determined that the angle and bar concept for the same depth was heavier, was more susceptible to web buckling, provided less lateral compression chord stability, and required arc welding of all joints. The Butler design is available in the proper depth for drive unit clearance, can be obtained in lengths suitable for prototype fabrication, and is an existing, commercially available item which is being mass produced in an automated facility.

Other structural configurations were analyzed between the original and final concept which progressively enhanced the design by reducing the number of parts and the structural weight. These included a central support for the 1.22 x 1.22 m (4 x 4 ft) mirror module which enabled the length of the 6 truss members to be reduced from 8.5 m (28 ft) to 7.3 m (24 ft), and the torque tube span to be reduced from 6.2 m (20.5 ft) to 5.0 m (16.5 ft). A subsequent concept employed mirror modules which were 1.83 x 1.83 m (6.0 x 6.0 ft) arranged in a 4 x 4 matrix on the heliostat. A central module attachment method was again considered which enabled the number of support trusses to be reduced from 6 to 4, and the truss length to be reduced to 5.8 m (19.0 ft). However, this concept was discarded due to a severe cost penalty associated with the large 1.83 x 1.83 m (6.0 x 6.0 ft) mirror size.

The current approach uses a total of 12 mirror modules, each 1.22 x 3.66 m (4.0 x 12.0 ft). A total of 4 truss members are required for support, each of which is 6.4 m (21.0 ft) long. The spacing between the two trusses which support a given mirror module was chosen to be 2.13 m (7.0 ft). This support distance results in the gravity sag across the 3.66 m (12.0 ft) width always being concave-shaped for image enhancement. This truss-to-truss span coupled with the narrow elevation drive unit resulted in a required torque tube length of 2.8 m (9.2 ft) each.

With the Northrup design concept, the torque tube passes through the truss in the central triangular-shaped zone bounded by the web tubing and the bottom chord. The largest practical tube size which can pass through the truss opening is approximately 0.41 m (16 inches). This outside diameter and a wall thickness of 3.2 mm (0.125 inch) was originally selected for the torque tube. For the required length of 2.8 m (9.2 ft), this resulted in a weight of 88.5 kg (195 lb) per tube. At the time of selection, this presented no interface problem with the then-current drive unit (a relatively large 2-stage

worm and gear unit). However, subsequent drive studies led to a simpler, more compact drive unit. As a result, the large diameter torque tube created a match-up problem with the small drive. The trade-off options were to increase the drive unit size (which would involve a larger gear casting, housing, bearing, and seal), or to neck-down the torque tube using a concentric pipe fitting reducer, or to decrease the torque tube diameter for its entire length. The latter approach was selected. A standard 12 inch x Schedule 20 pipe having a 0.32 m (12.75 inch) outside diameter and a 6.35 mm (0.25 inch) wall thickness is now specified for the torque tube. Even though it is considerably heavier at 140.9 kg (310 lb) each, it is believed to be the most technically acceptable and economic of the alternatives.

3.3.4 Drive Unit Trade Studies

The drive unit has perhaps been the most "studied" of the various elements of the Northrup heliostat. It is the most costly element, and the most sensitive one in terms of dependence on wind loads, gravity loads, heliostat shape, electronic performance, motor characteristics, etc. The drive unit evaluation and selection was further complicated by the multiplicity of possible types of gearing available, the large number of gear ratio combinations for each type of gearing, the number of gear stages employed, the different stepper motor performance characteristics which accompany different electronic driver hardware and software techniques, and the wide variety of available physical options such as materials and bearing selection. A brief chronology of the Northrup drive unit evolution is as follows:

1. The originally proposed concept was based on using a stepper motor, and two worm gear stages for both the azimuth and elevation drive systems. An 80:1 ratio was planned for the input stage, and a 52:1 ratio for the output stage. A relatively large stepper motor (a Superior Electric Co. Model M172-FD306) and sophisticated TM-600 translator was required. Since the motor cost was quite high, an effort was initiated to seek a modification which would enable a smaller motor to be used.

2. The next evolutionary step maintained the two worm gear stages (80:1 stage 1 and 52:1 stage 2), but added a small 3:1 gear stage at the motor. The motor selected was a Superior Electric M112-FJ326 unit with a TM600-type of translator. Since the motor was considerably more expensive than the small gear box, a logical step was to increase the gear box ratio, and use a smaller motor. With an 11.5:1 gear box ratio, adequate torque and slew rate could be obtained with an M093-FD301 motor with an accompanying saving of nearly $200 per drive unit.

3. At this point, the drive unit employed three gear stages, a relatively small motor, and a sophisticated translator. An optimization study was next performed to determine if an economic and technical optimum set of gears could be obtained for the stage 1 and 2 worm gear set. Backlash, output torque, drive unit weight, tooth stress, and

material and gear costs were evaluated for over forty combinations of gear size, ratio, and diametral pitch. Figure 3-30 shows the results for nine such combinations. The main conclusion from this study was that no major cost or technical advantage was obtained by varying the stage 1 and stage 2 gearing over a wide range; i.e., the basic concept was performance, weight, and cost constrained. Any major saving would have to be obtained by a change in concept rather than an optimization within the confines of the three stage concept.

4. To reduce unit weight and cost, and to simplify the design, an effort was initiated to eliminate the first worm gear stage by employing a larger ratio gear box at the motor. A low cost, triple reduction gear box, Model 030-415-0115, manufactured by Bison Gear & Engineering Corp. was selected for the input stage. It provided a 115:1 gear ratio, an output torque capability of 2886 kg-cm (2500 lb-in), and a considerably higher efficiency than a comparable worm gear stage. However, the size of output worm gear and its ratio increased significantly to a 1.09 m (43 inch) pitch diameter and 172:1 ratio. In spite of this large size, the overall material and gear cost for the complete drive was reduced by about 15% with this concept. Figure 3-31 presents the performance characteristics for this drive unit. Figure 3-32 shows a perspective rendering of the one-worm configuration which highlights the use of the azimuth gear as a turn-table for the elevation drive, the 1/3 sector elevation worm gear, and the use of Camroll bearings for motion and support.

5. A cost trade-off between the use of the small, Model M092-FD310, stepper motor and its companion TM600 electronic translator versus using a somewhat larger, Model M112-FJ326, stepper motor and its TBM-105 translator was next performed. It was found that even though the larger motor is higher in cost, the combined motor and translator cost is less. Hence, a change was made to the M112-FJ326 stepper motor and TBM-105 translator which has been maintained through the current approach. (Note: A recent problem with the planetary efficiency has necessitated a further motor change to a higher torque M112-FJ327 motor).

Figure 3-30

PERFORMANCE FOR 2-STAGE WORM DRIVE CONCEPT

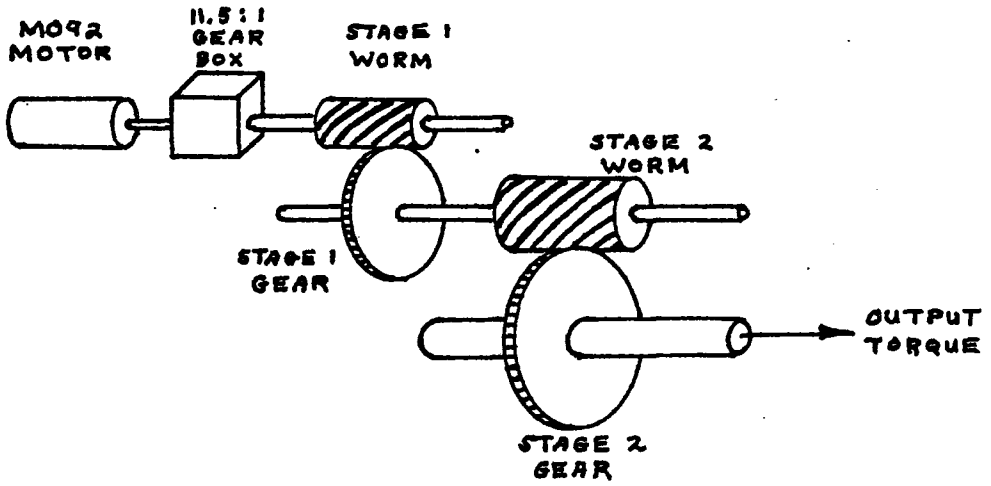

DRIVE UNIT PERFORMANCE

STAGE 2 WORM AND GEAR	STAGE 1 WORM AND GEAR		
D. P. = 1.5 GEAR P.D. = 16" WORM P.D. = 4" RATIO = 24:1 BACKLASH 0.63 mrad	8 D. P. 144:1 GEAR P.D. = 18" T = 10979 ft-lb S = 10745 psi W = 1681 lb C = $1528	6 D. P. 120:1 GEAR P.D. = 20" T = 9680 ft-lb S = 5440 psi W = 1693 lb C = $1561	5 D. P. 120:1 GEAR P.D. = 22" T = 9355 ft-lb S = 2961 psi W = 1717 lb C = $1660
D. P. = 2 GEAR P.D. = 20" WORM P.D. = 4" RATIO = 40:1 BACKLASH 0.50 mrad	8 D. P. 96:1 GEAR P.D. = 12" T = 10305 ft-lb S = 11374 psi W = 1699 lb C = $1533	6 D. P. 96:1 GEAR P.D. = 16" T = 10881 ft-lb S = 4825 psi W = 1719 lb C = $1566	5 D. P. 100:1 GEAR P.D. = 20" T = 11928 ft-lb S = 2326 psi W = 1731 lb C = $1665
D. P. = 2 GEAR P.D. = 27" WORM P.D. = 4" RATIO = 54:1 BACKLASH 0.37 mrad	8 D. P. 80:1 GEAR P.D. = 10" T = 11632 ft-lb S = 10197 psi W = 1755 lb C = $1575	6 D. P. 72:1 GEAR P.D. = 12" T = 11079 ft-lb S = 4771 psi W = 1769 lb C = $1601	5 D. P. 70:1 GEAR P.D. = 14" T = 11350 ft-lb S = 2478 psi W = 1772# C = 1670

Figure 3-31

INITIAL CONFIGURATION OF A 1-STAGE WORM DRIVE

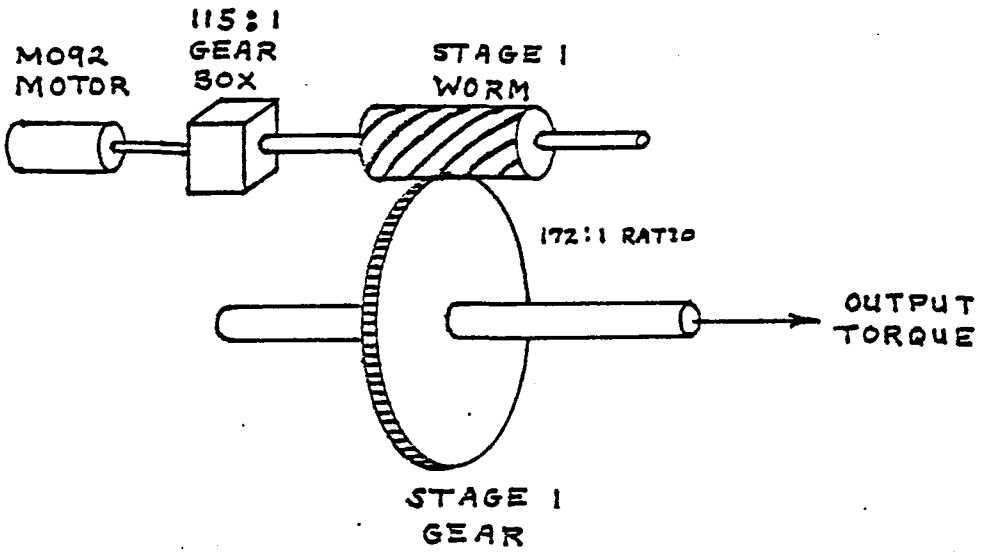

CHARACTERISTICS

	WORM	GEAR
DIAMETRAL PITCH	4	4
PITCH DIAMETER	3.00"	43.00"
NO. OF THREADS/TEETH	1	172
THREAD/TOOTH STRESS	34009 psi	10769 psi
MATERIAL	STEEL	CAST IRON
WEIGHT, AZIM	6 lb	102 lb
WEIGHT, ELEV	6 lb	34 lb
FACE WIDTH	3.50"	1.50"
MAXIMUM TORQUE	-	9640 ft-lb
BACKLASH EFFECT	-	0.23 mrad

Figure 3-32

PERSPECTIVE VIEW OF THE INITIAL

NORTHRUP 1-WORM DRIVE UNIT

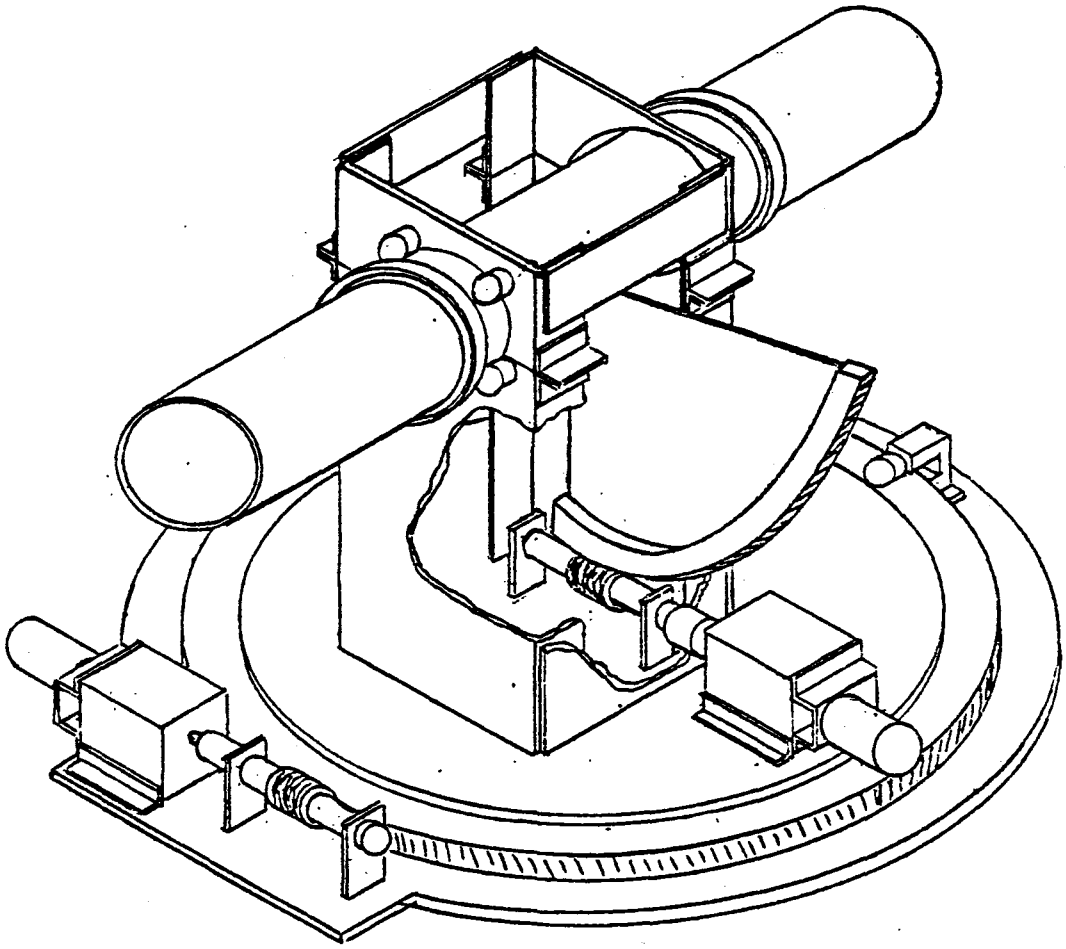

6. With the large worm gear size which resulted from using the 115:1 helical gear box, an interference problem between the azimuth motor and the mirror modules occurred. Rather than increasing the drive off-set to achieve more clearance, it was determined that the problem could be more cleanly resolved by fixing the azimuth gear (i.e., a non-revolving azimuth gear) and allowing the worm instead to "crawl-around" the azimuth gear. With this change the protruding azimuth and elevation motors always maintain the same relative position to the mirror modules during azimuth maneuvers; i.e., the motors always protrude in a direction opposed to the azimuth pointing vector. Additional changes involved the elimination of the internal support structure and sheet metal cover, and the addition of a load-carrying, cast-iron enclosure. Figure 3-33 presents an exploded view of this fixed-azimuth drive unit concept. It will be noted that Camroll bearings are employed in 19 places to provide the necessary rotating supports.

7. During the latter stages of the drive unit evolution, the Winsmith Division of UMC Industries was working closely with Northrup as a potential fabricator and alternate-design consultant. Winsmith proposed a concept employing a large-ratio, high-torque planetary unit which replaces the triple reduction helical gear box. This higher planetary ratio (450.45:1 vs 115:1) enabled the worm gear stage to be greatly decreased in ratio and size. The decreased gear size in turn enabled the use of two ball-and-race bearings of a size which became cost-competitive with the 19 individual Camroll bearing elements. Furthermore, the bearing emplacement opens the possibility for a future simplification and cost reduction by using the housing and gear body as the bearing race. The bearing support would then be achieved by simply inserting the steel balls during the drive assembly. Figure 3-34 presents a perspective view of the Winsmith drive unit.

The trade-off study between the helical gear box/large worm gear/Camroll bearing concept and the planetary gear stage/small worm gear/ball-and-race configuration resulted in a virtual tie.

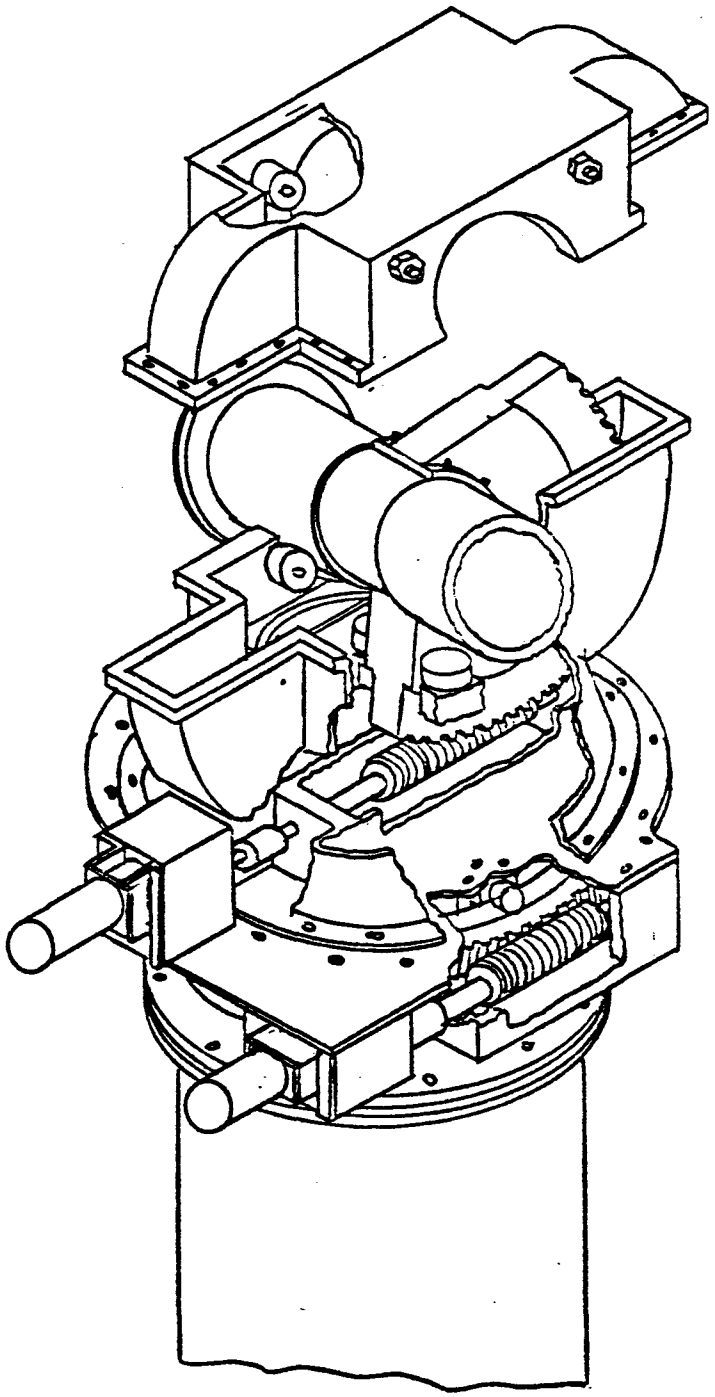

Figure 3-33

NORTHRUP FIXED-AZIMUTH DRIVE
EXPLODED VIEW

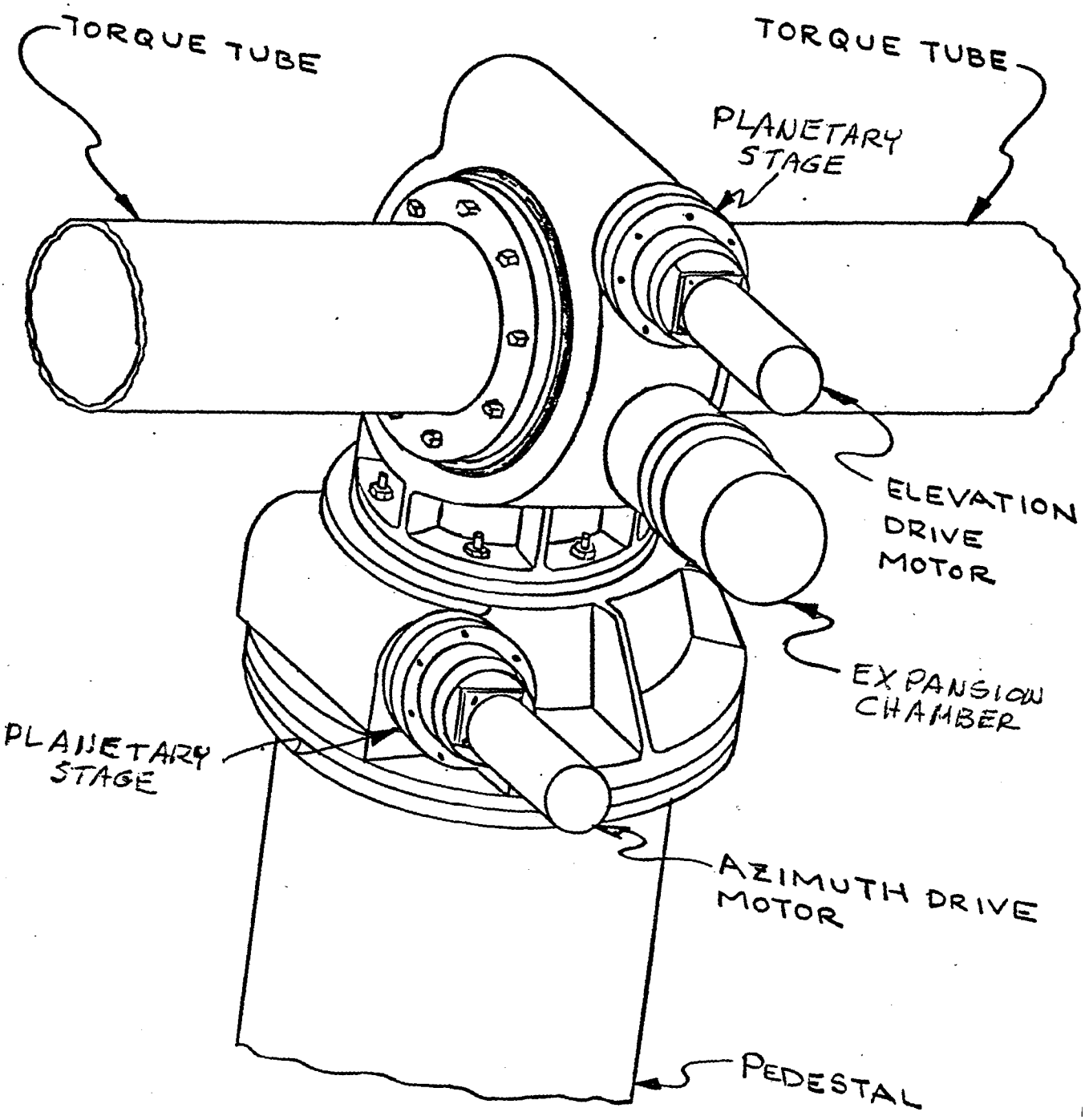

Figure 3-34

Perspective View of Northrup Drive Unit

The output torque characteristic, drive efficiency, total unit weight, total material and piece part cost, and slew rate-at-required torque were within a few percent of each other. The Winsmith drive concept was selected based on several decisive features:

1. Possibility for future cost savings using integral bearing concept.

2. Unit is oil-filled and sealed versus oil-bathed and vented for the alternate. The moisture condensation concern is eliminated, and the bearings are subjected to continuous lubrication.

3. The planetary gear box offers flexibility in future motor-gear ratio trade-offs. The planetary gear ratio can be varied over a very large range without changing the size of the enclosure envelope or interface. Future advances in the motor drive translator and software might enable the use of a smaller (but higher pulse rate) motor which might in turn necessitate a higher planetary gear ratio.

4. The selected drive unit is simpler and has significantly fewer parts, fewer machining operations, and fewer assembly adjustments than the alternate using discrete Camroll bearings. Even though the material and piece parts costs for the two alternates are comparable, the assembly time and cost are projected to be less with the selected approach.

3.3.5 Stow Position Trade Studies

The baseline Northrup heliostat is designed to be stowed in either a vertical position or a face-up horizontal position. Vertical is the preferred orientation to enable natural rain washing of the mirrored surface. The horizontal, face-up orientation is an optional stowage position which may be selected for any given day if high winds are anticipated in locations where blowing sand or debris might result in mirror damage. The choice of these options is controlled by the computer software.

An additional stowage option is available on the Northrup heliostat which permits a face-down horizontal stow position. Two torque tube adapters are required with this option; the primary purpose of the adapters being to provide a central slot which enables the mirror modules to clear the pedestal during the "turn-under" maneuver. A second function of this adapter is to provide a center-line offset between the torque tube and the elevation drive axis. This offset essentially eliminates the gravity moment, which at its maximum is approximately 596 kg-m (4300 ft-lb). However, since the maximum gravity moment and maximum wind moment occur at different elevation angles, the maximum combined moment for a 22 m/s (50 mph) wind is only reduced from 1607 kg-m (11624 ft-lb) to 1313 kg-m (9497 ft-lb). Figure 3-35 shows the design of the torque tube adapter.

The two baseline heliostats delivered to Sandia-Albuquerque do not include the torque tube adapters for face-down stow. However, heliostat #3 at the Northrup-Hutchins test facility is outfitted with the adapters. Figures 3-36a and 36b present a series of photographs of this configuration.

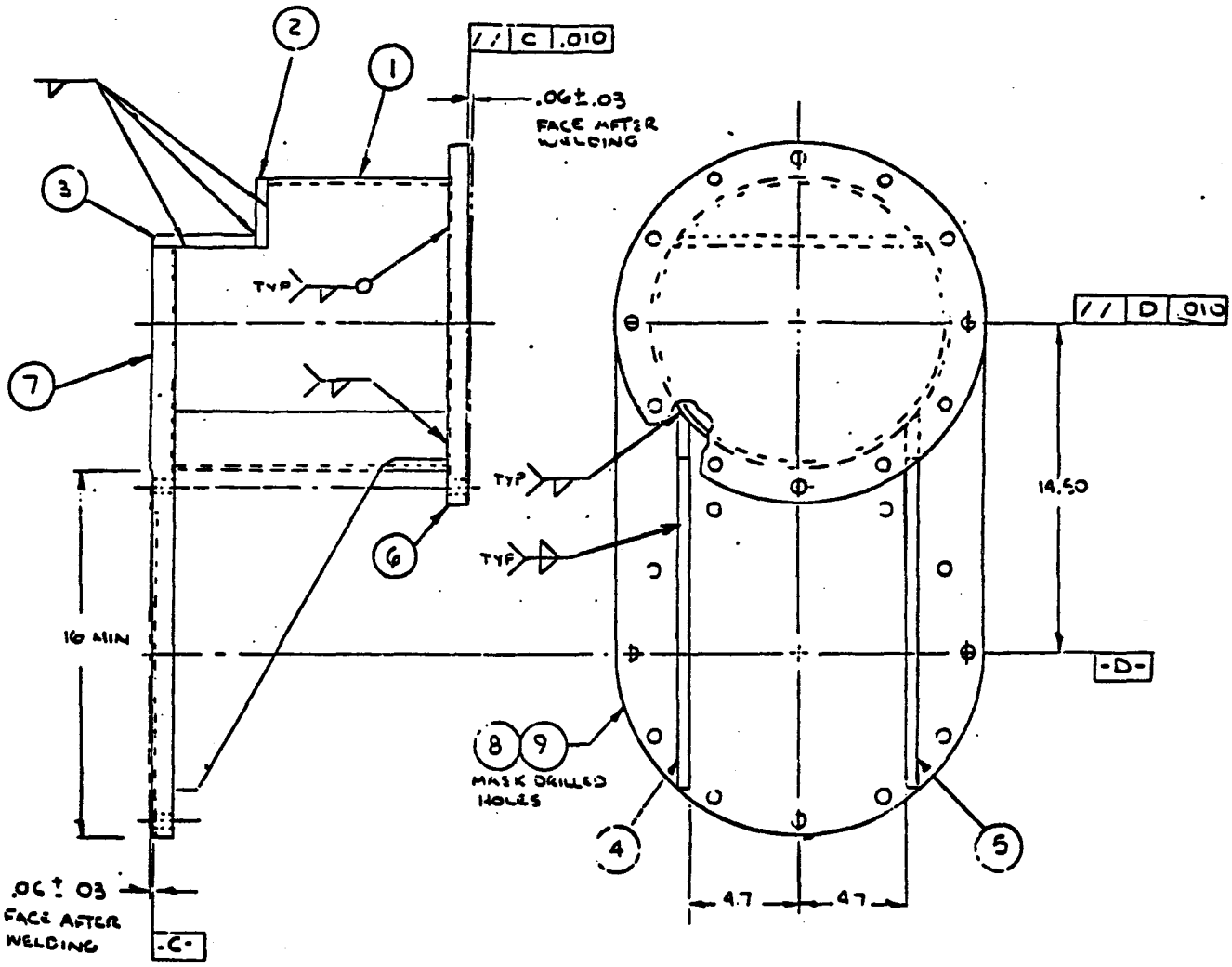

Figure 3-35

Torque Tube Adapter For Face Down Stow Option and Reduced Gravity Moment

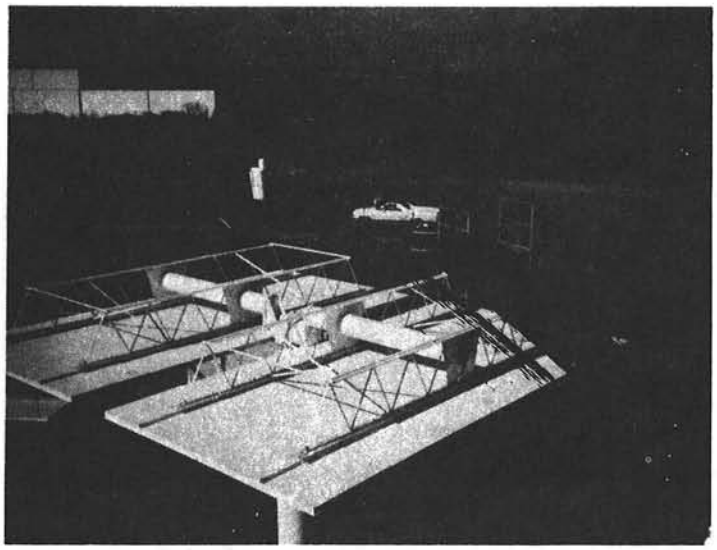

FACE DOWN STOWAGE FEATURE
RESULTING FROM REDUCED MOMENT ADAPTER
HELIOSTAT #3 AT HUTCHINS, TEXAS

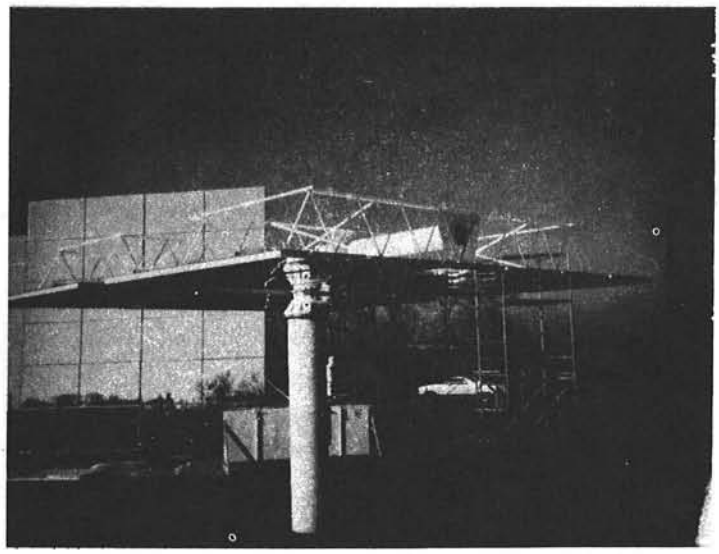

Figure 3-36a

SLOTTED HELIOSTAT CONFIGURATION
RESULTING FROM REDUCED MOMENT ADAPTER
HELIOSTAT #3 AT HUTCHINS, TEXAS

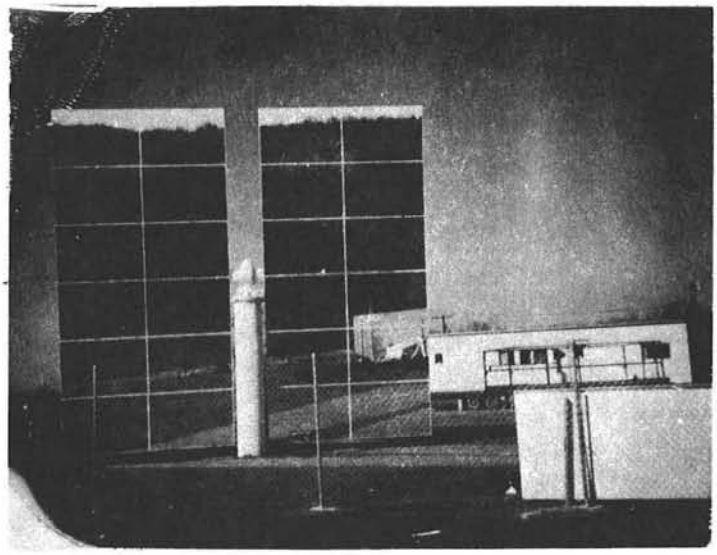

Figure 3-36b

3.4 SUMMARY OF TEST RESULTS

The following section presents the test results pertinent to the current, baselined Northrup II heliostat design. Additional tests and fabrication development experiments were performed on the Northrup I drive unit and a variety of mirror module candidates. The results of these tests were useful in the design progression, but are not included in this report as they are no longer relevant.

Appendix G provides a more detailed description of the test conditions and results.

3.4.1 Electronic Tests Summary

3.4.1.1 Limit Switch Tests

The accuracy of the electronics and stepper motors is dependent on the position reference offered by the home position switch. In order to verify part specifications and obtain confidence in the design a limit switch tester was constructed. This tester consisted of a small stepper motor driving an actuator through several stages of gear reduction. Special software was designed to drive the motor into the switch, back it off, and record the position. The accuracy of each step of the motor was .000047 inch which amounts to .0047 mr for a 10" arm. The test was performed over a period of three days and a few hundred data points obtained. The repeatability was within plus or minus 3 steps. Results of some of the tests are shown in Figure 3-37.

3.4.1.2 Translator Tests, Bench and Heliostat

Three different translators were procured and a fourth designed and built. The results of the evaluation is explained in Section 9.4.4.

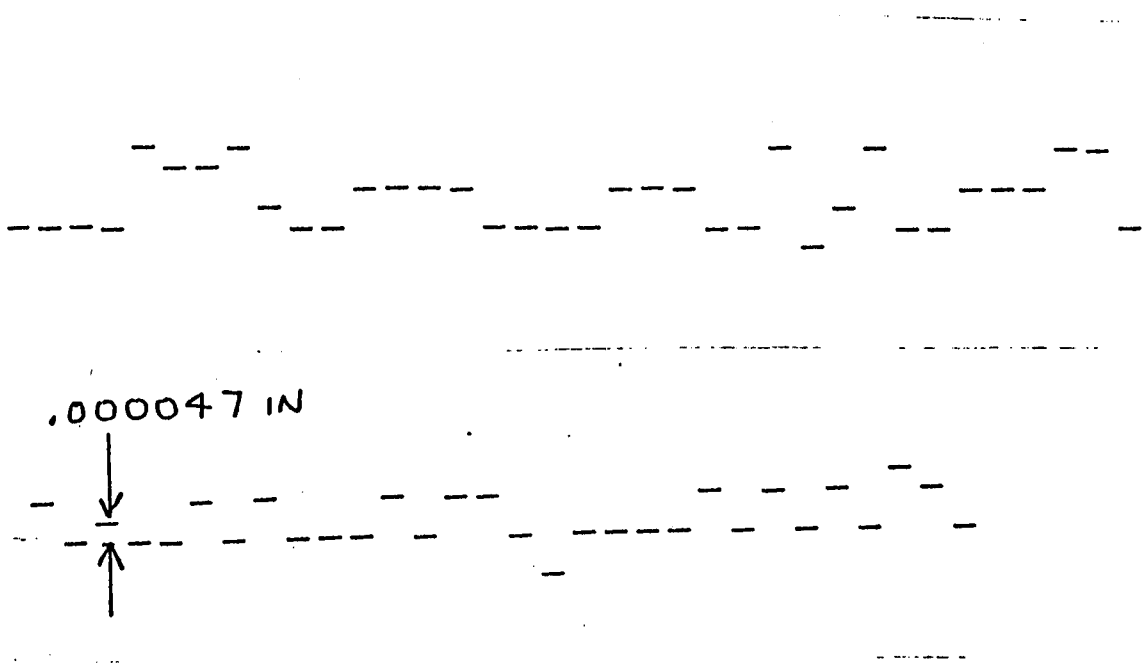

Fig.3-37 Limit Switch Test Position Repeatibility Data Chart

The first type of translator tested was the Superior Electric STM 101. This unit consisted of power drivers and sequential switching logic. This translator required either external pulses or allows internal speed control. The design simulates constant current to the motor with high supply voltage and series resistors. This translator has the disadvantage of dissipating more power when the motor is at rest than when moving. The power supply required is 24 volts at 6 amperes. Since the motor windings see a constant voltage source in series with a resistor, the motor quickly runs out of torque at the higher speeds due to the back emf generated. The internal logic in the translator converts input pulses to a logic configuration shown in Figure 3-38. This logic can be easily generated by a microprocessor.

A simplified translator was built and software designed to drive the heliostat in a tracking mode. This translator was tested on the Northrup I heliostat. The Commodore computer was used to drive the translator. A BASIC program was used to calculate the step commands from time of day, heliostat and target coordinates. The step commands were then passed to a machine language program that drove the translator. The translator interfaced to the computer through a 6522 versatile interface adapter. A small stepper motor was used to drive the Northrup I heliostat through the existing motor and gearhead. This was enough to demonstrate tracking but not slew. Slewing was accomplished with the AC Bodine motor. Good tracking was demonstrated with the stepper motor for about a six hour period.

A low power mode was demonstrated with the Northrup translator design. This was accomplished by adding a fifth mode to the logic table that turned off all the transistor switches at once. The drawback to this method is that no holding torque is available during the low power mode. Test results on the heliostat showed no loss of steps during the low power mode on elevation and some loss of steps in azimuth. Later analysis of the azimuth problem showed an abnormal amount of backdrive in the drive mechanism due to a soft rubber coupling between the original motor and the Stage 1 worm shaft.

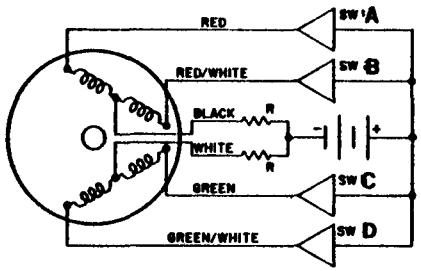

DC Stepper Motor and Control Switching Schematic

STEP	Sw. A	Sw. B	Sw. C	Sw. D
1	On	Off	On	Off
2	On	Off	Off	On
3	Off	On	Off	On
4	Off	On	On	Off

CW Motor Rotation Winding Sequence Logic

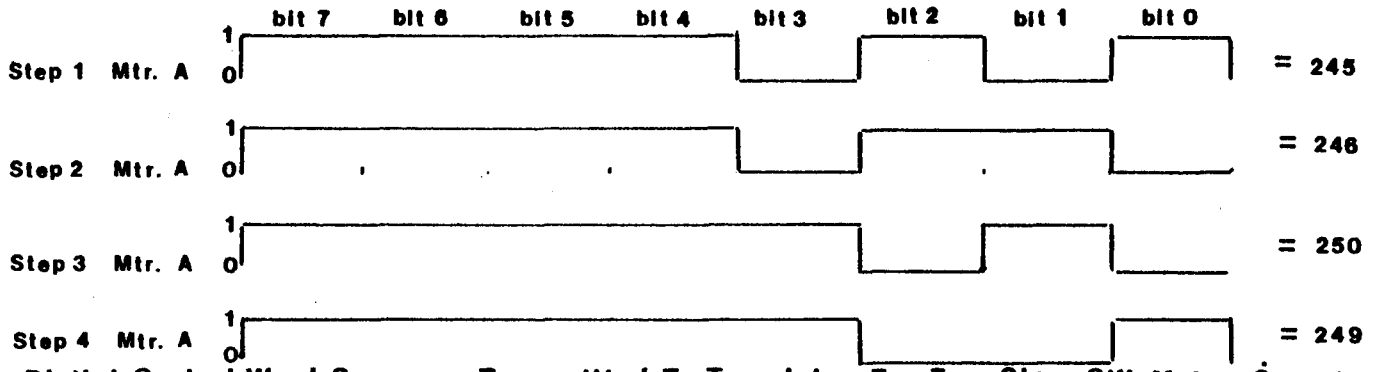

Digital Control Word Sequence Transmitted To Translator For Four Step CW Motor Operation

Fig. 3-38 Stepper Motor and Translator Control Word Logic Sequence, CW Motor Operation

Software for driving the translator was developed for a stand-alone heliostat controller. By using the Commodore computer for the development system we were able to change from the BASIC heliostat driver to a machine language driver in one computer and a serial data transfer to another computer. Once the machine language program was checked out, the program was burned in a 2716 EROM that was plugged into the Commodore computer and tested. Once checked out, a breadboard was built and checked for driving the stepper motors through the Northrup translator. After checking out the motor speed torque characteristics on a dynamometer it indicated a need for improved torque at high speeds. Several software strategies were developed for slewing the motor at high speeds. These techniques involved pulsing the motor during each step. This technique showed the need for analog feedback to control the motor current in the absence of current limiting resistors.

Procurement of the switching translators showed that an involved method of current and pulse feedback along with high voltage on the motor windings would afford much higher speed and torque.

3.4.1.3 TC 600 Translator Tests

The Superior Electric TC 600 translator was tested for performance with the M112-FJ326 and the M092-FD810 motors. The results showed good torque/speed performance and a high amount of heating in the stand-by mode. The translator required four external supplies one of which was 70 volts at 10 amperes peak current. The unit generated high current switching transients at a frequency higher than the stepping rate.

3.4.1.4 TBM 105 Translator Tests

The TBM 105-0214 and the TBM 105-1230 were tested with the M092-FD310 and the M112-FJ326 respectively. The results showed moderate torque/speed performance and small amount of motor heating. The translator was self contained and only required a 110 volt supply. The only transients generated were the stepping signals to the motor.

3.4.2 Mechanical Test Summary

3.4.2.1 Summary of Heliostat Wind Tunnel Tests

The ASCE flat plate aerodynamic data are generally considered reliable and can be used with confidence for static wind loads predictions on isolated flat plate heliostats. Also dynamic wind loading does not appear to be a problem area needing investigation. Therefore in order to reduce the predicted large wind induced pitching moment loads on the elevation drive mechanism of the heliostat (the maximum occurred at 20-degrees angle of attack), it was decided to wind tunnel test various slotted and offset-panel heliostat configurations.

Three model heliostat configurations were wind tunnel tested. Two configurations had air slots formed by displacing the mirror modules laterally (in the plane of the mirrors). The third configuration had an offset panel where several of the heliostat individual mirror modules were displaced perpendicular to the plane of the mirrors to form slots.

All tests were conducted in the University of Texas at Arlington low-speed wind tunnel at a Reynolds number of approximately 700,000 and at a free stream dynamic pressure of 14.5 lb/sq. ft. In order to minimize scaling effects and wind tunnel boundary effects, each model configuration was tested with open slots and then immediately re-tested with tape covering the slots (thus forming a solid model). These tests results were compared with each other to determine the relative effects of the slots. The results are presented in Figures 3-39, 3-40, and 3-41. They are plotted as ratios of slotted model aerodynamic moments (or forces) divided by solid model aerodynamic moments (or forces). These moments and forces have been adjusted (normalized) to correspond to equal-reflective-area heliostats.

The results of the wind tunnel tests indicate that in general the slots caused reductions in lift, drag, and pitching moments about the mid-chord position (middle) of the models. The amount of reduction in pitching moment at 20-degrees angle of attack varied from approximately 10% for a lateral slot configuration to approximately 30% for the offset configuration. These reductions indicate that there should also be reductions in the maximum wind induced loads on the elevation drive mechanism of the full-sized heliostat.

FIGURE 3-39

WIND TUNNEL TESTS - PICTURE FRAME SLOTS

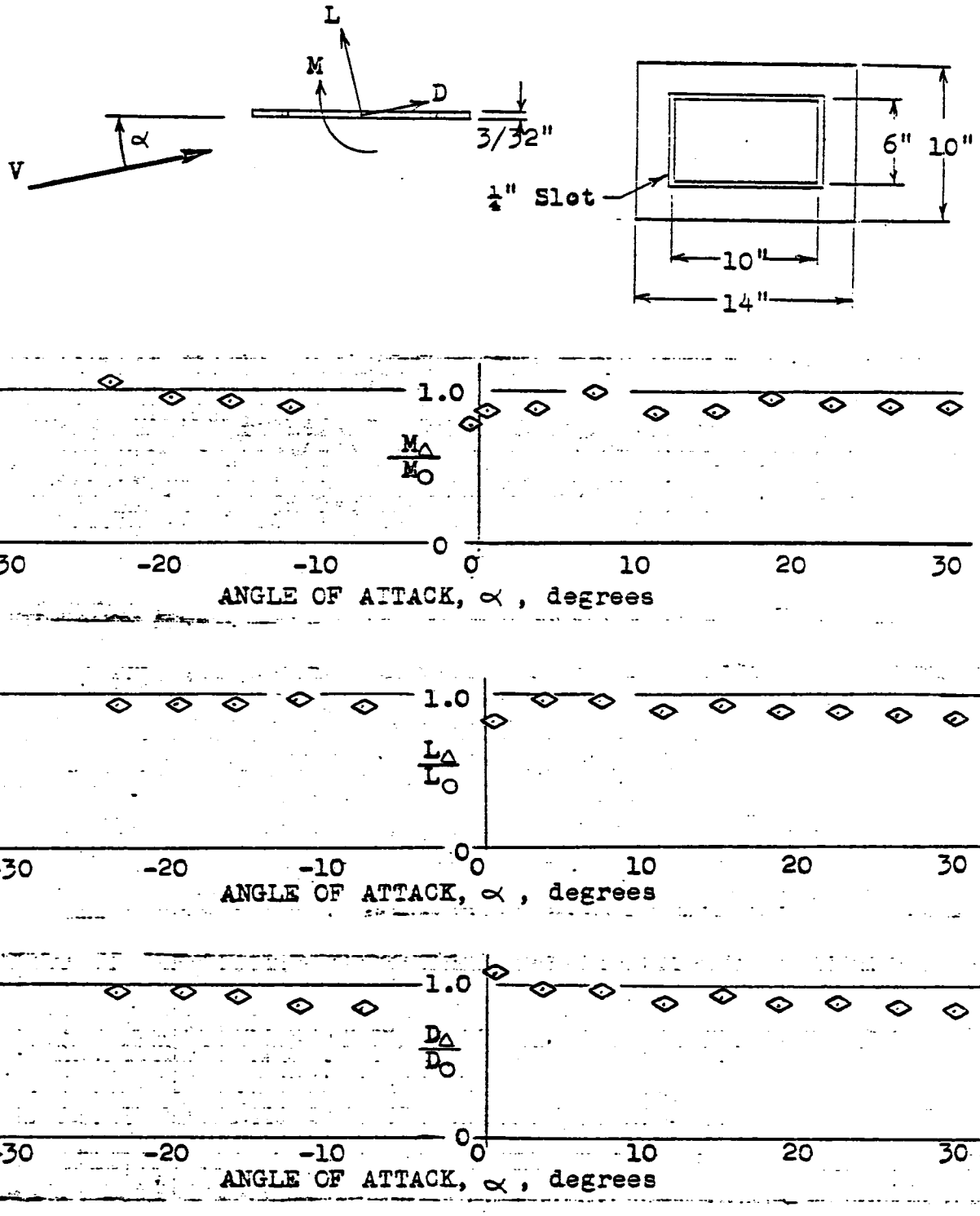

Wind tunnel test results for heliostat model #3 with outside facets laterally separated to form slots. Ratios graphed are for the slotted model pitching moment, lift, and drag divided by the solid model pitching moment, lift, and drag, respectively.

FIGURE 3-40
WIND TUNNEL TESTS - THRU SLOTS

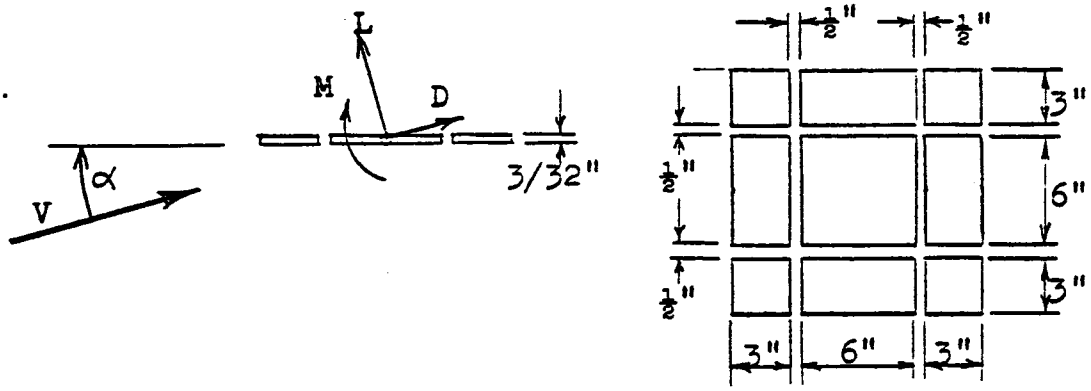

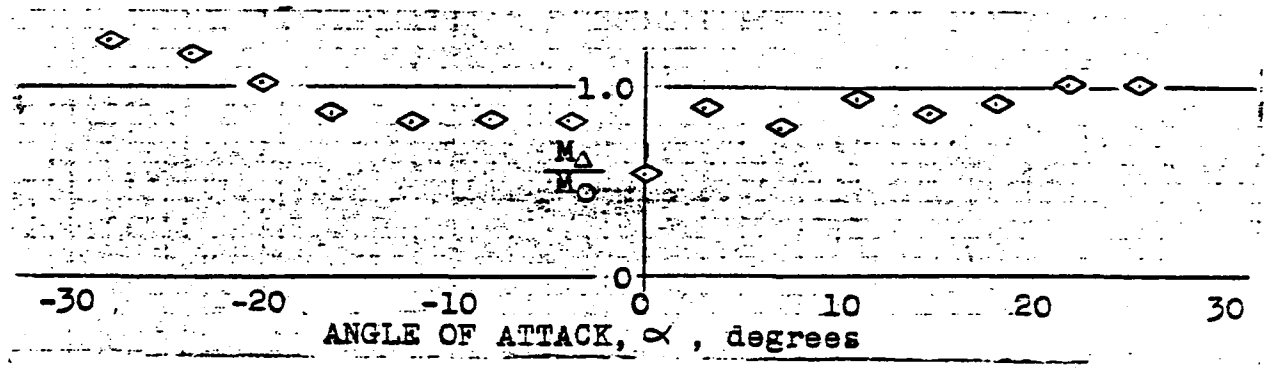

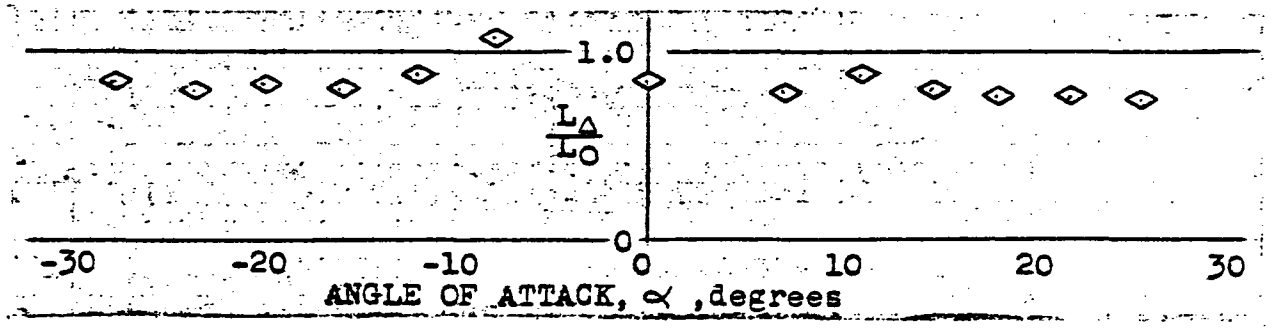

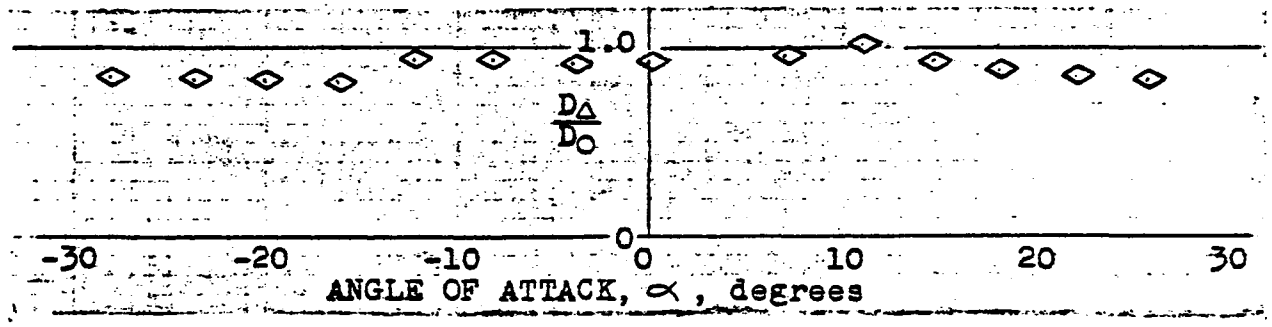

Wind tunnel test results for heliostat model #4 with outside facets laterally separated to form slots. Ratios graphed are for the slotted model pitching moment, lift, and drag divided by the solid model pitching moment, lift, and drag, respectively.

FIGURE 3-41

WIND TUNNEL TESTS - OFFSET FACETS

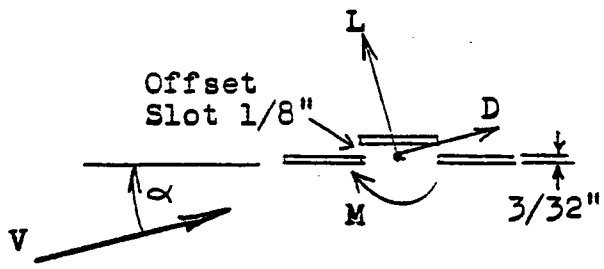

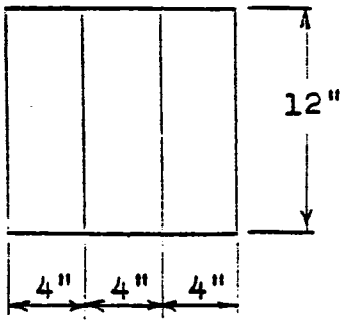

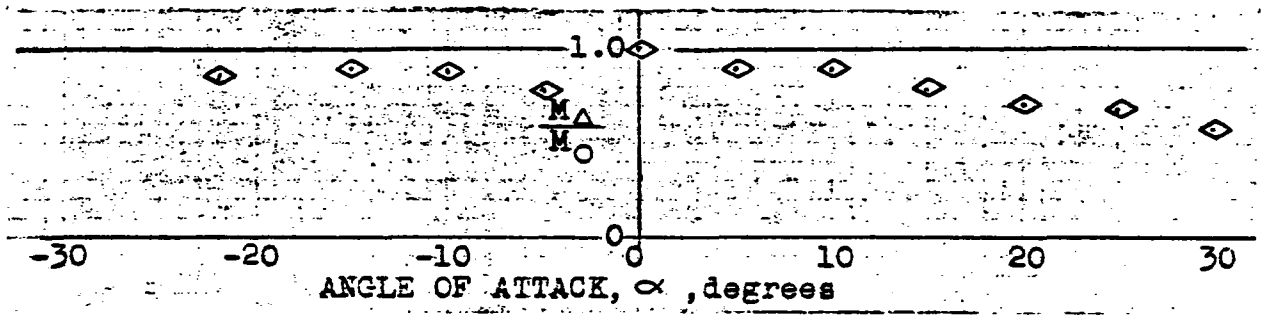

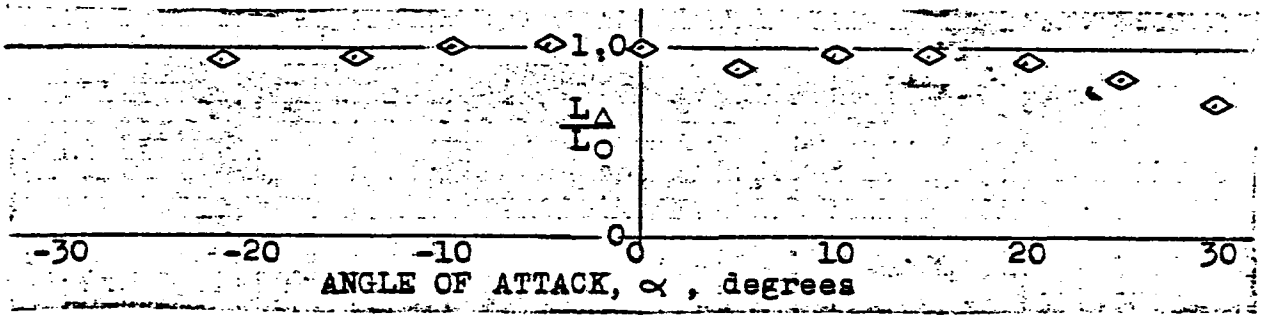

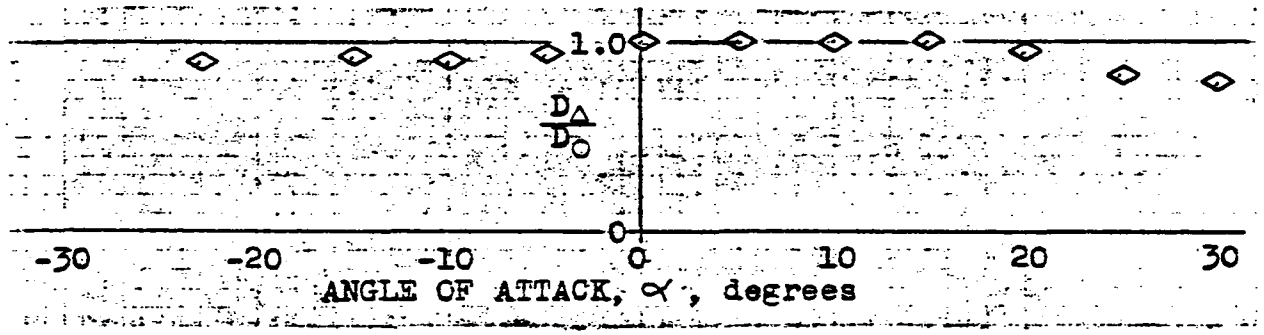

Wind tunnel test results for heliostat model #5 with central facets offset from the plane of the mirrors. Ratios graphed are for the slotted model pitching moment, lift, and drag divided by solid model pitching moment, lift, and drag, respectively.

3.4.2.2 Humidity Tests, Silicone Grease

A humidity test of the silicone grease was performed to measure its effectiveness as a mirror backing protection. Mirror samples were suspended in a 60°C (140°F), 100% relative humidity-condensing environment for a total of 1600 hours. The mirror samples were of the "hardware-store" variety, and had no supplemental paint protection on the backside. One sample was coated with the light viscosity silicone grease (Dow Corning #7 compound), one sample with the medium viscosity silicone grease currently specified for the mirror modules (Dow Corning #4 compound), and a third sample was ungreased. The ungreased specimen showed major silvering degradation, the light viscosity silicone specimen showed one small blackened area where a support string was tied, and the specimen coated with the medium viscosity #4 compound showed no degradation. The conclusion reached is that the Dow Corning Silicone Compound #4, which was developed as an aircraft ignition system moisture sealant, offered excellent mirror silvering protection.

3.4.2.3 Mirror Module Hail Test

Extensive mirror module hail tests have been performed throughout the contract period to verify the adequacy of the mirror-silicone grease-steel substrate to resist breakage. Some initial tests were performed with "specification" ice balls of 0.75 inch diameter at speeds of 65 ft/sec. However, breakage was virtually non-existant, so subsequent tests were all performed with "margin" ice balls of 1.0 inch diameter.

A pneumatically-powered hail gun was constructed at the Northrup-Hutchins facility. Photoelectric sensors were employed to measure the time interval over a fixed, known distance which enabled the velocity to be computed. Various velocities were achieved by adjusting the chamber pressure which propelled the hail balls. The firing of an ice ball was accomplished by an electrical switch which in turn would trigger a solenoid valve to release the high pressure air into the barrel. Spherical ice balls of 1.0 inch diameter were made in a 2-piece aluminum mold which was fabricated specifically for this purpose. To insure adequate hardness, the ice balls were frozen and chilled to 20°F maximum.

For ice balls fired into the mirror interior area (away from the edges), velocities as high as 140 ft/sec could be tolerated without breakage. Edge hits would generally pass velocities up to 100 ft/sec. Infrequent breaks would occur at or near the edges at velocities near 75 ft/sec. It is believed that these were generally caused by an existing edge defect such as a minute crack or chip, and an impact in the near vicinity would cause the defect to propagate from the defect to the impact zone. Generally, breakage was very infrequent even with the "margin" ice balls of 1.0 inch diameter, and velocities well above 75 ft/sec. Hence, the mirror module design is felt to be very adequate from the hail impact standpoint.

3.4.2.4 Mirror Module Thermal Cycling-Freeze/Thaw

A single mirror module (S/N 200078) was subjected to a series of thermal cycles in the Northrup environmental control room. A total of 10 cycles were performed. A thermal cycle consisted of heating to 120°F at the rise rate of 60°F/hour, stabilizing at this level for 30 minutes, spraying with ambient temperature water for 2-3 minutes, ramping down at 60°F/hour to 15°F, stabilizing at this level for 30 minutes, spraying with ambient temperature water for 2-3 minutes, and then cycling back to 120°F.

The objective of this test was to demonstrate the functional and structural integrity of the mirror module. The primary aim was to determine if any damage results from thermal cycling, thermal shock, or freezing. Another equally important goal was to visually check the appearance for distortions or curvatures at the temperature extremes.

The test instrumentation consisted of 4 thermocouples for measuring mirror module temperature at the following locations:

a. Backside module sheet-adjacent to 48" rectangular cross support member-left side.

b. Backside module sheet-adjacent to 48" rectangular cross support member-right side.

c. Mirror face-left end-approximately 3" inboard and near center of 48" width.

d. Mirror face-right end-approximately 6" inboard and near center of 48" width.

In addition to these temperature measurements, an optical "zebra-board" was constructed to enable a qualitative evaluation of mirror distortion and/or curvature to be made. The "zebra-board" was fabricated from a 4' x 12' mirror-less mirror module, painted white, and gridded with 1/2-inch wide black stripes on 4-inch centers. The "zebra-board" image in the mirror module being tested was visually examined and photographed at each temperature extreme.

The test results indicated a complete success. No damage resulted from the thermal cycling, the thermal shock from the water spray, or from the resulting freeze-thaw cycles. The visual observations of the "zebra-board" revealed no observable curvature or change in distortion.

3.4.2.5 Mirror Module Survival Wind Load Test

The objective of the mirror module survival wind load test was to verify the structural integrity of the adhesive bond joints and primary load paths through the attachments and adjacent rib members when subjected to loads comparable to a 90 mph wind.

Figure3-42illustrates the test set-up used for the mirror module survival wind load test. Since the test objective was to evaluate the mirror module adhesive and structure, a module with broken mirrors was used. The broken mirrors were removed prior to testing. The module was suspended from the 3 attachment studs (i.e., face down orientation), and dead-weight loaded with wet sand on the backside. Only one-half of the module area was loaded on test #1, and the opposite end was loaded on test #2 to enable two potentially destructive tests to be accomplished on the same module.

The instrumentation used on this test consisted of a load gage to measure the sand weight, and 7 dial indicators to measure deflections. The dial indicators were attached such that the deflections being measured excluded deflections of the load gage and the test fixture main support member. The 7 dial indicators were located beneath each of the 7 longitudinal mirror module ribs.

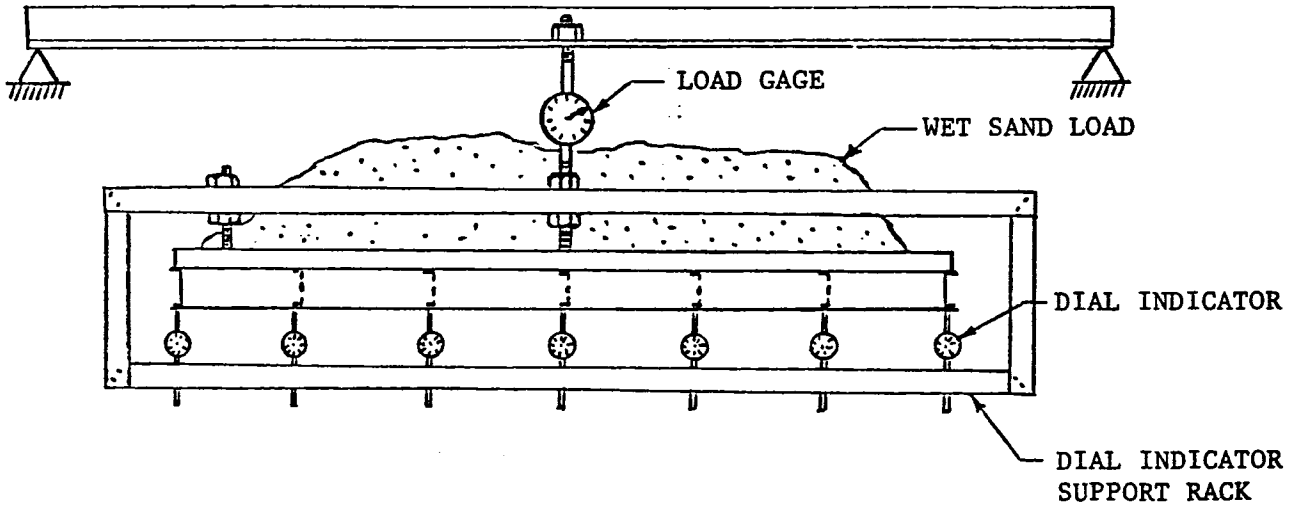

FIGURE 3-42

MIRROR MODULE SURVIVAL WIND LOAD TEST

The test loads were based on a 90 mph wind impacting a heliostat in the vertical stow position. This represents an over-test condition because a heliostat would normally be stowed horizontally if a high wind were anticipated. With a 90 mph wind normal to the heliostat, a peak pressure at the geometric center of 2.38 times the dynamic pressure occurs. This corresponds to a loading of 37.4 lb/ft^2. Since only one-half of the mirror module area (24.0 ft^2) was loaded on each test an 897.6 lb sand weight simulates the worst case 90 mph wind condition. This load was applied in 100 lb increments with dial indicator readings taken at each increment.

No bond failures or problems were noted at the 90 mph, 897.6 lb test condition. The load was increased in 100 lb increments to a maximum of 1500 lbs in an attempt to cause a bond failure. On test #1 an abrupt deflection change was noted on one dial indicator at 1400 lbs load which indicated local bond failure at one rib. Test #2 on the other one-half of the mirror module survived the full 1500 lb load limit without any problem or evidence of bond failure.

3.4.2.6 Mirror Module Imperfection Evaluation

Several tests were performed to evaluate mirror module and/or mirror-only surface imperfections. One of these was a laser ray trace performed by Sandia-Albuquerque on two mirror modules. Another related test was performed by Northrup-Hutchins on a mirror-only. On this latter test a mirror facet was placed on a 5 x 7 ft flat, level granite surface plate. An 8-inch long calibrated Starret level was used to measure surface angles at 45 locations on the mirror. The following tabulation shows the results of both the laser ray test, and the mirror-only surface angle measurements.

COMPLETE MODULE-LASER RAY TRACE

Mirror Module	Scan #	Scan Direction	RMS Reflected Beam Deviation x - component	y - component
A	4	y (48")	0.394 mrad	1.386
A	5	y (48")	0.756	1.296
A	6	y (48")	0.558	0.958
A	7	y (48")	0.544	1.638
B	4	y (48")	2.230	1.876
B	5	y (48")	0.922	1.736
B	6	y (48")	0.510	1.680
B	7	y (48")	0.608	1.358
B	1	x (144")	0.794	0.926
B	2	x (144")	0.750	0.946
B	3	x (144")	0.600	0.692
RMS of y-scans (48" direction)			0.987	1.517
RMS of x-scans (144" direction)			0.719	0.862
RMS of both scans			0.863	1.233

MIRROR FACET ONLY - STARRET LEVEL

RMS OF 45 READINGS	0.771	0.706

The implication is a strong one, and is one which is consistant with visual observations: a large portion of the distortion on a mirror module is inhèrent in the mirror glass.

Since obtaining these data, two changes have been made to the mirror modules delivered to Sandia to improve the imperfection distortions.

1. The edge moulding has been redesigned.
2. A "select" grade of glass is now used for the mirrors.

The original edge moulding was a commercial edging known as Bailey "C"-Sash. It mechanically gripped the mirror edge so tightly that edge distortions occurred. The new edge seal employs a simple "U" cross-sectional shape which is attached with a cure-in-place RTV silicone rubber. It also gives a very tight edge grip, but via adhesion rather than a mechanical grip, and as such is nearly distortion-free.

3.4.2.7 Water Spray Test

The objective of the water spray test was to simulate a wash and/or driving rain of potentially sensitive components such as the drive unit, motors, and exposed cable harnesses.

A test method consisted of spraying the area around the drive unit and pedestal from a distance of approximately 10 feet using an ordinary garden-variety hose and nozzle for a period of 20-25 minutes on 5 or more different days. The spray technique was to adjust the nozzle to achieve a droplet pattern and velocity similar to a wind-driven rain; i.e., a solid-stream jet was avoided. The heliostat was allowed to warm to a mid-afternoon ambient temperature, and then sprayed with cool tap water. Following the water spray operation, the heliostat was operated for approximately 15 minutes.

Due to schedule limitations at the Hutchins test site on the heliostat #1 unit, some deviations to the plan were necessary. The heliostat #1 unit was selected for test because it had a drive unit which had excessive backlash and was due to be returned to Winsmith for tear-down and re-work. This provided an excellent opportunity to determine if any water penetration had occurred. Due to the test schedule and replacement of this drive unit, only 3 water spray cycles were performed on the complete drive unit/ heliostat assembly. However, an additional 4-day period of actual heavy rain conditions (i.e., 10 inches of rainfall) had been encountered previously, so a considerable exposure was actually encountered. In addition, the drive unit was subjected to an additional 6 cycles of water spray after its removal from the heliostat and prior to its return to Winsmith for tear-down. These 6 cycles were more severe than would normally be encountered for several reasons:

a. The drive unit was painted a dark gray in color, and therefore, would warm more than the current white painted configuration.

b. The drive unit was stored in a sunny area at the test site and was not shaded as it would be when installed on a heliostat. During the 6 cycles of spraying, the drive unit was first warmed to a mid-afternoon ambient temperature, and then sprayed with cool water.

c. The drive unit being tested did not have the expansion chamber which is currently installed on all production units for the purpose of preventing differential pressures between the inside of the drive and the external ambient pressure.

The results of the water spray test and actual rain exposure were as follows:

1. The tear-down of the drive unit at Winsmith revealed no perceptible water in the oil, and no evidence of any rust on any internal parts.

2. Water did enter the pedestal and wet the electronics during the actual heavy rain period. It was found that a small passage existed between the drive unit base and the pedestal tapered shims/flange. The opening was plugged with a small amount of duct-seal, and no direct water penetration was noted thereafter.

3. Some rusting was noted at flange interfaces such as between the motor and drive, between the torque tube flanges and drive unit, and between the drive unit base and pedestal tapered shims/flange. These surfaces are now being coated with a layer of silicone grease (to both coat the surfaces with a protective moisture barrier, and to fill the minute cracks and crevices which were acting as capillary paths for water draw-in).

A related observation is that some moisture was noted inside the pedestal walls and on electronic chassis surfaces even without water spray or rain. The phenomenon is undoubtedly caused by high humidity and cool pedestal/electronic temperatures. These temperatures were occasionally falling below the dew point, and the water vapor in the air condensed on the cool surfaces. No visible damage or failures occurred from this condensation, but since it was undesirable, a technique was developed wherein the electronic cooling fan was always kept running. The small amount of power plus the moving air apparantly maintained the internal temperatures above the dew point so condensation no longer occurred.

3.4.2.8 Drive Unit Backlash Test

The free backlash was measured on three separate heliostats in both the elevation and azimuth directions. The backlash was measured with dial indicators as the rack/mirror structure was moved back and forth under light forces of 20 to 25 lbs (up to 100 lbs on elevation) to move the drives within their backlash range. The heliostats were horizontal for the elevation tests and were vertical for the azimuth tests. The results are presented in Table 3-26 below in terms of milliradians of rotation.

Table 3-26
Drive Backlash Test Results

	Azimuth Rotation	Elevation Rotation
Heliostat #1	.785 mrad	1.102 mrad
Heliostat #2	.174	1.176
Heliostat #3	.660	1.167
Average	.539	1.148

3.4.2.9 Pointing Accuracy With Operational Wind Loads Test

Reflected beam motion due to wind moment was experimentally determined, by applying wind moment loads during actual tracking operations. Both the elevation and azimuth axis motion were tested for 27 mph and 35 mph wind loads.

This test was performed to demonstrate the requirement that the pointing error of the reflective surface (excluding foundation) is less than 3.6 mrad in a 27 mph wind. The test was performed at the 35 mph wind condition to determine the magnitude of the error, as the heliostat is required to track, but has no accuracy requirement during this wind condition.

The moments applied during the tests were 2768 ft lbs for 27 mph wind and 4651 ft lbs for 35 mph wind.

The beam motion was recorded by actual photographs of the image on the target with and without the loading.

During the testing, loads were applied and released in a short time span, to eliminate the possibility of tracking errors which could occur over a longer span of time. Rapid loading was accomplished in the azimuth tests by backing a scissor lift test rig until weights were lifted by a loading cable which loaded the heliostat. Then the rig was driven forward, released and moved to the other side for the reversing load. The azimuth test sequences were accomplished in approximately 10 minutes. Rapid loading in the elevation tests was accomplished by using a hand hoist on each weight attached to the rack structure and simply lifting the weight off the ground to apply load, then lowering it to release load.

A summary of the beam pointing results is as follows:

Azimuth	27 mph	$\pm$ 2.0 mrad
	35 mph	$\pm$ 2.9 mrad
Elevation	27 mph	1.5 mrad (down)
	35 mph	2.4 mrad (down)

It should be noted that the displacement at the target is the "reflected beam" displacement. Therefore, half of this displacement represents the mirror surface motion, which is compared to the 3.6 mrad requirement after pedestal contribution is subtracted.

3.4.2.10 Elevation Axis Test - 90 mph Wind Horizontal Stow

The objectives of the Elevation Axis Test are to: (a) verify the structural integrity of the drives and major structural components to withstand loads induced by 90 mph winds while in the horizontal stow position and (b) measure deflections of the drives and major structural components for comparison with pointing accuracy requirements at lower wind conditions.

The 90 mph elevation axis wind condition produces the largest moment (20,477 ft lbs) about the elevation drive axis of any condition; thus it produces the largest elevation drive main gear tooth force. This tooth force is 29,250 lbs tangential load. This condition along with the cross-elevation axis condition produces the highest azimuth bearing moment (245,710 inch lbs).

The test was performed with the heliostat in the horizontal position, which simulates horizontal stow. Moment load was applied about the elevation drive axis which simulates the moment induced by a frontal 90 mph wind at 10 degrees from horizontal.

The test was performed by incrementally applying load to 110% limit load. Loads were applied by hanging six 55 gallon barrels from the rack trusses with ropes and filling the barrels to the appropriate level with water. Two test runs were made. The loading setup is shown below.

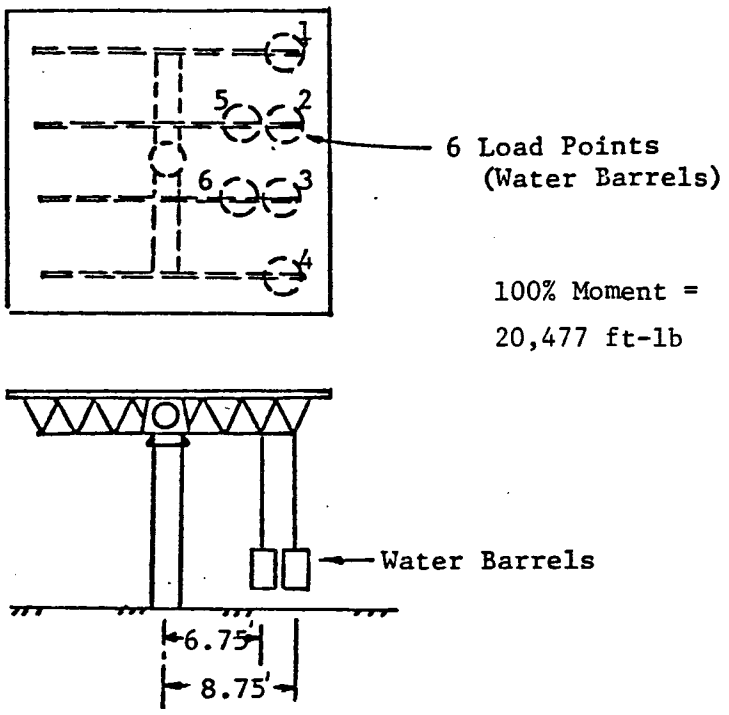

Deflections at critical locations on the structure and drive were monitored with dial indicators at each load increment. Rotational displacements at 100% load are summarized in Table 3-27.

Table 3-27

ROTATIONAL DISPLACEMENTS AT 100% LOAD

Rack Rotation (Total)		10.98 mrad
Elevation Drive Rotation (Worm)		5.07
Azimuth Bearing Rotation		2.22
Pedestal Tip Rotation-Calculated (Rough measurement confirmation)		1.33
Pedestal-set	Approx	.1 mrad

3.4.2.11 Cross-Elevation Axis Test - 90 mph Wind Horizontal Stow Condition

The objectives of the Cross-Elevation Axis Test are identical to those of the Elevation Axis Test, except that this test was to verify structural integrity and measure deflections for wind in the cross-elevation axis.

The 90 mph cross-elevation axis wind is the condition that produces

(a) The highest elevation drive bearing moment (267,645 inch lbs)

(b) The highest azimuth drive bearing moment (245,710 inch lbs). This is the same as the elevation axis condition (actual test load was 6.6% higher than the elevation axis test because the torque tube root moment was simulated).

(c) The highest torque tube root bending moment (20,874 ft lbs)

(d) The highest Butler truss bending moment and shear load (Moment = 6174 ft lbs, Shear = 1008 lbs)

The test was performed with the heliostat in the horizontal position, which simulates horizontal stow. Moment load was applied about the cross elevation axis which simulates the moment induced by a 90 mph side wind at 10 degrees from horizontal.

The test was performed by incrementally applying load to 110% limit load. Loads were applied by hanging six 55 gallon barrels from the outboard rack truss with ropes and filling the barrels to the appropriate level with water. One test run was made. The loading setup is shown in Figure 3-43.

Deflections at critical locations on the structure and drive were monitored with dial indicators at each load increment. Rotational displacements at 100% load are summarized in Table 3-28.

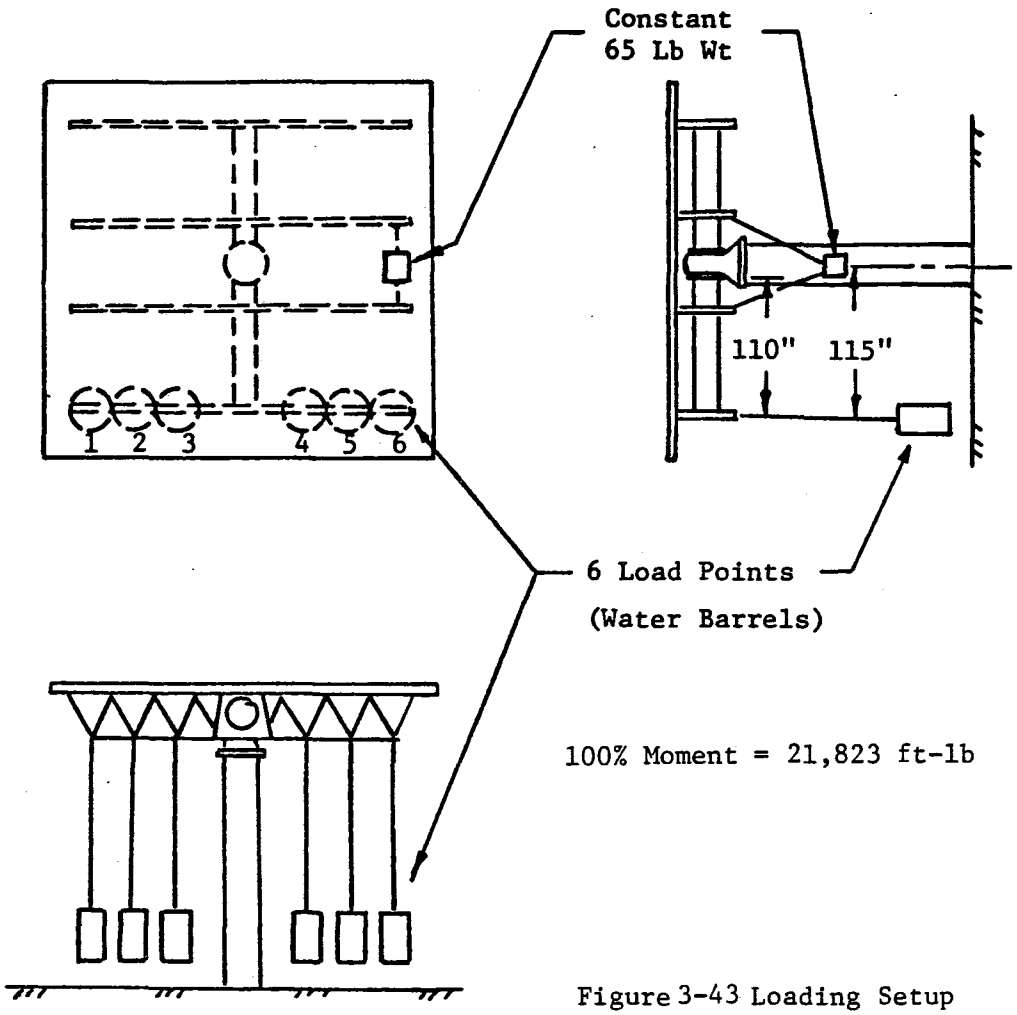

Figure 3-43 Loading Setup

Table 3-28

Rotational Displacements at 100% Load

Rack Rotation (Total)		11.13 mrad
Elevation Bearing Rotation		5.47
Azimuth Bearing Rotation		2.73
Pedestal Tip Rotation-Calculated (Rough measurement confirmation)		1.41
Pedestal Set	Approx.	.07

3.4.2.12 Azimuth Axis Test - 50 mph Vertical Condition

The objectives of the Azimuth Axis Test were to: (a) verify the structural integrity of the drives and major structural components to withstand loads induced by 50 mph winds while in the vertical drive or stow position, and (b) measure deflections of the drives and major structural components for comparison with pointing accuracy requirements at lower wind conditions.

The 50 mph azimuth wind condition produces the largest moment (9497 ft lbs) about the azimuth axis of any condition. Therefore, it produces the largest azimuth drive main gear tooth force of 13,560 lbs (tangential load). This condition also produces the largest pedestal twisting moment.

The test was performed with the heliostat in the vertical position, which simulates vertical stow or driving to stow. Moment load was applied about the azimuth drive axis which simulates the moment induced by a 50 mph wind at 70 degrees from the mirror surface normal.

The test was performed by incrementally applying load to 110% limit load. Moment load about the azimuth axis was applied by hanging two 55 gallon barrels from a cable and pulley system designed to provide a horizontal force to a wood beam inserted into the torque tube. The barrels were then filled to the appropriate level with water. Two test runs were made. The loading setup is shown in Figure 3-44.

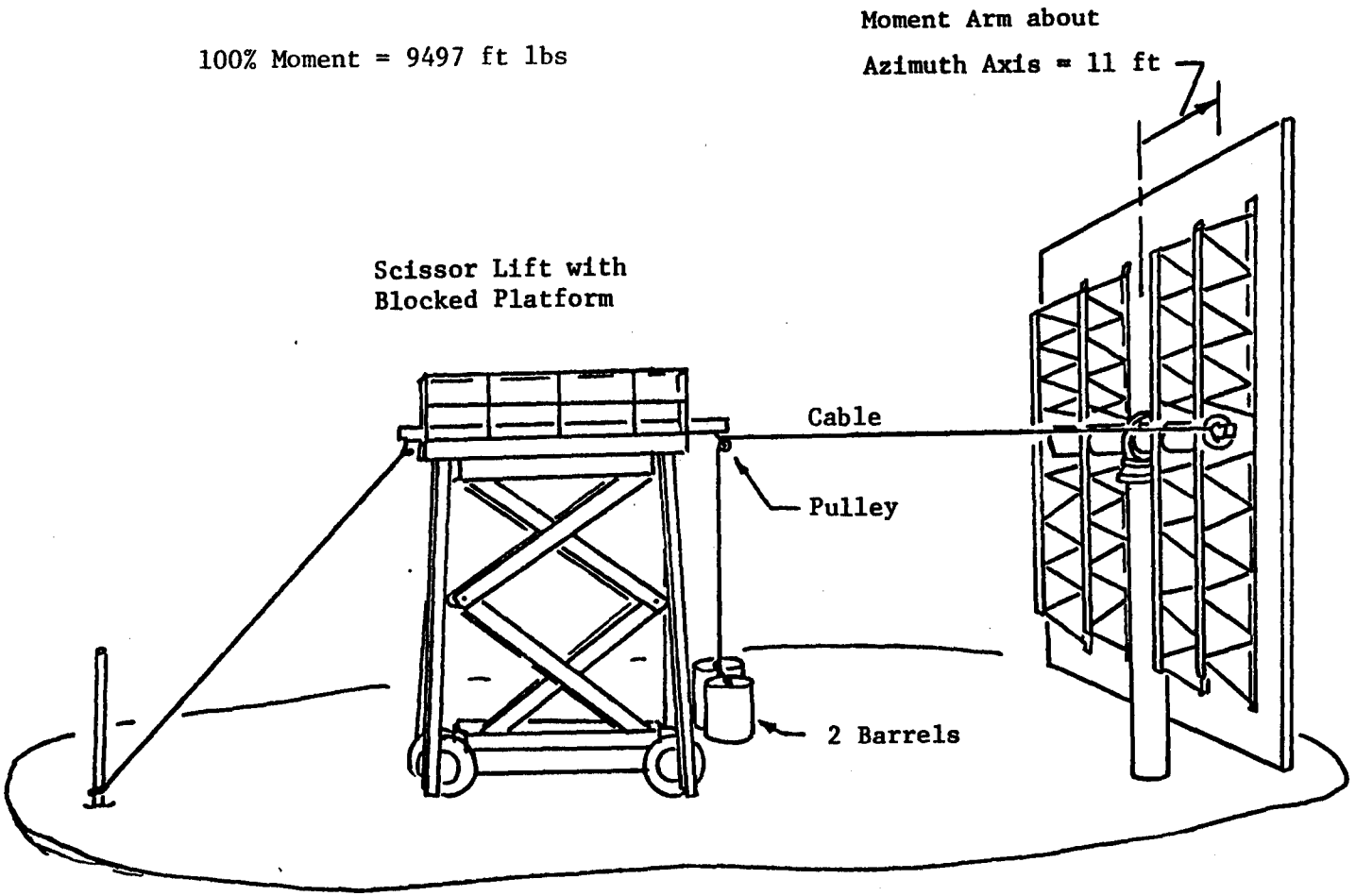

Figure 3-44 Test Loading Setup

Deflections at critical locations on the structure and drive were monitored with dial indicators at each load increment. Rotational displacements at 100% load are summarized in Table 3-29.

Table 3-29

Rotational Displacements at 100% load

	Test 1*	Test 2
Rack Rotation (Total)	8.75 mrad	5.39 mrad
Elevation Bearing	4.74	1.00
Azimuth Worm	5.93	1.87
Pedestal Tip Twist - Calculated	.74	.74
Pedestal Twist Set Approx.	.017	.005

*A "shift" in both the elevation and azimuth drives was experienced during Test 1, between 20 and 40% load.

A distinctive shift of approximately 3 milliradians occurred in both the elevation "bearing" and the azimuth "worm" measurements of the drive unit. This shift occurred between 20% and 40% load and was accompanied by a distinct sound at the time of loading. It is believed that the cause of the shift was some combination of backdriving in the azimuth drive and/or the hard setting of bearings or bearing races in the drives that would not have occurred under light loads. It is also believed that the shock effect of the initial set in one drive (elevation or azimuth) caused the other one to set. The subsequent data taken during the first and second test runs followed a linear pattern and no yielding is believed to have occurred, and certainly no failure occurred.

It should be noted that a post-test inspection of the drive unit by both Winsmith and the bearing manufacturer (Keene Corp.) revealed no damage of any kind following these load tests.

3.4.2.13 Motor Torque Adequacy

Extensive testing was performed to determine the motor torque adequacy for driving against wind loads, gravity loads, and frictional losses within the drive unit. For a 22 m/s (50 mph) wind the worst-case combined wind and gravity moments are 1313 kg-m (9497 ft-lb) for azimuth, and 1607 kg-m (11624 ft-lb) for elevation.

Shortly after erecting heliostats #1, #2, and #3 at the Northrup test facility, preliminary motor stall tests were performed which indicated a torque problem existed. With the Superior Electric M112-FJ326 stepper motor and TBM105-1230 control-translators, motor stall occurred at loads (moments) between 829 kg-m (6000 ft-lb) and 1106 kg-m (8000 ft-lb). An interim attempt to resolve the problem by raising the translator voltage resulted in a slight improvement to 1270 kg-m (9200 ft-lb).

The problem cause was identified by using a D-C motor to drive the heliostat, and recording the input current trace to provide an input torque measurement. The current traces obtained showed torque oscillations at a frequency consistent with the planet gear rotation. It was deduced that insufficient backlash existed between planet and ring gear teeth, and that under load, the small axial movement of the worm bearing plus some worm shaft bending could create a slight misalignment which resulted in a "pinch-point" interference during each revolution of the two planet gears.

Since an immediate solution to the low output torque of the drive was needed to enable the delivery schedule to be met, a change to a higher torque stepper motor was made. The motor selected was a Superior Electric M112-FJ327 with a TBM105-1218 translator. The size, weight and cost for these is essentially the same as for the original motor and translator; the major difference lies in the motor windings and translator voltage. The new motor provided a higher peak torque (863 oz-in versus 612 oz-in), but this added torque was achieved at the expense of motor speed. With the new motor, peak torque occurs at 150 rpm (500 steps/sec pulse rate) versus 300 rpm (1000 steps/sec pulse rate) with the original

motor. As a result, the slew rate is only one-half of the desired rate.

With the new motor-translator combination, the current motor stall torque has been significantly increased to a level between 1553 kg-m (11,250 ft-lb) and 1670 kg-m (12,100 ft-lb) for the sample of drive units tested.

One notable problem was experienced with the heliostat #1 azimuth drive delivered to Sandia-Albuquerque. A motor stall was experienced at a relatively low load of approximately 662 kg-m (4800 ft-lb). Subsequent disassembly of the planetary stage of this unit revealed a slight interference of the planet carrier assembly and the two halves of the housing. The cause was an insufficient gasket thickness between the two housings. A thicker gasket was installed which provided more clearance. A subsequent re-test at a load of 1410 kg-m (10,215 ft-lb) showed satisfactory operation and no motor stalling.

3.4.2.14 Operations and Accuracy Tests

Operations and tracking accuracy tests were performed informally on the three heliostats installed in Hutchins during the Sept. 12 to Oct. 30 period and on the two heliostats installed at the Albuquerque CRTF during the Nov. 11-20 period. Formal testing for the "Second Generation Heliostat" program evaluation began Dec 4 with the "Control System Operational Modes" test.

3.4.2.14.1 "Test 1 - Control System Operational Modes"

The objective of the control system operational mode test is to "Determine whether heliostats can perform such required functions as tracking, stowing, and assuming a commanded orientation." (ref. "Second Generation Heliostat Test Plan, p. 1)

Three sets of tests were performed over the two day period of Dec. 4 and 5th to demonstrate the control capability of the heliostat hardware and software. These were tests 1.3.1 Standard Modes, 1.3.2 Special Modes, and 1.3.4 Control Drive Repeatability.

Test 1.3.1 Standard (Control) Modes

In separate operational tests each heliostat was operated through the mode sequences of a normal operating day.

a. Stow to Standby Line Bottom
b. Standby Line Bottom to Standby Line Top
c. Standby Line Top to Target Tracking
d. Target Tracking to Standby Line Top
e. Standby Line Top to Stow

Both heliostats demonstrated full compliance with the test requirements.

Test 1.3.2 Special Control Modes

In separate operational tests each heliostat was operated at slew speed to the extremes of both elevation and azimuth travel to evaluate individual slew rates, combined slew rates, limit switch functional status, and establish limit switch base positions. Both heliostats properly traversed in commanded slew directions in all tests. No 1 heliostat primary limit switches limited up, down, east, and west travel

properly. No. 2 heliostat primary limit switches limited up, down, and east travel properly, but the west travel was stopped by the back up limit switch before the primary was reached. A bracket bent in shipping was found to be the cause. After restoring the bracket position normal west limit control was demonstrated.

Test 1.3.4 Control/Drive Repeatability

The control/drive repeatability test consists of up to 10 operational cycles between stow positions and an initial commanded position established by a laser image on a target located 250 ft behind the test heliostat. (3 inches on the laser target = 1 mrad).

During the initial sequence, between "vertical stow" and the "control command position", repeatability was demonstrated within .25 inches (0.08 mrad) in "no wind"conditions and 1.75 inches (0.58 mrad) when winds sufficient to toggle azimuth backlash were present. Throughout this sequence the pedestal was shaded.

During the second sequence, between "horizontal stow" and the "control command position", repeatability was demonstrated within a 2 inch x 2 inch (.67 mrad x .67 mrad) envelope. Pedestal bending from periods of solar exposure between "horizontal stow" and the "test" position is believed responsible for the slightly increased inaccuracy. It should be noted that this pedestal solar exposure is not a normally encountered condition during tracking for the basic configuration Northrup II heliostat.

3.4.2.14.2 Beam Centroid Pointing Accuracy

The objective of the "Beam Centroid Pointing Accuracy" test is to "measure beam centroid pointing error with the Beam Characterization System (BCS) while tracking the sun". The compliance with the specification beam pointing requirement is 1.5 mrad for each axis (equivalent to axis pointing of 0.75 mrad) is defined by the performance in this BCS monitored test.

Baseline beam centroid pointing accuracy testing was performed with both heliostats Dec 12 (Day 347) and Dec 18 (Day 353). Summarized numerical results are shown in Tables 3-30 (Dec 12) and 3-31 (Dec 18). Graphic plots for Dec 12 are shown in Figures 3-45 and 3-46 and for Dec 18 are shown in Figures 3-47 and 3-48.

The baseline tracking accuracy data indicated #2 heliostat to be within specification limits, 0.2597 mrad rms elevation error and 0.5532 mrad rms azimuth error. The #1 heliostat was beyond limit for the elevation error, 1.0270 mrad rms elevation error and 0.5442 mrad rms azimuth error. Correlation of the elevation error patterns for morning and afternoon against elevation angle show repeating patterns for #2 and a hysteresis effect between am elevation and pm elevation for #1. This generally correlates with the tilt data difference between the two heliostats (#1 tilt = 1.81 mad; #2 tilt = 0.27 mrad).

The Dec. 18, 1980 data confirmed the characteristic tracking performance pattern of higher accuracy for #2 heliostat than #1. The final point for each heliostat was with low sun angles and illustrates the increasing atmospheric refraction effect on the sun's apparent position at low sun angles. A correction model for the atmospheric refraction has been incorporated in the software subsequent to these tests.

The negative offset of azimuth data sets on Dec. 18 is believed to be the result of a slow clock. Current practice is to set the computer clock with WWV time each morning.

Table 3-30

Baseline Beam Centroid Pointing Accuracy

For Second Generation Northrup Heliostats

a) N-1 CRTF Heliostat (171.38, 1016.37, 102.88 target coordinates)

Dec 12 (Day 347)

Time	Azimuth Axis		Elevation Axis	
	Angle degrees from West	Mean Axis Pointing Error for 30 Data Points, mrad	Angle, degrees from Vertical	Mean Axis Pointing Error for 30 Data Points, mrad
9:45-9:48	100.96	-1.40	15.88	0.13
10:22-10:25	96.69	-0.22	17.39	0.39
10:59-11:03	92.41	-0.31	18.41	0.49
11:38-11:41	87.31	-0.59	18.86	0.42
12:12-12:15	83.10	0.28	18.78	1.02
12:48-12:50	78.72	0.47	18.23	1.41
13:51-13:54	71.27	-0.26	16.10	1.30
14:48-	65.11	1.05	13.01	1.37
RMS For Full Day		0.5442		1.0270

Figure 3-45 No 1 Northrup Heliostat - Dec 12, 1980

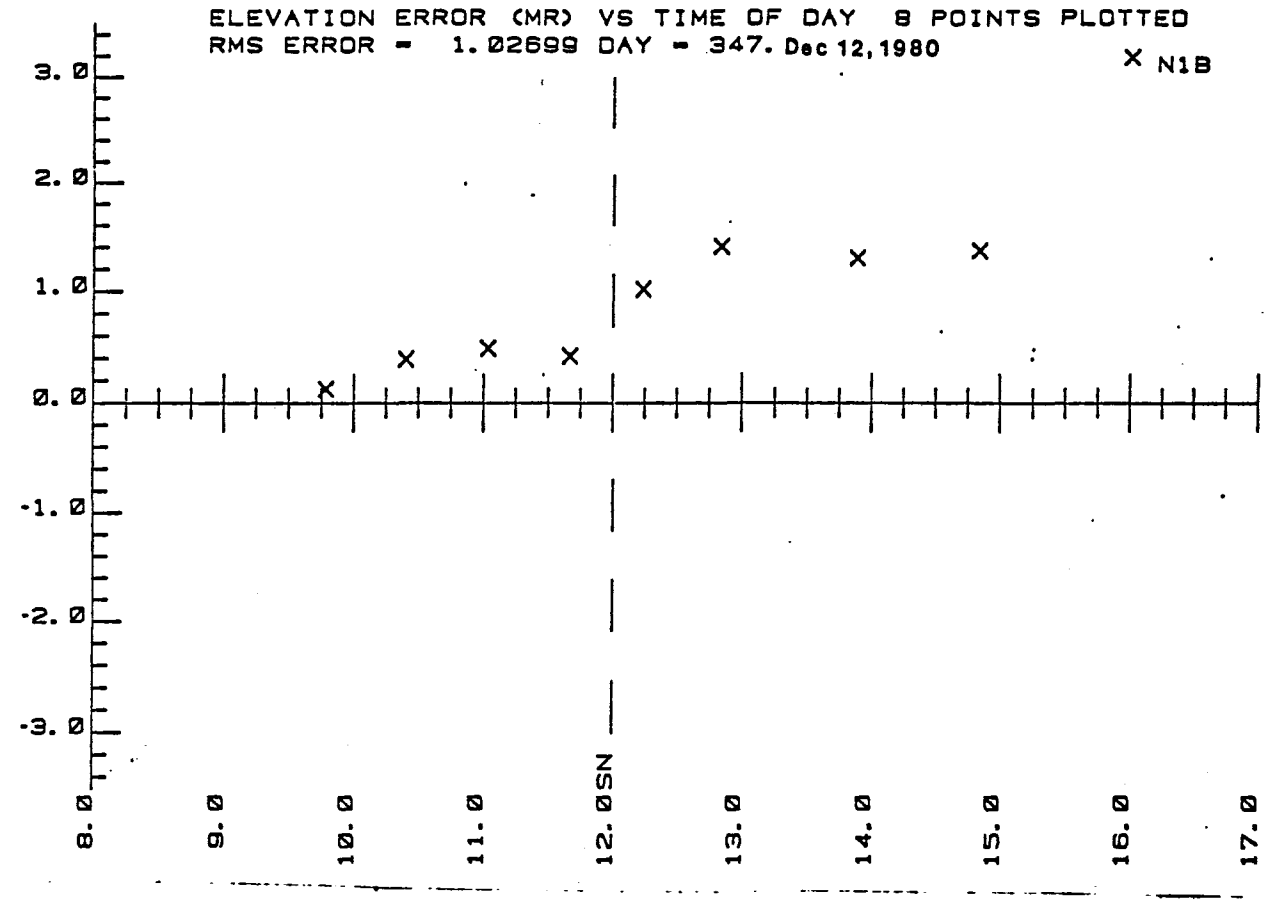

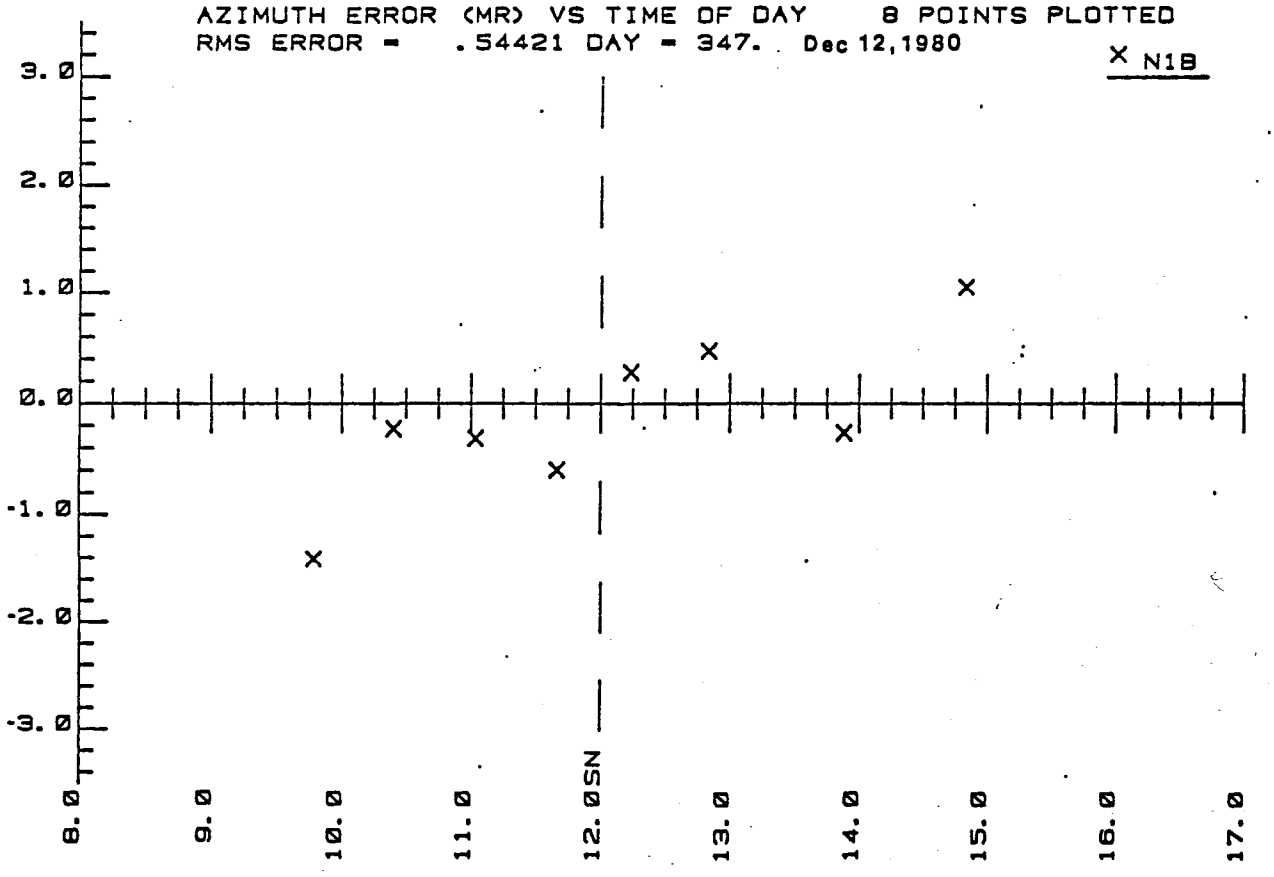

Table 3-30

b) N-2 CRTF Heliostat (-65.26, 769.55, 107.36 target coordinates)

Dec 12 (Day 347)

Time	Azimuth Axis		Elevation Axis	
	Angle, degrees from West	Mean Axis Point Error For 30 Data Points, mrad	Angle, degrees from Vertical	Mean Axis Pointing Error for 30 Data Points, mrad
9:53-9:56	107.72	-1.06	16.78	-0.44
10:30-10:34	103.36	-0.71	18.33	+0.02
11:08-11:11	98.86	-0.72	19.36	+0.19
11:46-11:49	94.13	-0.52	19.88	+0.26
12:20-12:23	89.86	-0.38	19.88	+0.05
12:55-12:57	85.57	-0.15	19.42	+0.43
14:00-14:03	77.79	-0.36	17.33	-0.08
15:02-15:05	71.17	-0.22	13.96	-0.56
RMS For Full Day		.5532		.2597

Figure 3-46 No. 2 Northrup Heliostat December 12, 1980

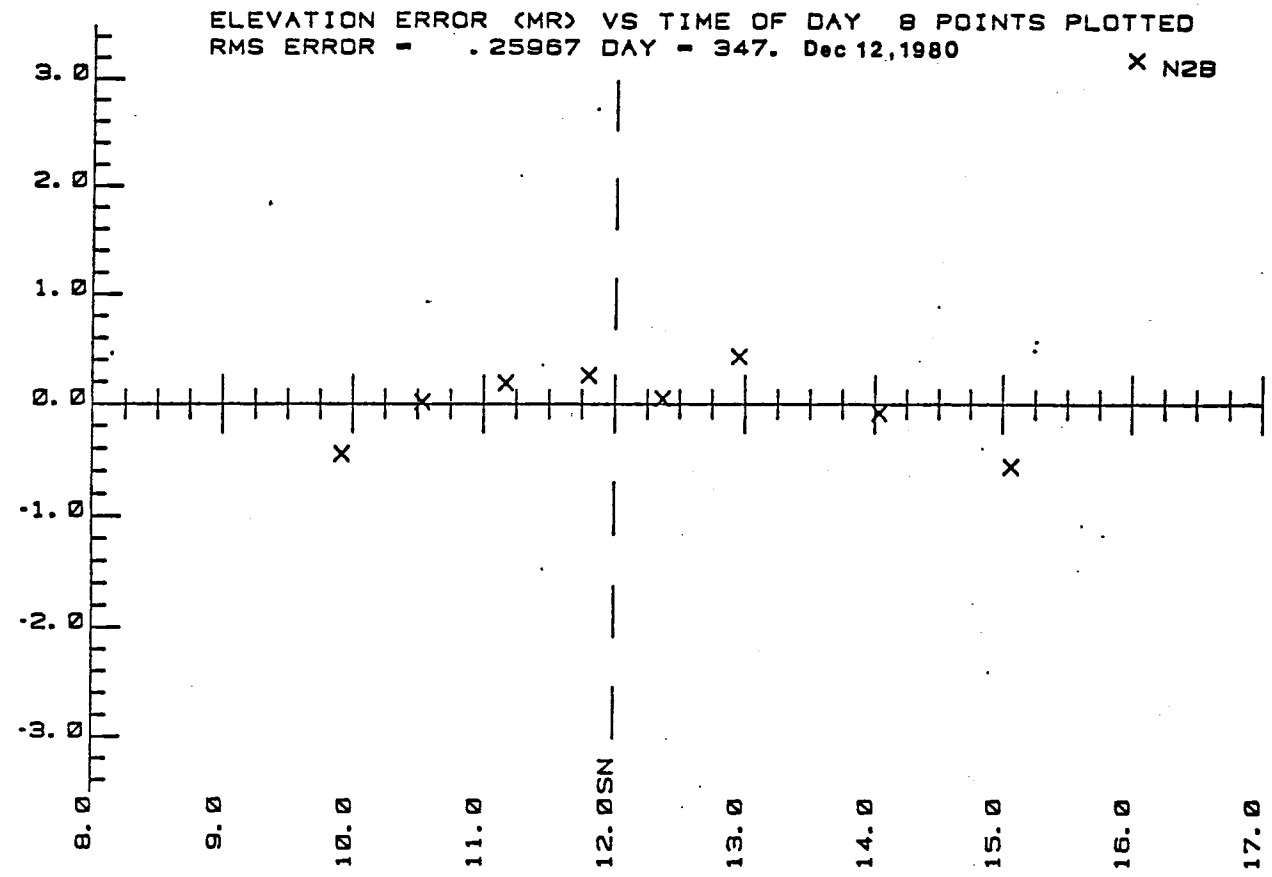

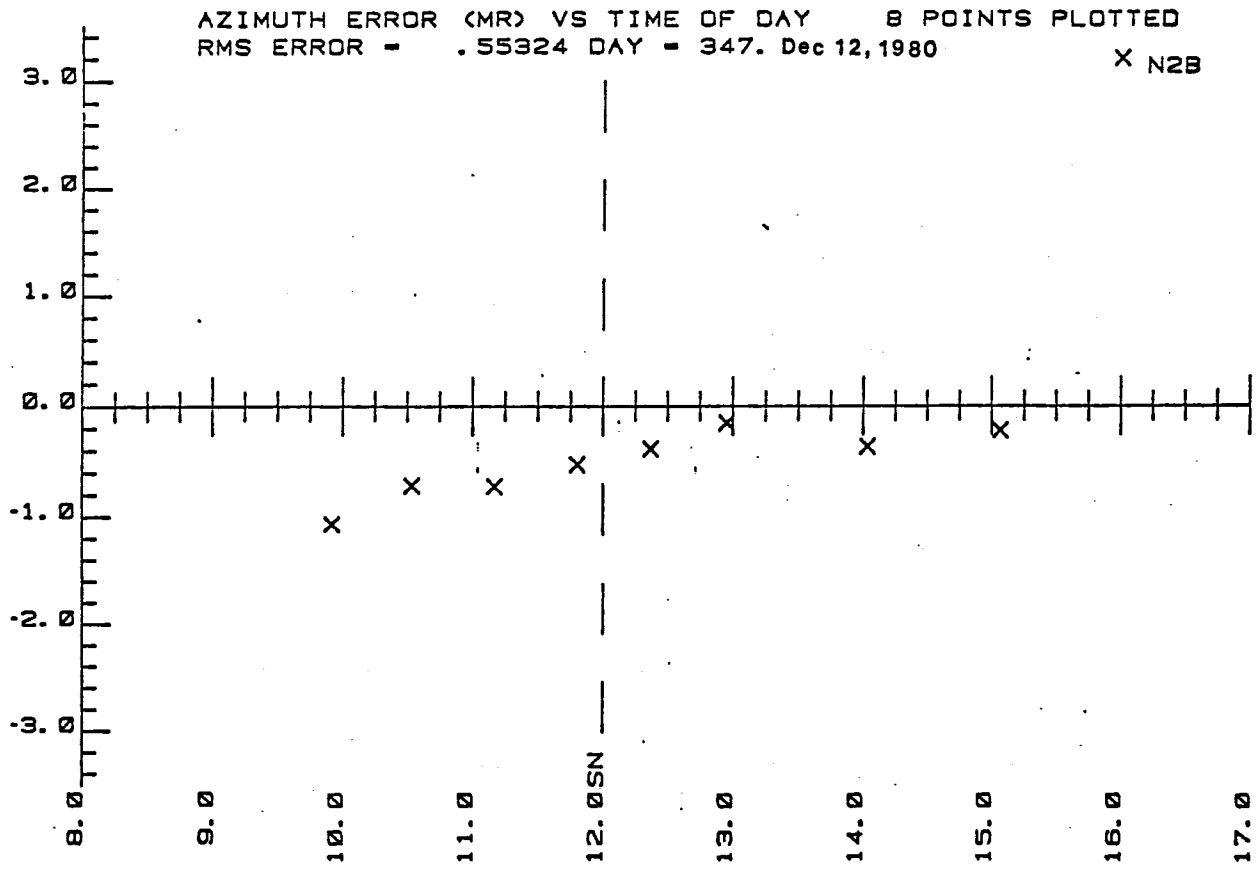

Table 3-31

Baseline Beam Centroid Pointing Accuracy For Second Generation Northrup Heliostats

(a) N-1 CRTF Heliostat (171.38, 1016.37, 102.88 target coordinates)

Dec 18, 1980 (Day 353)

Time	Azimuth axis		Elevation axis	
	Angle, degrees from West	Mean Axis Pointing Error for 30 Data Points, mrad	Angle,degrees from Vertical	Mean Axis Pointing Error for 30 Data Points, mrad
10:13- 10:16	98.038	-0.76	16.821	-0.47
11:13- 11:17	90.773	-0.53	18.446	-0.78
12:17- 12:23	82.863	-0.63	18.623	-0.42
13:10- 13:13	76.368	-1.37	17.579	- .02
15:19- 15:23	62.447	- .53	11.021	- .36
16:36- 16:39	55.685	.69	4.511	-1.11
RMS First 5 sets		.9292		.5663
RMS All 6 sets		.9005		.7531

Figure 3-47 No. 1 Northrup Heliostat Dec 18, 1980

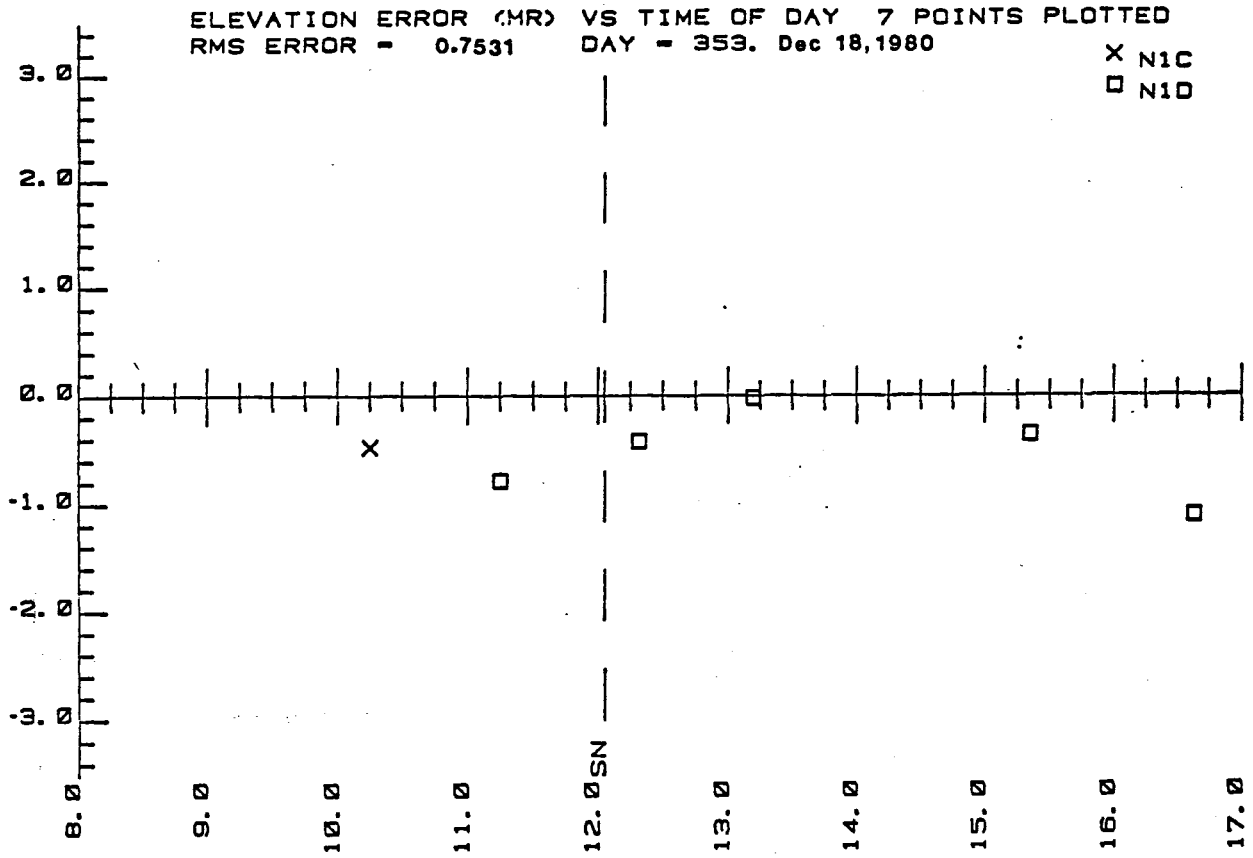

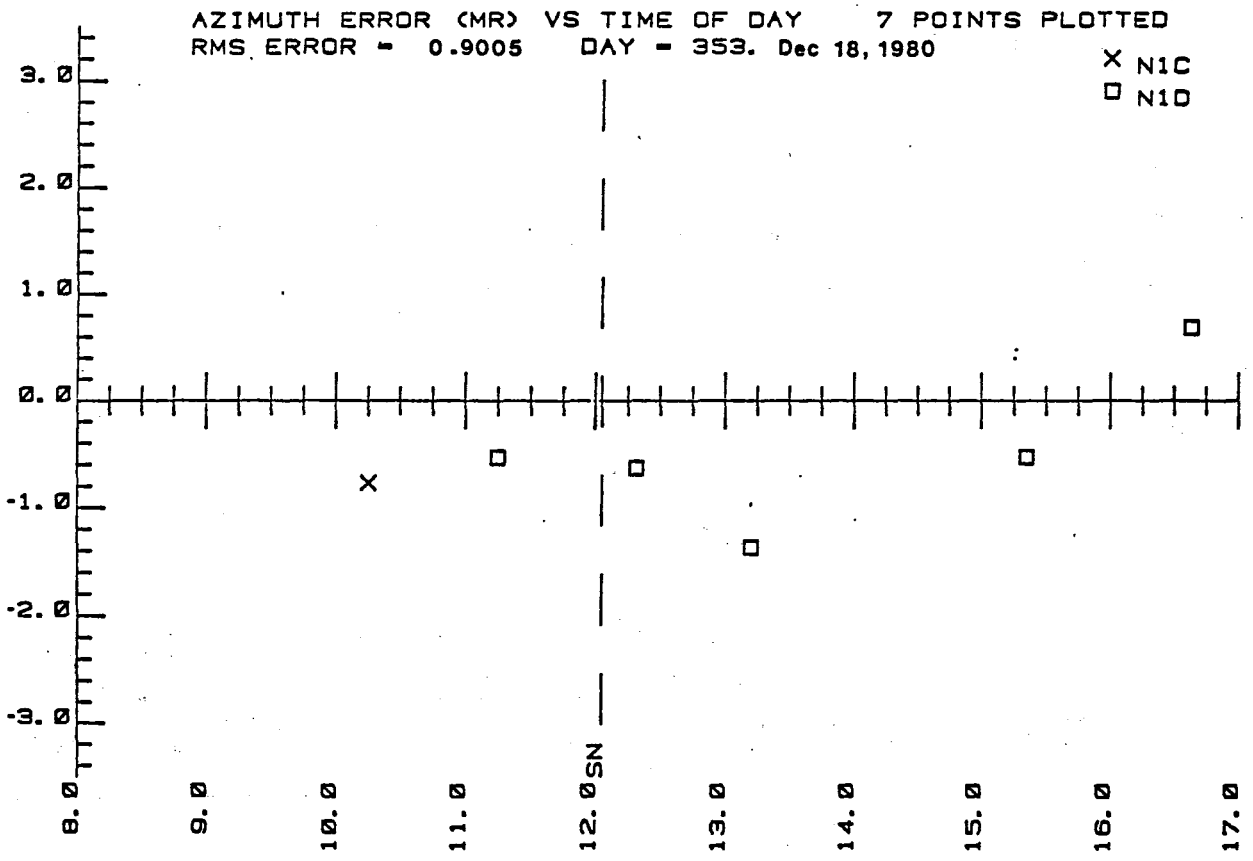

Table 3-31

Baseline Beam Centroid Pointing Accuracy For Second Generation Northrup Heliostats

(b) N-2 CRTF Heliostat (-65.26, 769.55, 107.36 target coordinates)

Dec 18, 1980 (Day 353)

Time	Azimuth axis		Elevation axis	
	Angle, degrees from West	Mean Axis Pointing Error for 30 Data Points, mrad	Angle, degrees from Vertical	Mean Axis Pointing Error for 30 Data Points, mrad
10:02-10:05	106.93	-1.21	16.94	-0.09
11:25-11:29	96.99	-0.55	19.49	0.13
12:28-12:31	89.23	-0.76	19.70	-0.05
13:48-13:51	79.57	- .46	17.81	- .30
15:39-15:42	67.69	- .46	11.20	- .34
16:44-16:47	62.22	- .14	5.37	-2.99
RMS First 5 sets		.8250		0.2666
RMS all 6 sets		.6532		.7044

Figure 3-48 No 2 Northrup Heliostat Dec 18, 1980

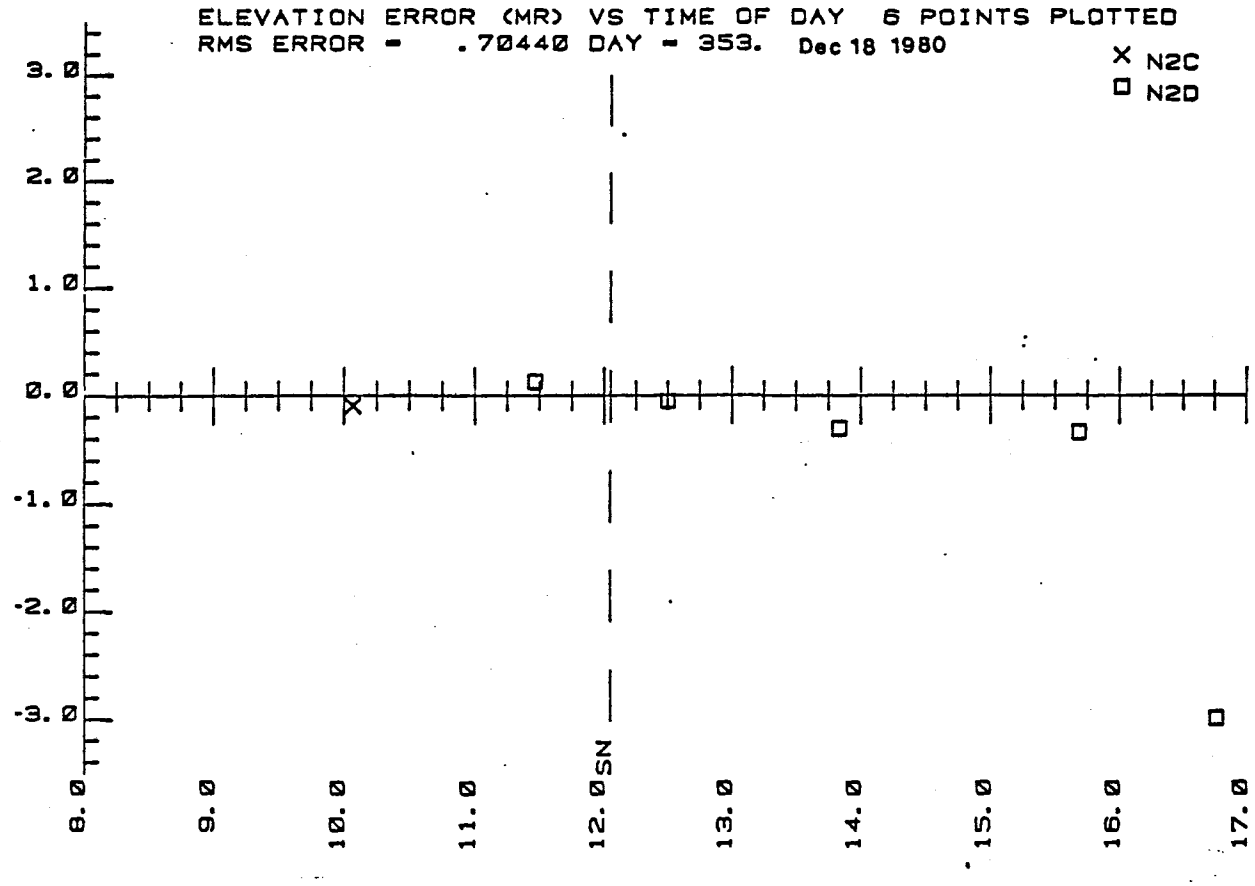

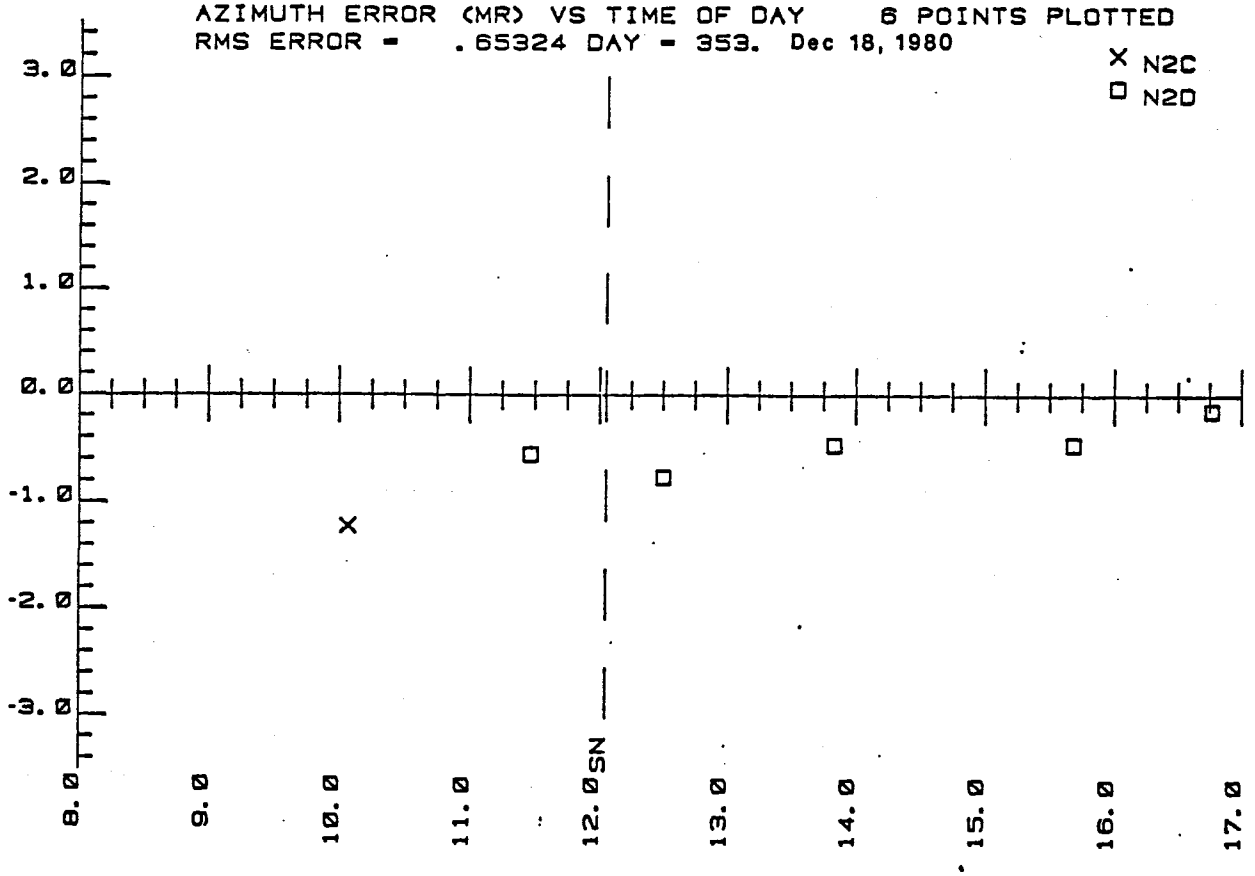

3.4.2.14.3 Beam Quality

Initial "Beam Quality" tests were run on both heliostats Dec. 10,1980. The focal beam pattern for both heliostats was more diffuse than the "helios model" beam generated for the individual heliostats and the test time. Near-noon charts for the 90% power contour with the "helios model" points overlaid are shown in Figures 3-49 (No. 1 Northrup heliostat) and 3-50 (No. 2 Northrup heliostat).

Inspection of the mirror modules revealed a "built-in convex cant" of up to 1.4 mrad between the two facets of a single module. Inspection of the assembly tables indicated a position shift from the original alignment which caused the out of flat cant.

A design change decision to build in a concave cant matched to the slant range was made and implemented. Replacement modules were built and installed on both heliostats at CRTF. Beam quality data with a canted facet heliostat was taken Feb 5, 1981 on No. 2 heliostat. The 90% contour and 90% "helios" model plots are shown in Figure 3-51. Numerical data from the beam quality tests are summarized in Table 3-32 . The gain in image size achieved by the canted facet mirror modules is quantified by the reduction in size of the 90 percent contour footprint from 19.88-19.97 m^2 in the Dec 10 test to 14.3-15.5 m^2 in the Feb. 5th test. The contour still exceeds the specified helios model by 1.5 m^2. Refinement of the "Y Direction" canting procedure is expected to improve this value.

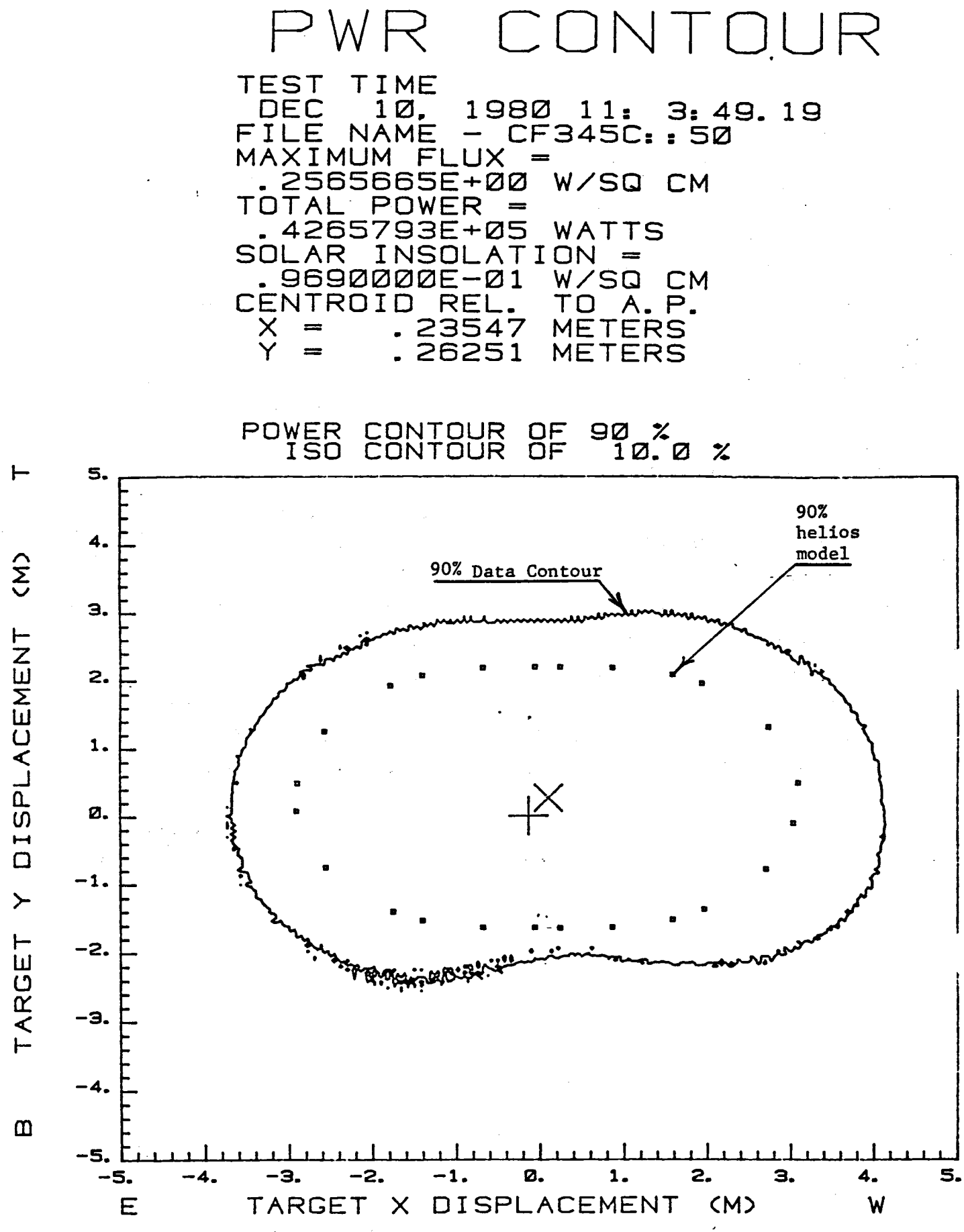

Fig. 3-49 "Beam Quality" Comparison Northrup #1

PWR CONTOUR

TEST TIME
DEC 10. 1980 11:22:56.17
FILE NAME - CF345D::51
MAXIMUM FLUX =
.3338382E+00 W/SQ CM
TOTAL POWER =
.4106595E+05 WATTS
SOLAR INSOLATION =
.9630001E-01 W/SQ CM
CENTROID REL. TO A.P.
X = 0.00000 METERS
Y = -.48126 METERS

POWER CONTOUR OF 90 %
ISO CONTOUR OF 13.0 %

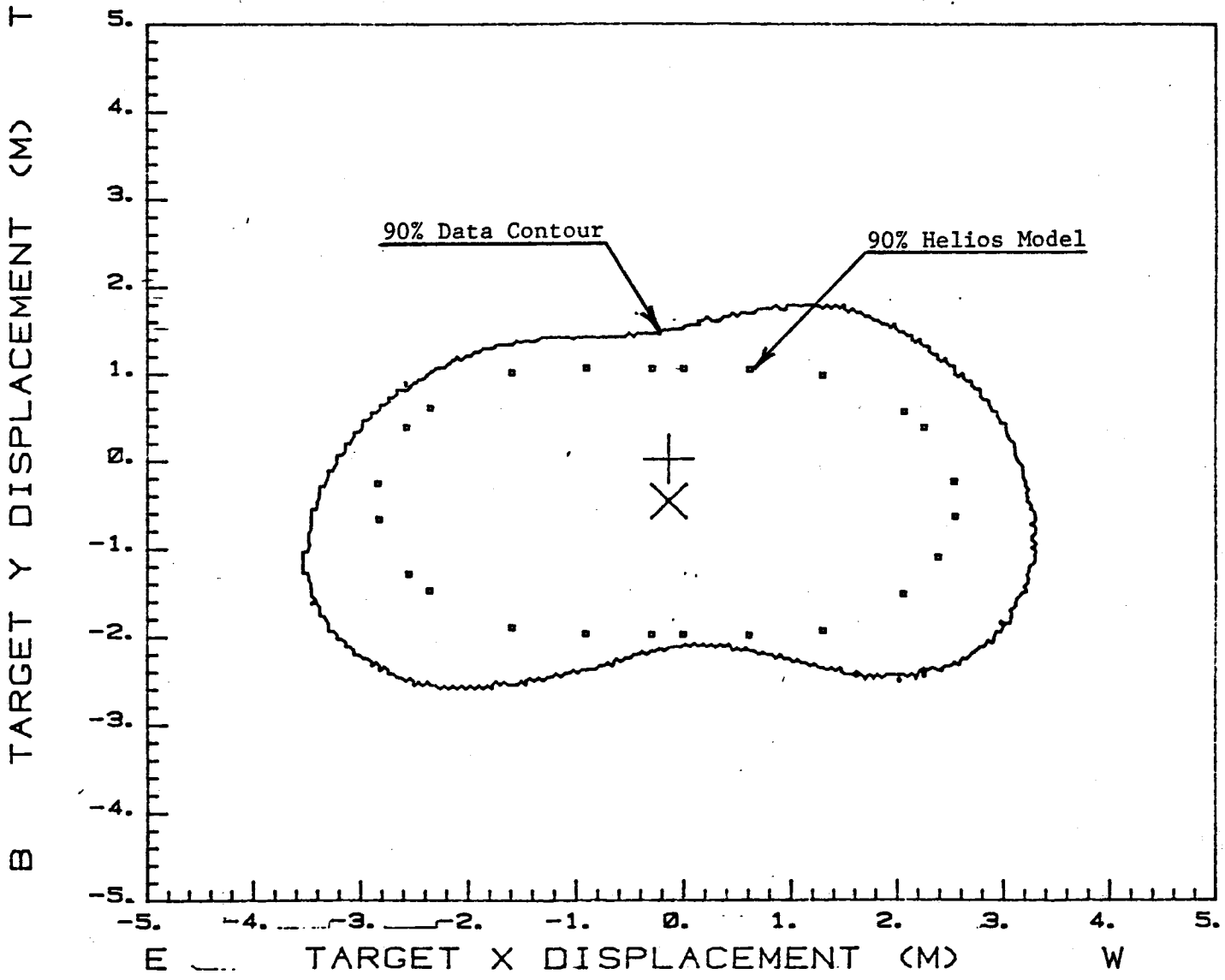

Figure 3-50 "Beam Quality" Comparison Northrup #2

PWR CONTOUR

TEST TIME
FEB 5, 1981 15:11:53.23
FILE NAME - CF036B::62
MAXIMUM FLUX =
.5428509E+00 W/SQ CM
TOTAL POWER =
.3454443E+05 WATTS
SOLAR INSOLATION =
.9460001E-01 W/SQ CM
CENTROID REL. TO A.P.
X = -.34290 METERS
Y = -.59821 METERS

POWER CONTOUR OF 90 %
ISO CONTOUR OF 8.5 %.

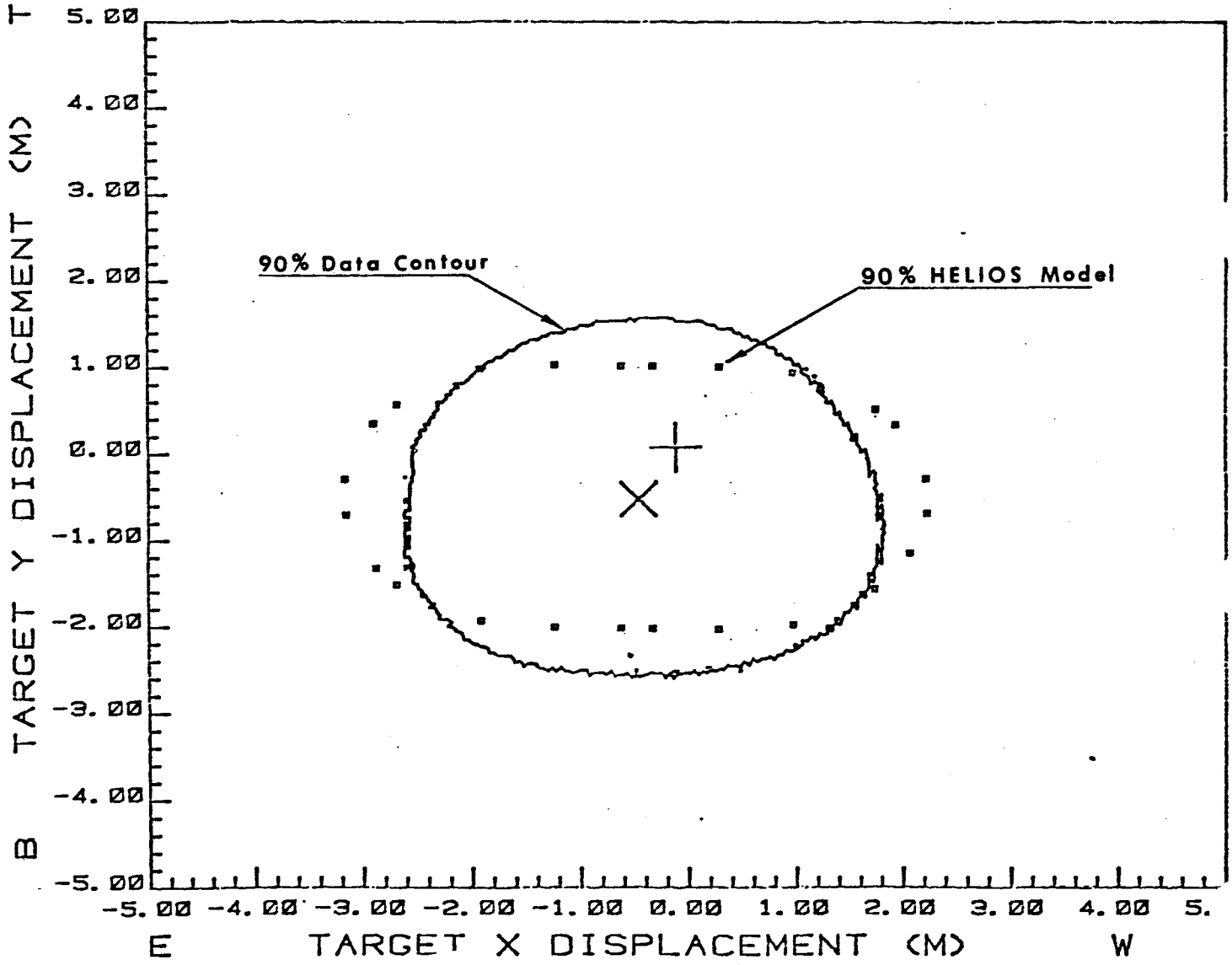

Figure 3-51 "Beam Quality "Northrup #2 Canted Modules

Table 3-32 "Beam Quality" Data Summary

Heliostat & Test time	Total Power kwt	Insolation w/m^2	Max Flux, w/m^2	90% Power Contour Area	Helios Model 90% Contour Area
No 1- Dec 10 11:03:49	42.658	969	2565.7	31.488	18.096
No 1-Dec 10 15:16:14	34.101	794	1980.2	30.345	17.887
No 2- Dec 10 11:22:56	41.066	963	3338.4	19.967	12.737
No 2-Dec 10 14:53:14	34.487	863	3060.2	19.877	12.968
No 2- Feb 5 11:28:41	40.544	1022	5192.0	15.528	not available
No 2- Feb 5 15:11:53	34.544	946	5428.5	14.299	12.797

3.4.2.14.4 Life Cycle Tests

Life cycle testing software was developed on the bench test electronics unit in Littleton and incorporated in the CRTF Software Jan. 12. Either 1 or 2 heliostats are operated in a simulated half day cycle which spans a $\pm$ 67 degree range in elevation and a $\pm$ 50 degree range in azimuth every hour.

The cycle count is recorded on the same type plot used during tracking operation where the lines are composed of plotted points for each tracking update. Figure 3-52 shows a typical plot for dual heliostat cycling showing the twenty four operating cycles and the simulation cycle.

As of Feb. 4, 1981 heliostat #2 had operated 380 cycles without any problems being encountered.

Figure 3-52 Life Cycle Test Chart for 2 Heliostats

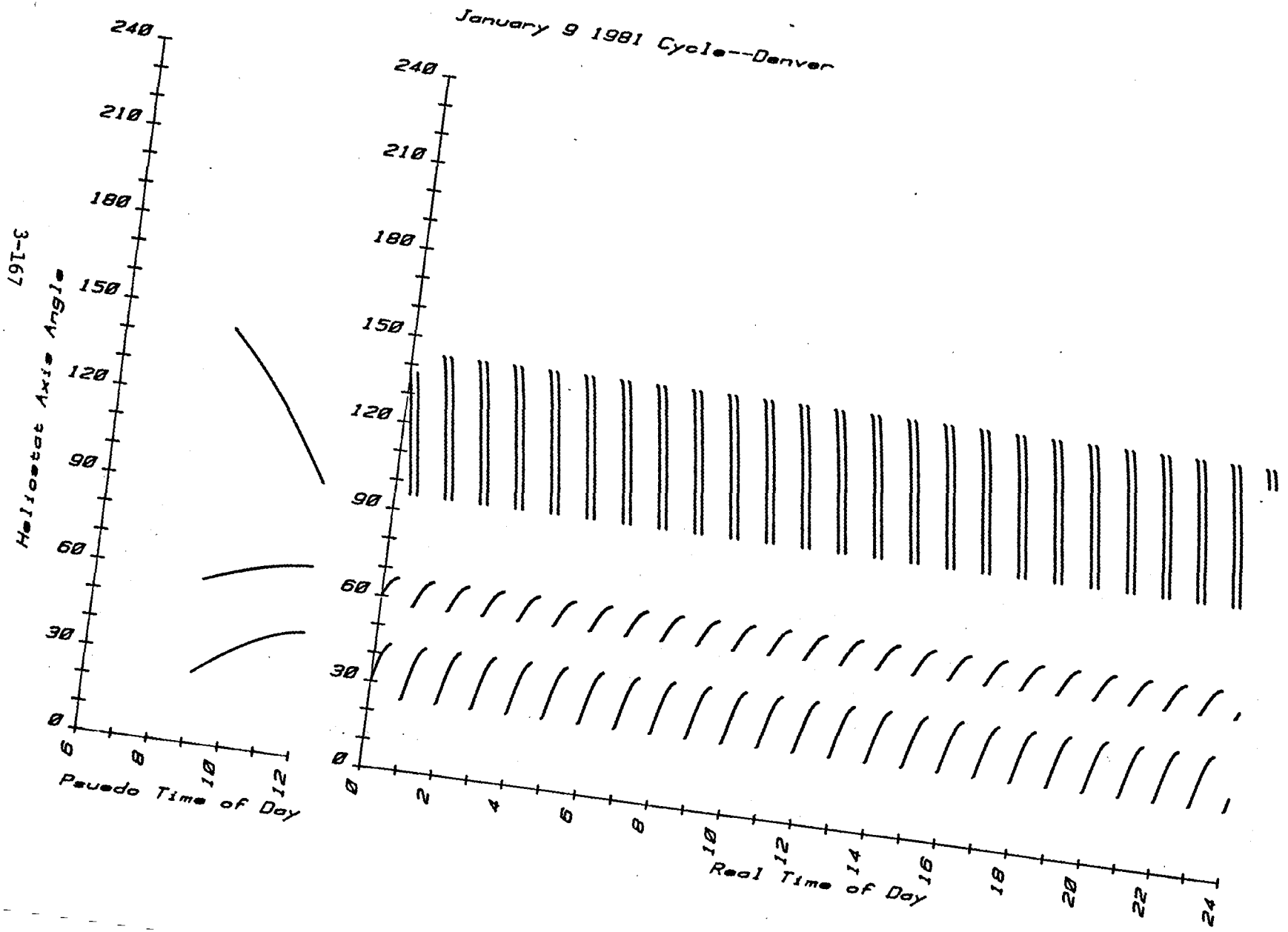

UNLIMITED RELEASE

INITIAL DISTRIBUTION

UC-62d (350)

U.S. Department of Energy
600 E Street NW
Washington, D. C. 20585
Attn: W. W. Auer
G. W. Braun
K. Cherian
M. U. Gutstein
L. Melamed
J. E. Rannels

U.S. Department of Energy
San Francisco Operations Office
1333 Broadway
Oakland, CA 94612
Attn: S. D. Elliott
S. Fisk
R. W. Hughey
W. Nettleton

U.S. Department of Energy
Solar Ten Megawatt Project Office
P. O. Box 1449
Canoga Park, CA 91304
Attn: M. Slaminski

U.S. Department of Energy
Solar Ten Megawatt Project Office
5301 Bolsa Ave. MS14-1
Huntington Beach, CA 92649
Attn: R. N. Schweinberg

USAF Logistics Command
P. O. Box 33140
Wright-Patterson AFB
Ohio 45433
Attn: G. Kastanos

UCLA
900 Veteran Avenue
Los Angeles, CA 90024
Attn: F. Turner

Georgia Institute of Technology
Engineering Experiment St.
Atlanta, GA 30332
Attn: S. H. Bomar, Jr.

University of Houston
Houston
Solar Energy Laboratory
4800 Calhoun
Houston, TX 77004
Attn: A. F. Hildebrandt
L. L. Vant-Hull

U.S. Department of Interior
Water & Power Res. Service
P.O. Box 427
Boulder City, NV 89005
Attn: J. Sundberg

Acurex
485 Clyde Avenue
Mountain View, CA 94042
Attn: J. Hull

Aerospace Corporation
Solar Thermal Projects
Energy Systems Group, D-5
Room 1110
P.O. Box 92957
El Segundo, CA 90009
Attn: P. deRienzo
P. Mathur

Airesearch Manufacturing Co.
2525 West 190th Street
Torrance, CA 90509
Attn: M. G. Coombs
For: P. F. Connelly

AMFAC
700 Bishop Street
Honolulu, HI 96801
Attn: G. St. John

ARCO
911 Wilshire Blvd
Los Angeles, CA 90017
Attn: J. H. Caldwell, Jr.

Arizona Public Service
P. O. Box 21666
Phoenix, AZ 85036
Attn: D. L. Barnes
For: E. Weber

Arizona Solar Energy Commission
1700 W. Washington - 502
Phoenix, AZ 85007
Attn: R. Sears

Babcock & Wilcox
91 Stirling Avenue
Barberton, OH 44203
Attn: G. Grant
For: J. Pletcher
M. Seale

Babcock & Wilcox
P. O. Box 1260
Lynchburg, VA 24505
Attn: W. Smith

Babcock & Wilcox
20 S. VanBuren Avenue
Barberton, OH 44203
Attn: M. Wiener

Badger Energy, Inc.
One Broadway
Cambridge, MA 02142
Attn: F. D. Gardner

Battelle Pacific Northwest Labs
P. O. Box 999
Richland, WA 99352
Attn: M. A. Lind

Bechtel National, Inc.
P. O. Box 3965
San Francisco, CA 94119
Attn: E. Lam
For: J. B. Darnell
R. L. Lessley

Black & Veatch
P. O. Box 8405
Kansas City, MO 64114
Attn: C. Grosskreutz
For: J. E. Harder
S. Levy

Boeing Engineering & Construction
P. O. Box 3707
Seattle, WA 98124
Attn: R. L. Campbell
R. Gillette
J. R. Gintz

Booz, Allen & Hamilton, Inc.
8801 E. Pleasant Valley Road
Cleveland, OH 44131
Attn: W. Hahn

Brookhaven National Laboratory
Upton, NY 11973
Attn: G. Cottingham

Burns and Roe, Inc.
550 Kinderkamack Rd.
Oradell, NJ 07649
Attn: J. Willson

Burns and Roe, Inc.
185 Crossways Park Drive
Woodbury, NY 11797
Attn: R. Vondrasek

Busche Energy Systems
7288 Murdy Circle
Huntington Beach, CA 92647
Attn: K. Busche

California Public Utilities Commission
350 McAllister St., Room 5024
San Francisco, CA 94102
Attn: B. Barkovich
For: C. Waddell

Chevron Research
P. O. Box 1627
Richmond, CA 94804
Attn: L. Fraas

Chevron Oil Research
P. O. Box 446
La Habra, CA 90631
Attn: W. Peake
For: J. Ploeg
W. Stiles

Colt Industries
Trent Tube Division
East Troy, WI 53170
Attn: J. Thackray

Corning Glass Works
Advanced Products Dept.
M/S 25
Corning, NY 14830
Attn: W. M. Baldwin
A. Shoemaker

Custom Metals Enterprises, Inc.
3288 Main Street
Chula Vista, CA 92011
Attn: T. J. Bauer

Data Science Corp.
1189 Oddstad Drive
Redwood City, CA 94063
Attn: M. Liang

Electric Power Research Institute
P. O. Box 10412
Palo Alto, CA 93403
Attn: J. Bigger

El Paso Electric Company
P. O. Box 982
El Paso, TX 79946
Attn: J. E. Brown

Energy, Inc.
P. O. Box 736
Idaho Falls, ID 83401
Attn: G. Meredith

Exxon Enterprises-Solar Thermal Systems
P. O. Box 592
Florham Park, NJ 07932
Attn: P. Joy
For: D. Nelson
G. Yenetchi

Ford Aerospace
3939 Fabian Way, T33
Palo Alto, CA 94303
Attn: I. E. Lewis
For: H. Sund

Foster-Miller Associates
135 Second Avenue
Waltham, MA 02154
Attn: E. Poulin

Foster Wheeler Dev. Corp.
12 Peach Tree Hill Road
Livingston, NJ 07039
Attn: A. C. Gangadharan
For: R. Zoschak

GAI Consultants, Inc.
570 Beatty Rd.
Monroeville, PA 15146
Attn: H. Davidson

General Atomic Company
P. O. Box 81608
San Diego, CA 92138
Attn: H. A. Chiger

General Electric Company
Advanced Energy Programs
P. O. Box 8661
Philadelphia, PA 19101
Attn: A. A. Koenig

General Electric Company
1 River Road
Schenectady, NY 12345
tric Company
1 River Road
Schenectady, NY 12345
Attn: J. A. Elsner
For: R. N. Griffin
R. Horton

GM Transportation System Center
GM Technical Center
Warren, MI 48090
Attn: J. Britt

GM Corp. Harrison Rad. Division
A and E Building
Lockport, NY 14094
Attn: A. Stocker

Houston Lighting and Power
P. O. Box 1700
Houston, TX 77001
Attn: J. Ridgway

Institute of Gas Technology
Suite 218
1825 K Street, NW
Washington, D. C. 25006
Attn: D. R. Glenn

Jet Propulsion Laboratory
Building 520-201
4800 Oak Grove Drive
Pasadena, CA 91103
Attn: M. Adams
H. Bank
W. Carley
E. Cuddihy
J. Sheldon
J. Swan
V. Truscello

Kaiser Engineers, Inc.
300 Lakeside Drive
Oakland, CA 94612
Attn: I. Kornyey

Lawrence Berkeley National Laboratory
University of California
Berkeley, CA 94720
Attn: A. J. Hunt

Los Alamos National Laboratory
P. O. Box 1663
Los Alamos, NM 87545
Attn: S. W. Moore

Los Angeles Water and Power
111 North Hope Street
Los Angeles, CA 90051
Attn: B. M. Tuller
R. Radmacher

Martin Marietta Corporation
P. O. Box 179
Denver, CO 80201
Attn: P. R. Brown
A. E. Hawkins
T. Heaton
L. Oldham
H. C. Wroton

McDonnell Douglas Astronautics Co.
5301 Bolsa Avenue
Huntington Beach, CA 92647
Attn: P. Drummond
R. L. Gervais
D. A. Steinmeyer
L. Weinstein

Meridian Corporation
5515 Cherokee Avenue
Alexandria, VA 22312
Attn: B. S. Macazeer

Nielsen Engineering. & Research
510 Clyde Avenue
Mt. View, CA 94043
Attn: R. Schwind

Northrup, Inc.
302 Nichols Drive
Hutchins, TX 75141
Attn: J. A. Pietsch

ARCO Power Systems
Suite 301
7061 S. University Boulevard
Littleton, CO 80122
Attn: J. Anderson
F. Blake

Olin Corporation
275 Winchester Avenue
New Haven, CT 06511
Attn: S. L. Goldstein

OSC Department of Commerce
341 West 2d Street
San Bernardino, CA 92401
Attn: M. G. Heaviside

Pacific Gas and Electric Co.
77 Beale Street
San Francisco, CA 94105
Attn: P. D. Hindley
For: J. F. Doyle
A. Lam

Pacific Gas and Electric Co.
3400 Crow Canyon Road
San Ramon, CA 9426
Attn: H. Seielstad
For: J. Raggio

Phillips Chemical Co.
13-D2 Phillips Building
Bartlesville, OK 74004
Attn: M. Bowman

Pittsburgh Corning
800 Presque Isle Drive
Pittsburgh, PA 15239
Attn: W. F. Lynsavage

Pittsburgh Corning
723 N. Main Street
Port Allegany, PA 16743
Attn: W. J. Binder
For: R. Greene

PPG Industries, Inc.
One Gateway Center
Pittsburgh, PA 15222
Attn: C. R. Frownfelter

Public Service Co. of New Mexico
P. O. Box 2267
Albuquerque, NM 87103
Attn: A. Akhil

Research and Development
Public Service Co. of Oklahoma
P. O. Box 201
Tulsa, OK 74102
Attn: F. Meyer

Rockwell International
Energy Systems Group
8900 De Soto Avenue
Canoga Park, CA 91304
Attn: T. Springer

S. C. Plotkin & Associates
6451 West 83rd Street
Los Angeles, CA 90045
Attn: W. Raser

Safeguard Power Transmission Co.
Hub City Division
P. O. Box 1089
Aberdeen, SD 57401
Attn: R. E. Feldges

Sargent and Lundy
55 East Monroe
Chicago, IL 60603
Attn: N. Weber

Schumacher & Associates
2550 Fair Oaks Blvd., Suite 120
Sacramento, CA 95825
Attn: J. C. Schumacher

Sierra Pacific Power Co.
P. O. Box 10100
Reno, NV 89510
Attn: W. K. Branch

Solar Energy Research Institute
1617 Cole Boulevard
Golden, CO 80401
Attn: L. Duhham, TID
G. Gross
B. Gupta
D. W. Kearney
L. M. Murphy
R. Ortiz, SEIDB
J. Thornton

Solar Thermal Test Facility
User Association
Suite 1205
First National Bank East
Albuquerque, NM 87112
Attn: F. Smith

Solar Turbines International
P. O. Box 80966
San Diego, CA 92138
Attn: P. Roberts

Southern California Edison
2244 Walnut Grove Road
Rosemead, CA 91770
Attn: J. Reeves
For: C. Winarski

Southwestern Public Service Co.
P. O. Box 1261
Amarillo, TX 78170
Attn: A. Higgins

Standard Oil of California
555 Market Street
San Francisco, CA 94105
Attn: S. Kleespies

Stanford Research Institute
333 Ravenswood Avenue
Menlo Park, CA 94025
Attn: A. Slemmons

Stearns-Roger
P. O. Box 5888
Denver, CO 80217
Attn: W. Lang
For: J. Hopson

Stone & Webster Engineering Corp.
245 Summer Street
P. O. Box 2325
Boston, MA 02107
Attn: R. Kuhr

Townsend and Bottum
9550 Flair Drive
El Monte, CA 91731
Attn: R. Schwing

US Gypsum
101 S. Wacker Drive
Chicago, IL 60606
Attn: Ray McCleary

US Water & Power Resources Service
Bureau of Reclamation
Code 1500 E
Denver Federal Center
P. O. Box 25007
Denver, CO 80225
Attn: S. J. Hightower

Van Leer Plastics
15581 Computer Lane
Huntington Beach, CA 92649
Attn: Larry Nelson

Veda, Inc.
400 N. Mobile, Building D
Camarillo, CA 90310
Attn: L. E. Ehrhardt
For: W. Moore

Westinghouse Corporation
Box 10864
Pittsburgh, PA 15236
Attn: J. J. Buggy
For: R. W. Devlin
W. Parker

Winsmith
Division of UMC Industries
Springville, NY 14141
Attn: W. H. Heller

K. R. Miller, 3153
G. E. Brandvold, 4710; Attn: J. F. Banas, 4716
J. A. Leonard, 4717
B. W. Marshall, 4713; Attn: D. L. King
A. B. Maish, 4724
R. G. Kepler, 5810; Attn: L. A. Harrah, 5811
J. G. Curro, 5813
F. P. Gerstle, 5814
J. N. Sweet, 5824; Attn: R. B. Pettit and E. P. Roth
T. B. Cook, 8000; Attn: A. N. Blackwell, 8200
B. F. Murphey, 8300
C. S. Hoyle, 8122; Attn: V. D. Dunder
R. J. Gallagher, 8124; Attn: B. A. Meyer
D. M. Schuster, 8310; Attn: R. E. Stoltz, 8312, for M. D. Skibo
A. J. West, 8314
W. R. Even, 8315
R. L. Rinne, 8320
C. T. Yokomizo, 8326; Attn: L. D. Brandt
P. L. Mattern, 8342
L. Gutierrez, 8400; Attn: R. A. Baroody, 8410
D. E. Gregson, 8440
C. M. Tapp, 8460
C. S. Selvage, 8420
V. Burolla, 8424; Attn: C. B. Frost
R. C. Wayne, 8450
T. D. Brumleve, 8451
W. R. Delameter, 8451
P. J. Eicker, 8451 (5)
R. M. Houser, 8451
C. L. Mavis, 8451
W. L. Morehouse, 8451
H. F. Norris, Jr., 8451
W. S. Rorke, Jr., 8451
D. N. Tanner, 8451
S. S. White, 8451
A. C. Skinrood, 8452
W. G. Wilson, 8453
Publications Division, 8265/Technical Library Processes Division, 3141
Technical Library Processes Division, 3141 (2)
M. A. Pound, 8214, for Central Technical Files (3)

☆ U.S. GOVERNMENT PRINTING OFFICE: 1981 - 771-815/325 0-II